FREQUENCY DOMAIN OPTIMIZATION OF DRY FRICTION DAMPERS USED FOR EARTHQUAKE VIBRATION DAMPING OF BUILDINGS

A THESIS SUBMITTED TO
THE GRADUATE SCHOOL OF NATURAL AND APPLIED SCIENCES
OF
MIDDLE EAST TECHNICAL UNIVERSITY

BY

ZÜHTÜ EREN ERİŞEN

IN PARTIAL FULFILLMENT OF THE REQUIREMENTS
FOR
THE DEGREE OF MASTER OF SCIENCE
IN
MECHANICAL ENGINEERING

FEBRUARY 2012

Approval of the thesis:

FREQUENCY DOMAIN OPTIMIZATION OF DRY FRICTION DAMPERS USED FOR EARTHQUAKE VIBRATION DAMPING OF BUILDINGS

Submitted by **ZÜHTÜ EREN ERİŞEN** in partial fulfillment of the requirements for the degree of **Master of Science in Mechanical Engineering Department, Middle East Technical University** by,

Prof. Dr. Canan Özgen
Dean, Graduate School of **Natural and Applied Sciences** _____

Prof. Dr. Suha Oral
Head of Department, **Mechanical Engineering** _____

Assist. Prof. Dr. Ender Ciğeroğlu
Supervisor, **Mechanical Engineering Dept., METU** _____

Examining Committee Members:

Prof. Dr. Y. Samim Ünlüsoy
Mechanical Engineering Dept., METU _____

Assist. Prof. Dr. Ender Ciğeroğlu
Mechanical Engineering Dept., METU _____

Prof. Dr. Mehmet Çalışkan
Mechanical Engineering Dept., METU _____

Assist. Prof. Dr. Gökhan O. Özgen
Mechanical Engineering Dept., METU _____

Assist. Prof. Dr. Serdar Göktepe
Civil Engineering Dept., METU _____

Date: 08-02-2012

I hereby declare that all information in this document has been obtained and presented in accordance with academic rules and ethical conduct. I also declare that, as required by these rules and conduct, I have fully cited and referenced all material and results that are not original to this work.

Name Surname: ZÜHTÜ EREN ERİŞEN

Signature:

ABSTRACT

FREQUENCY DOMAIN OPTIMIZATION OF DRY FRICTION DAMPERS USED FOR EARTHQUAKE VIBRATION DAMPING OF BUILDINGS

Erişen, Zühtü Eren

M.Sc., Department of Mechanical Engineering

Supervisor: Assist. Prof. Dr. Ender Ciğeroğlu

February 2012, 148 pages

There are many active and passive vibration control techniques to reduce the effect of energy on structures which emerges during an earthquake and reduce the displacement of buildings that is caused by ground acceleration. Main advantage of passive vibration control techniques over active vibration control techniques is; no external power or a sensor is required for passive vibration control devices (PVCDs) and it results in lower installation and maintenance costs. However, PVCDs require a predefined optimum damping ratio and optimum damping distribution along the structure since they are not adaptive to changing ground acceleration values. During the design of the PVCDs numerous factors such as building properties and earthquake characteristics should be considered. Dry

friction damper is an example of PVCD and has an extensive usage in many different fields due to its high energy damping capacity with low cost and ease of installation. In this thesis, damping of seismic energy at buildings with dry friction dampers is investigated and a new optimization method is developed in frequency domain by employing Describing Function Method (DFM) which reduces the computational effort compared to the time domain and finite element solutions drastically. The accuracy and verification of the presented method is investigated by comparing the frequency domain results with time marching solutions. Furthermore, damper placement and slip forces on the dampers are optimized for single and multi-story buildings equipped with dry friction dampers by utilizing the developed method.

Keywords: Dry friction damper, optimal damper placement, optimum slip force, earthquake vibration damping, damper optimization

ÖZ

BİNALARDA DEPREM SIRASINDA OLUŞAN TİTREŞİMLERİN SÖNÜMLENMESİ İÇİN KULLANILAN KURU SÜRTÜNMELİ SÖNÜMLEYİCİLERİN FREKANS DÜZLEMİNDE OPTİMİZASYONU

Erişen, Zühtü Eren

Yüksek Lisans, Makine Mühendisliği Bölümü

Tez Yöneticisi: Yrd. Doç. Dr. Ender Ciğeroğlu

Şubat 2012, 148 sayfa

Deprem sırasında açığa çıkan enerjinin yapılar üzerindeki etkisini azaltıp binalarda yer ivmesinin sebep olduğu deplasmanı azaltmak amaçlı kullanılan birçok aktif ve pasif titreşim kontrol teknikleri vardır. Pasif titreşim kontrol tekniklerinin aktif titreşim kontrol tekniklerine göre temel avantajı; pasif titreşim kontrol cihazlarının harici enerjiye veya sensöre ihtiyaç duymamasıdır. Bu avantaj kurulum ve bakım maliyetlerinin azalmasını sağlamaktadır. Ancak pasif titreşim kontrol cihazları değişik yer ivmelerine karşı kendini adapte edemediğinden, önceden belirlenmiş optimum bir sönümleme oranı ve yapı boyunca bir sönümleme dağılımına ihtiyaç duymaktadırlar. Pasif titreşim kontrol cihazlarının dizaynı sırasında bina özellikleri

ve deprem karakteristiği gibi çok sayıda faktör göz önüne alınmalıdır. Kuru sürtünmeli sönümleyiciler pasif kontrol titreşim kontrol cihazlarına örnek olup, düşük maliyetine ve montaj kolaylığına karşın yüksek enerji sönümleme kapasitesine sahip olmaları sebebiyle birçok alanda yoğun olarak kullanılmaktadır. Bu çalışmada, binalarda sismik enerjinin kuru sürtünmeli sönümleyicilerle sönümlenmesi incelenmiş ve frekans düzleminde tanımlayıcı fonksiyonlar metodu kullanılarak, zaman tanım alanında ve sonlu elemanlar analiz yöntemi ile yapılmış çözümler ile karşılaştırıldığında, daha az hesaplama çabası gerektiren, yeni bir yöntem geliştirilmiştir. Anlatılan yeni yöntemin sonuçları zaman tanım alanında yapılan çalışmaların sonuçlarıyla karşılaştırılmış böylece yeni yöntemim doğruluğu ve geçerliliği gösterilmiştir. Buna ek olarak, sönümleyicilerin bina boyunca yerleşimi ve sönümleyiciler üzerindeki kayma kuvvetleri, tek ve çok katlı binalar için, yeni geliştirilen yöntem kullanılarak optimize edilmiştir.

Anahtar kelimeler: Kuru sürtünmeli sönümleyici, optimum sönümleyici yerleşimi, optimum kayma kuvveti, deprem titreşimlerinin sönümlenmesi, sönümleyici optimizasyon

To My Dear Family

ACKNOWLEDGEMENTS

First and foremost, I would like to express my sincere gratitude to my advisor Asst. Prof. Dr. Ender Ciğeroğlu for his invaluable guidance and continuous support to start and complete this study.

I would like to express my deepest gratitude to my parents Demet and Edip Erişen for everything that I have in my life and supporting me mentally and spiritually throughout my life. I am also deeply grateful to my sister Esra Erişen for her unconditional support.

I would like to thank my colleagues, Fuat Çağrı Demir, Ergin Kurtulmuş and Yusuf Eldoğan for their friendship and technical support during the thesis period.

TABLE OF CONTENTS

LIST OF TABLES

TABLES

LIST OF FIGURES

FIGURES

NOMENCLATURE

$[M]$	Mass matrix of the building
$[C]$	Damping matrix of the building
$[K]$	Stiffness matrix of the building
$\{x\}$	Displacement vector of the stories
$\{\dot{x}\}$	Velocity vector of the stories
$\{\ddot{x}\}$	Acceleration vector of the stories
$\{f_{NL}\}$	Nonlinear forcing vector
$\{f_{exc}\}$	Excitation vector
$\ddot{x}_g$	Earthquake acceleration
k_f	Friction damper stiffness
μ	Coefficient of friction
N	Normal load acting across the contact surface
k_b	Brace stiffness
k_{bd}	Damper assemblage stiffness
E_b	Elastic modulus of the brace
A_b	Cross sectional area of the brace
l_b	Length of the brace

$\left[M^{drift}\right]$	Mass matrix of the building for interstory drift solution
$\left[C^{drift}\right]$	Damping matrix of the building for interstory drift solution
$\left[K^{drift}\right]$	Stiffness matrix of the building for interstory drift solution
$\{y\}$	Interstory drift vector of the stories
$\{\dot{y}\}$	Interstory velocity vector of the stories
$\{\ddot{y}\}$	Interstory acceleration vector of the stories
$\{F\}$	Complex vector of amplitudes of external forces
ω	Excitation frequency
$\{X\}$	Complex vector of displacement amplitudes
$\{F_{NL}\}$	Complex vector of the nonlinear forcing amplitudes
α	Receptance of the linear system
$[\Delta]$	Generalized quasi-linear matrix
v	Harmonic input describing function
$[\Theta]$	Pseudo-receptance matrix
SR	Normalized damper stiffness
PS	Normalized slip load
E_d	Energy dissipated by the friction damper per cycle

CHAPTER 1

INTRODUCTION

1.1. Structural Response of a Building During an Earthquake

During an earthquake, structural vibrations occur on buildings due to the seismic energy transferred. As a result of these vibrations, structural damage or even failure may occur. Therefore; in order to decrease the vibration amplitude and minimize the effects of the earthquakes, a control system can be applied to the building.

This structural control system can be utilized by many different means such as modifying stiffnesses, masses, damping, or shape of the building and by providing passive or active counter forces [1].

The ways to accomplish a seismic response control are [2];

- Decreasing the energy transmission of the earthquake ground motion to the structure.

- Isolating the natural frequency of the building from the dominant frequency of the earthquake.

- Achieving the non-resonant state by providing nonlinear characteristics.

- Applying control forces to the building.

- Utilizing energy absorption mechanisms.

The hazard of earthquakes depend on many factors such as site condition, magnitude and distance of the earthquake to the site and structural properties of the building. Some building properties that affect the response during an earthquake can be given as;

- Natural frequency of the building

- Damping of the building

- Ductility of the building

- Stiffness of the building

Since there are many factors that affect an earthquake, it is totally a random process and due to this reason, it is hard to design and construct a building with an integrated passive vibration control system. In the standards and guidelines about earthquake resistant building design, some performance and modeling criteria are expressed for newly designed or seismically rehabilitated buildings. These guidelines also include hazard maps for different regions and present information for an artificially designed earthquake to use in calculations according to some parameters such as earthquake zone, soil characteristic and building type. However, all of the definitions, parameters, calculation methods are given for time domain solutions in these guidelines and there is very little information for the solution of non-linear systems such as buildings with dry friction dampers in frequency domain. Detailed information can be found in guidelines [3] and [4].

Takewaki et. al [5] has also stated that it is not so easy to find the most unfavorable ground motion for a building that may occur at the specified site as schematized in Figure 1.1. Nearly all of the code-specified design earthquakes are constructed by taking into account the knowledge from past observations and the

probabilistic insights. However, uncertainties in the occurrence of earthquakes still exist and shouldn't be disregarded.

Most important characteristics of an earthquake in terms of the damage that occurs on buildings are its amplitude and frequency. As can be seen from Figure 1.2, ground motion at a site is superposition of different frequencies with different amplitudes. If one of the dominant frequencies of an earthquake is far from the natural frequency of the building, then the building does not vibrate with a considerable amplitude and the damage caused is minimal. However, it is not always so practical to isolate the natural frequency of the building from these dominant frequencies due to constructive challenges; at which point vibration control systems are required. From the studies that have been done before, it is seen that most of the earthquakes are dominant in the range of 0.1 Hz - 10 Hz. [6, 7]

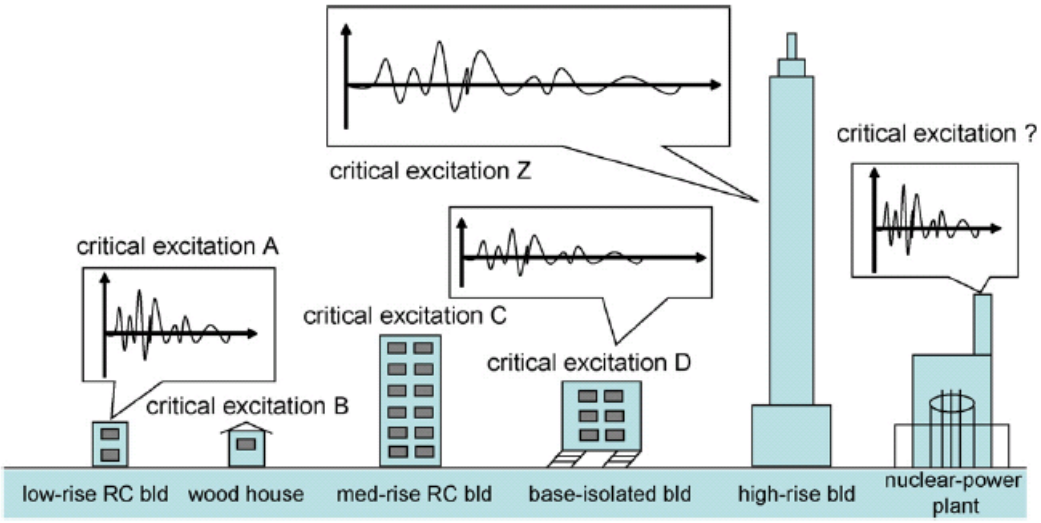

Figure 1.1 Various critical excitations for different type of buildings [5]

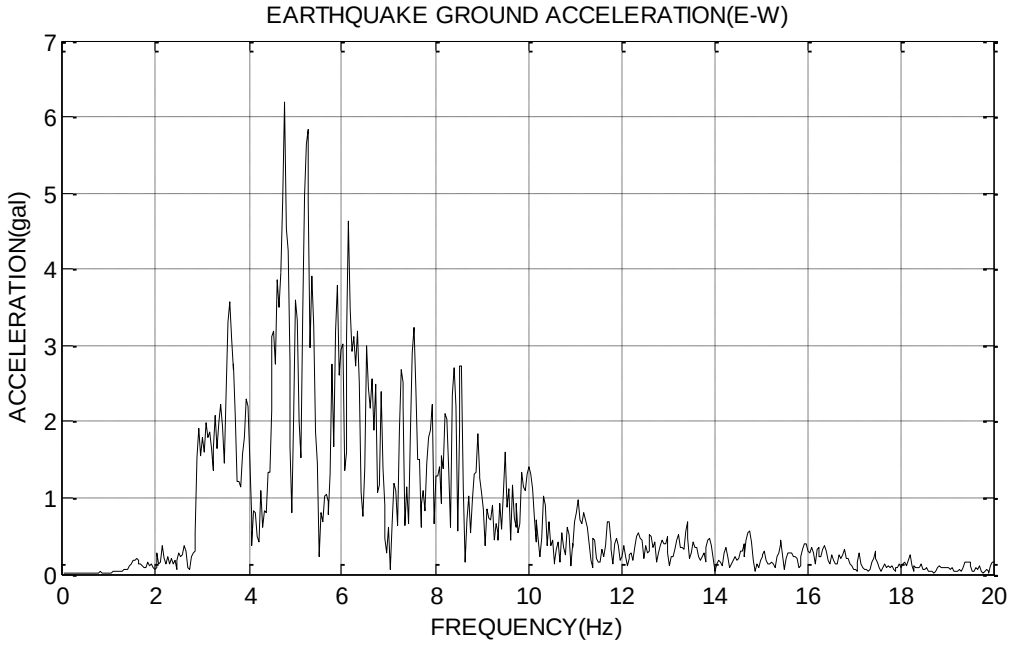

Figure 1.2 Frequency response function of 1992 ERZINCAN earthquake

1.2. Types of Structural Control Systems

Structural control systems can be classified in three main groups;

- Active Control Systems
- Passive Control Systems
- Semi active Control Systems

Specific advantages and disadvantages of these control system types are briefly summarized in this section.

1.2.1. Active Control Systems

Active control systems require an external power supply and an actuator to apply the required force to the building. Moreover, in this type of control systems, some different kinds of sensors are required to be placed at the ground and the building if active feedback system is applied. Although these systems are the most accurate way to decrease the vibration levels of buildings, they may be infeasible due to their high initial setup and operational cost. These systems are also not very reliable since they require an external power supply for operation.

A building with an active control system in Tokyo given in Figure 1.3, and Figure 1.4 shows the control diagram of the active control systems.

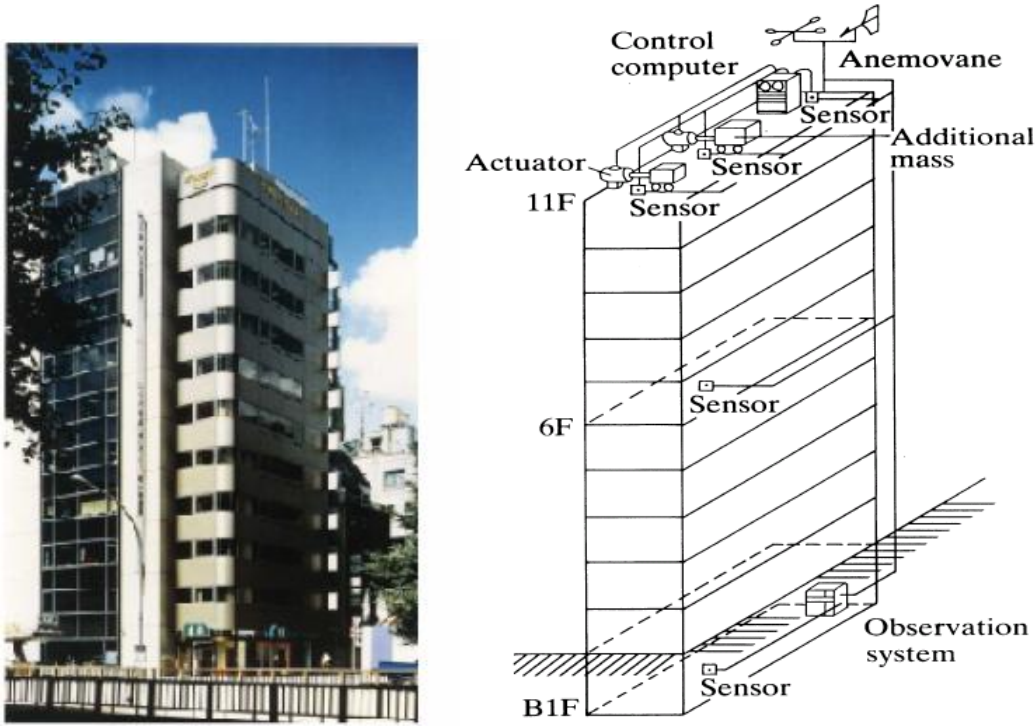

Figure 1.3 Kyobashi Seiwa building, Tokyo [8]

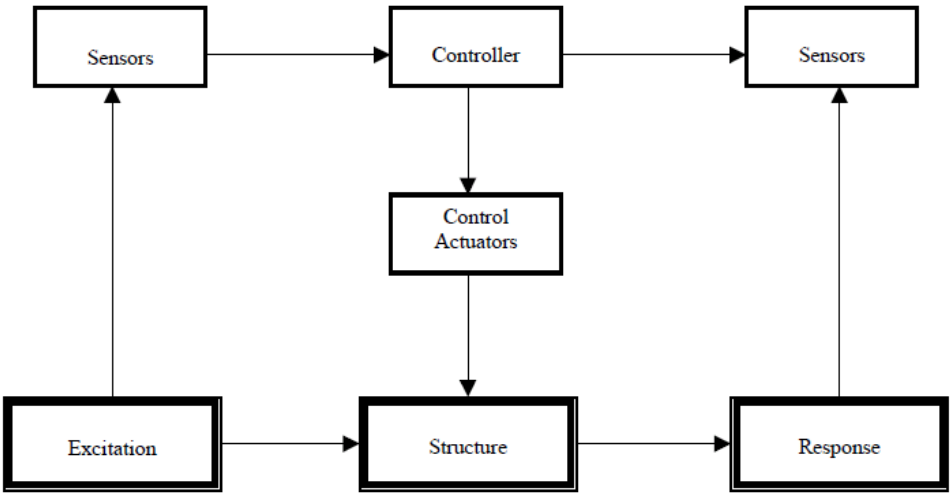

Figure 1.4 Schematic diagram of an active control system [8]

1.2.2. Passive Control Systems

In a passive control system, there is no need for an external power supply or a sensor and seismic energy is damped within the system in response to the motion of the building. However, since these systems are not adaptive, they require an optimum damping ratio and damping distribution along the structure. Metallic dampers, visco-elastic dampers, friction dampers and viscous dampers are among the passive control systems. The damping capacity of passive control system devices is directly related with the building properties and earthquake characteristic. Since they are practical to apply and less costly; in most cases they are preferred over active control systems.

1.2.3. Semi active Control Systems

Semi active control systems are a combination of passive and active control systems. In other words, semi active control devices can also be considered as controllable passive control devices. External energy required in these systems are considerably small compared to active control devices.

1.3. Building Models

In the literature, there are three main types of building models and they have been used for different purposes in earthquake studies. When the effects of each extra freedom need to be investigated, building model becomes more complex which leads to more time consuming and complicated analysis process.

1.3.1. Shear Building Model

Shear building model is the most widely used and the simplest building model as a lumped mass approach. In this model, every story of the building is idealized by a single column with a lumped mass at each floor level.

Since it is not easy to estimate the stiffness of all the elements without making a finite element analysis, most of the time only stiffness of the columns are considered in the calculations. Therefore, the stiffness of the idealized column is the total stiffness of all the columns in the actual structure [9].

In this model floors are assumed to be rigid, incompressible and columns are assumed to be axially rigid. As a result of these assumptions, displacements at each floor are described like a single degree of freedom (SDOF) system and the

number of degrees of freedom of the whole building is equal to the number of floors.

A sketch of the shear building model is given in Figure 1.5 and Figure 1.6 shows the horizontal response of the building to an earthquake where damping is neglected.

In this thesis shear building model is used since orientation of the dampers is not investigated and response in only one direction is studied at each floor for optimization purposes.

1.3.2. Shear Flexural Building Model

In this model, overall flexural behavior of the building can be investigated. It is an extension of the shear building model and number of degrees-of-freedom is two times that of the shear building model as shown in Figure 1.7 [5].

1.3.3. 3-D Shear Building Model

This model is a 3-D extension of the shear building model and can deal with torsional response of the buildings as shown in Figure 1.8 [5]. If it is required to study not only the location of the dampers but also their orientations, this model can be used.

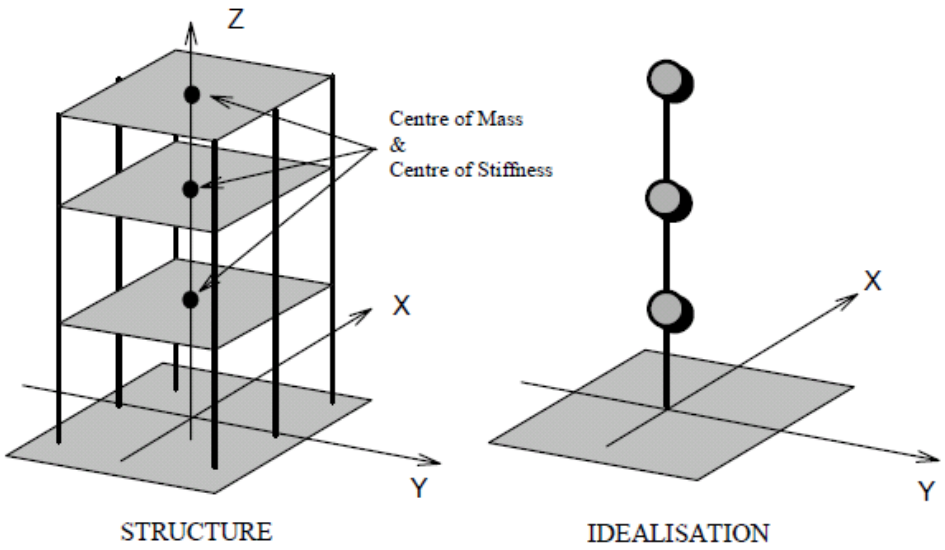

Figure 1.5 Shear building model [9]

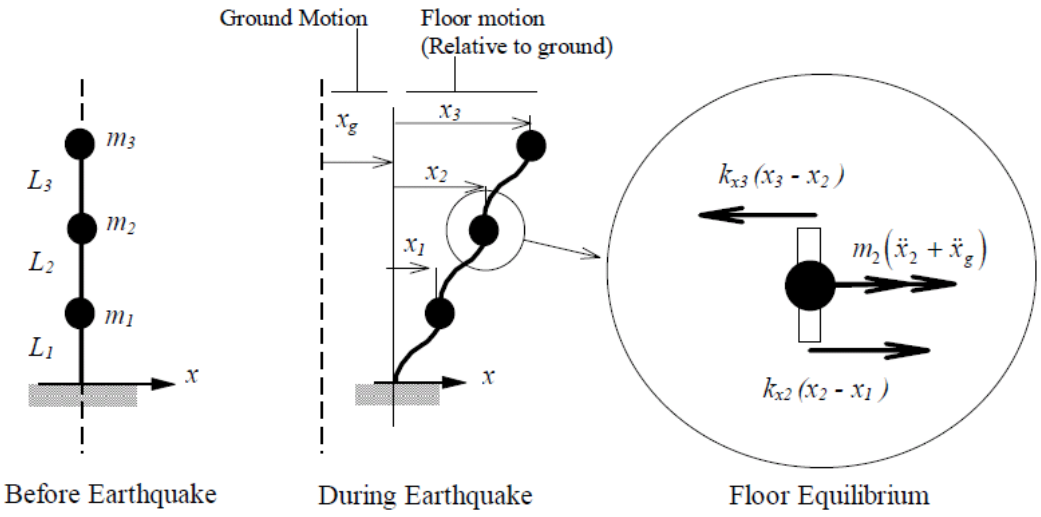

Figure 1.6 Horizontal response of a multistory building to earthquake [9]

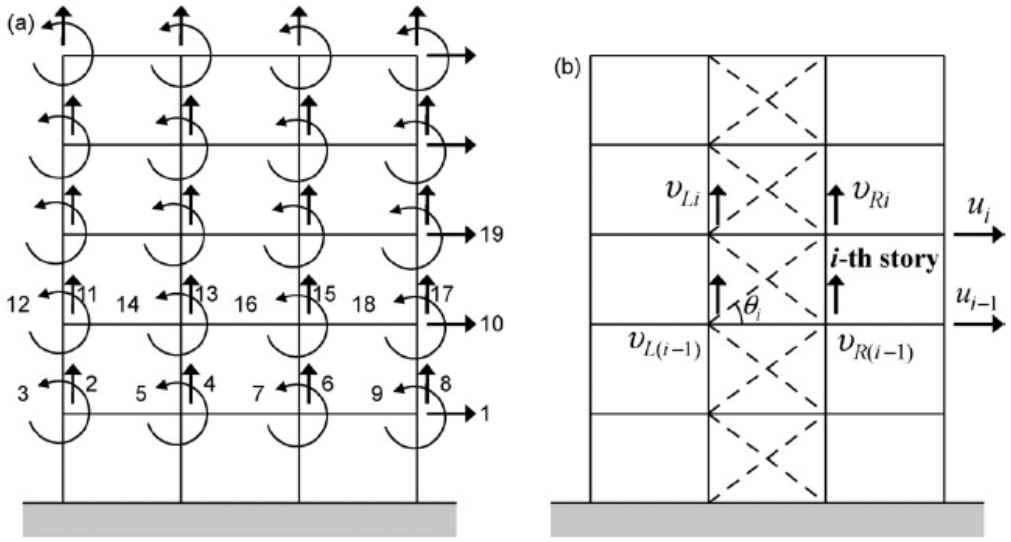

Figure 1.7 2-D planar building frame (shear-flexural building model) [5]

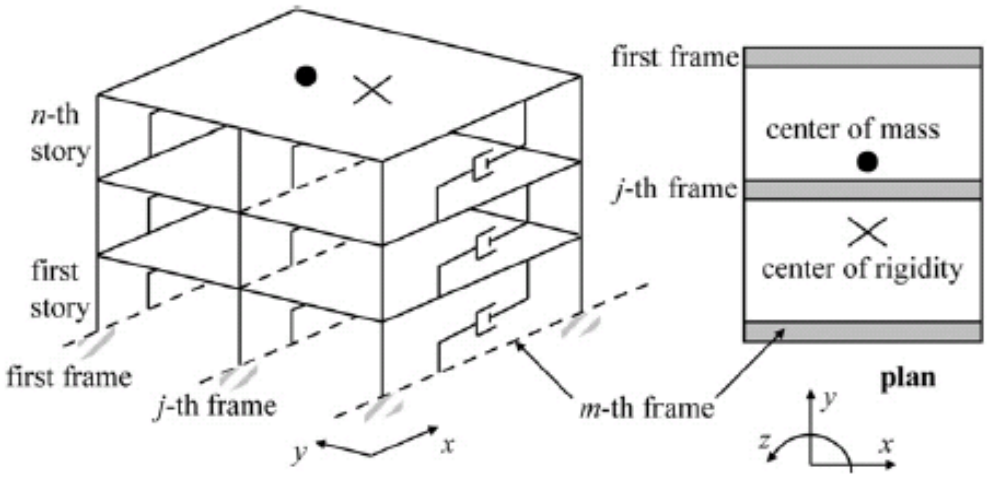

Figure 1.8 3-D shear building model [5]

1.4. Friction Damping

Friction can be defined as the resistance to the motion during sliding or rolling when one body is in tangentially contact with another body [10]. Although it is usually considered to be an undesirable phenomenon, it is used at various applications for energy damping such as automobile brakes, clutches and turbine blades. There are three types of friction between two bodies;

- Dry Friction: 2 solids with direct contact

- Fluid Friction: 2 solids separated with gas or liquid

- Boundary Friction: 2 solids separated with a thin film

Friction dampers are also extensively used at buildings as a passive control system method to reduce the displacement that is caused by ground acceleration during an earthquake. They can provide sufficient stiffness to the building and they have a good energy dissipation capacity [11].

During an earthquake, the friction damper begins to slip at a predetermined slip force and by this way dissipates the required energy. If slip load is too high, no slippage occurs at the damper so energy can not be dissipated. In the controversy, if it is too small, the damper usually travels at slip state but dissipated energy is less than required due to the low slip load. As a result of this dilemma, there is an optimum value of slip force for the damper which depends both on the structural properties and earthquake characteristics. At the same time, a friction damper can also shift the natural frequency of the building far from the earthquake dominant frequency under proper conditions.

1.4.1. Friction Modeling

Many researchers have investigated the friction phenomena and developed different models. Olsson and Åström[12] have investigated these models and summarized them in his study. In this thesis, "Coulomb Macro-Slip friction model" is used.

1.4.1.1. Coulomb Macro-Slip Model

Cigeroglu and Ozguven [13] stated that, the Coulomb macro-slip model is one of the widely used models for dry friction damping mechanisms due to its mathematical simplicity and also success in predicting actual responses for low normal loads.

In this model, all the friction surface is assumed to be in either stick or slip states and dry friction element is modeled like a spring as shown in Figure 1.9 where one end of it is as fixed and other end of it is free to slip if the force on the spring is greater than a predetermined value, which is referred as "slip force". This model will be investigated in more detail in Section 2.1.2.

1.5. Literature Survey

Mualla [14] studied dynamic response of single story buildings equipped with a novel friction damper device (FDD). Main parts of the damper and its principle of action are shown in Figure 1.10 and Figure 1.11. A 1/3 scaled steel building model with a friction damper was built for experiments. Numerical simulations based on non-linear time history were used to investigate the influence of excitation

frequency, displacement amplitude, bolt clamping force which effects the slip load of the damper and the number of loading cycles on the performance of the damper under lateral harmonic excitation. The results of the study showed that FDD is velocity independent within a certain range and linearly dependent on the displacement amplitude. Coulomb friction law was used to model the friction in the study.

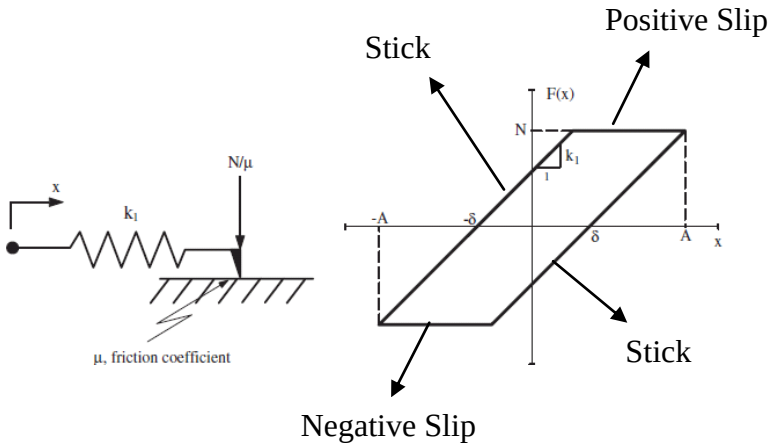

Figure 1.9 Schematic drawing of Coulomb macro-slip model and hysteresis curve [13]

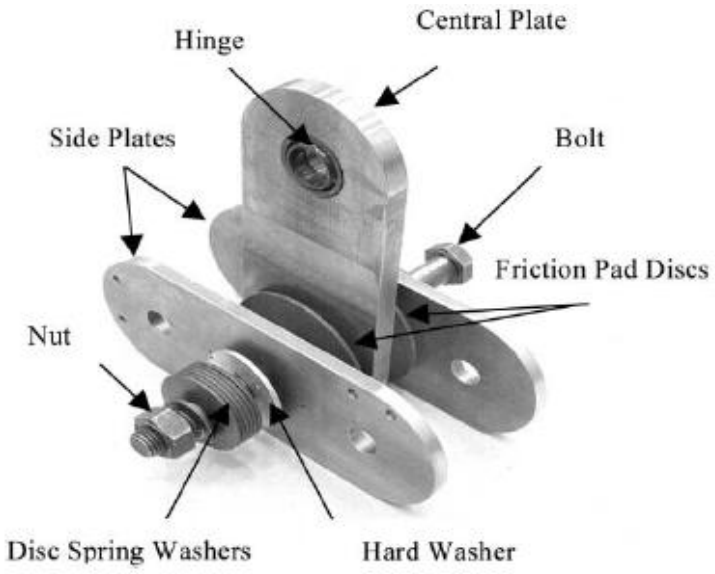

Figure 1.10 Main parts of the FDD [14]

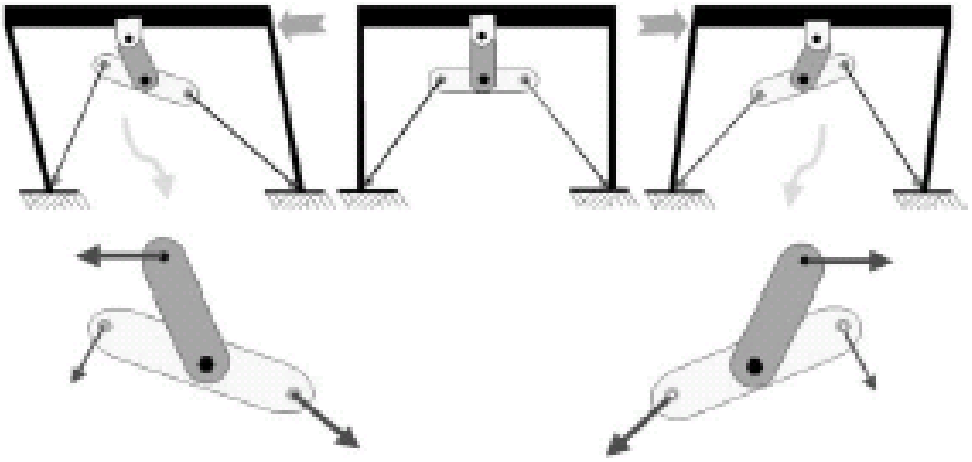

Figure 1.11 Principle of action of FDD [14]

In 2002, Pasquin et al. [15] studied the effects of the friction dampers on a nine-story building. Purpose of this study was the seismic upgrading of an existing building in Montreal. A total of 161 dampers were installed in single diagonal and chevron bracing and this upgrade reduced the drifts and base shear while greatly minimizing requirement of strengthening the existing members. Nonlinear time history dynamic analyses were performed to solve the system and optimize the dampers.

Chang et al. [16] made another rehabilitation study in 2003. 48 friction dampers were placed on "Monterey County Government Center" building to decrease structural deficiencies and meet the required safety levels as described in FEMA 356 guidelines. The building has 3 floors and a roof. 24 of the dampers which have a slip load of 250 kip were placed at the ground levels and 24 of them which have a slip load of 200 kip were placed at the 2^{nd} floor. After these modifications, the model was analyzed with both Basic Safety Earthquake 1 (BSE-1) and Basic Safety Earthquake 2 (BSE-2) time histories as required in FEMA 356. It was seen that maximum story displacement was reduced by 50% and story shear was reduced by 20% to 30%. In this study, the reasons of choosing friction dampers were given as;

- Energy dissipation capacity of friction dampers is very good
- Friction dampers are not so expensive and require no maintenance.

Lu et al. [17] utilized a discrete-time domain solution to find the dynamic response of a structural system equipped with multiple friction dampers. Based on the derived solution, a procedure is developed which allows the time interval of analysis to remain constant, even at the transition of stick and slip states.

Marko et al. [18] made a study about seismic mitigation of medium rise frame-shear wall structures using friction and visco-elastic dampers. Two building structures equipped with dampers in different configurations and in various locations are subjected to five different earthquake loadings. To model the dampers and structures, finite element techniques are used and effect of damper type, damper properties, configuration and location of the dampers to the building response are investigated. In this study, for contact analyses, Coulomb friction model is used. It was concluded that computation of tip deflection is a reasonable measure of the overall effect of the earthquake on the building.

In 2004, Liao et al. [19], performed a shaking table test to a three story steel frame structure equipped with a friction damper device which has already been investigated before by Mualla et al. [14]. In this study, only unilateral ground shaking of different earthquakes are used to investigate the seismic responses of the test structure. Numerical simulation results are compared with test results and it is seen that friction dampers have a very good performance in reducing the lateral story drifts. Numerical simulation results are given in Table 1.1.

Friction dampers are not only applied between the stories of a single building. They can also be applied to adjacent buildings. Bhaskararao and Jangid [20] investigated dynamic behavior of two adjacent single story structures connected with a friction damper under harmonic ground acceleration as shown in Figure 1.12. In this study, closed form expressions are derived to initiate stick and slip condition of the damper in terms of system parameters and differential equations of the system are solved both for the slip and stick states. To see the effects of

some design parameters, such as structure damping ratio and slip force, a parametric study is also carried out. At the end of the study, it is concluded that there is an optimum value of the slip force for the damper connecting two adjacent structures and dynamic response of the coupled structure can be decreased significantly with an optimized friction damper. Other conclusions of this study can be summarized as;

- Optimum slip force increases with the increase of natural frequency ratio of the buildings

- Optimum slip force is not the same for both buildings and it depends on the damping ratios of each building

- Optimum slip force increases with the increase of mass of the buildings

- Maximum displacement of the damper decreases with increasing slip load and increases with increasing ratio of the masses of the buildings.

Table 1.1 Interstory drifts for undamped and damped frame [19]

Earthquake	PGA (g)	Max. storey drift, with damper (mm)	Max. storey drift, w/o damper (mm)	Reduction (%)
El Centro, USA, 1940	0·36	18·96	38·5[a]	50·7
	0·26	15·06	32·9[a]	54·5
	0·05	2·31	13·63	83·1
Kobe, Japan, 1995	0·18	8·67	32·3[a]	73·2
	0·12	5·87	24·2[a]	75·8
	0·05	2·50	13·11	80·9
Chi-Chi, Taiwan, 1999	0·15	13·50	47·0[a]	71·3
	0·12	10·69	39·7[a]	73·1
	0·04	1·52	8·10	81·2

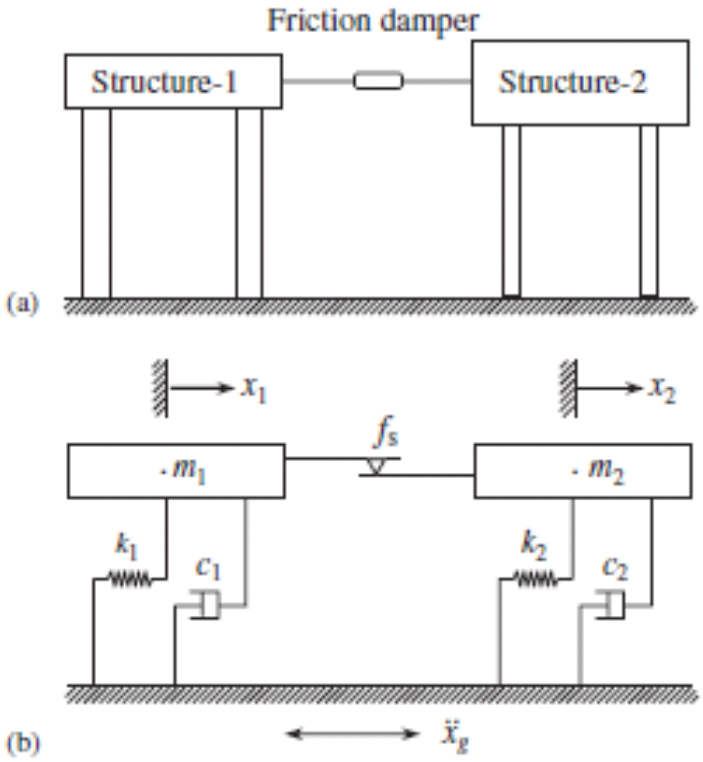

Figure 1.12 Adjacent Structures Connected with a Friction Damper and its Mechanical Model [20]

Bhaskararao and Jangid [21] also investigated the seismic response of multi-story adjacent buildings connected with friction dampers. In this study equations of motion and numerical study are presented for two cases;

- Dampers with same slip force

- Dampers with different slip force

A parametric study is also conducted to optimize the slip force of the dampers and number of dampers. It is shown that if proper slip force is selected for the dampers they are very effective in reducing the displacement of the buildings during an earthquake and it is not required to place the dampers between all the floors. The structural model used in this study is given in Figure 1.13. Friction is modeled as a fictitious spring which has very high stiffness (k_d) during non-slip mode and zero

stiffness during slip mode as shown in Figure 1.14. In this study, it is assumed that two buildings are symmetric and each adjacent floor is at the same level.

From the literature survey, it is seen that dry friction damper is an effective device to decrease the building vibration response during an earthquake, however slip force of the damper should be adjusted properly in order to use the damper with the best performance. Moreover, it is also seen that placement of the dampers at a multi-story building is an important parameter and should be optimized for cost reduction. In the literature, most of the studies are performed on a scaled model or utilized some kind of time integration methods which requires extensive computational effort.

1.6. Focus of the Thesis

Main focus of this thesis is the investigation of vibrations on buildings during an earthquake and developing a new methodology in frequency domain to optimize the characteristics of friction damper(s) in order to decrease the response of the buildings. By this way, difficulties of time domain methods are eliminated and computational effort is decreased.

In this thesis, design optimization will consist of;

- Optimization of the slip force(s)

- Optimization of the number of the damper(s)

- Optimization of the placement of the damper(s)

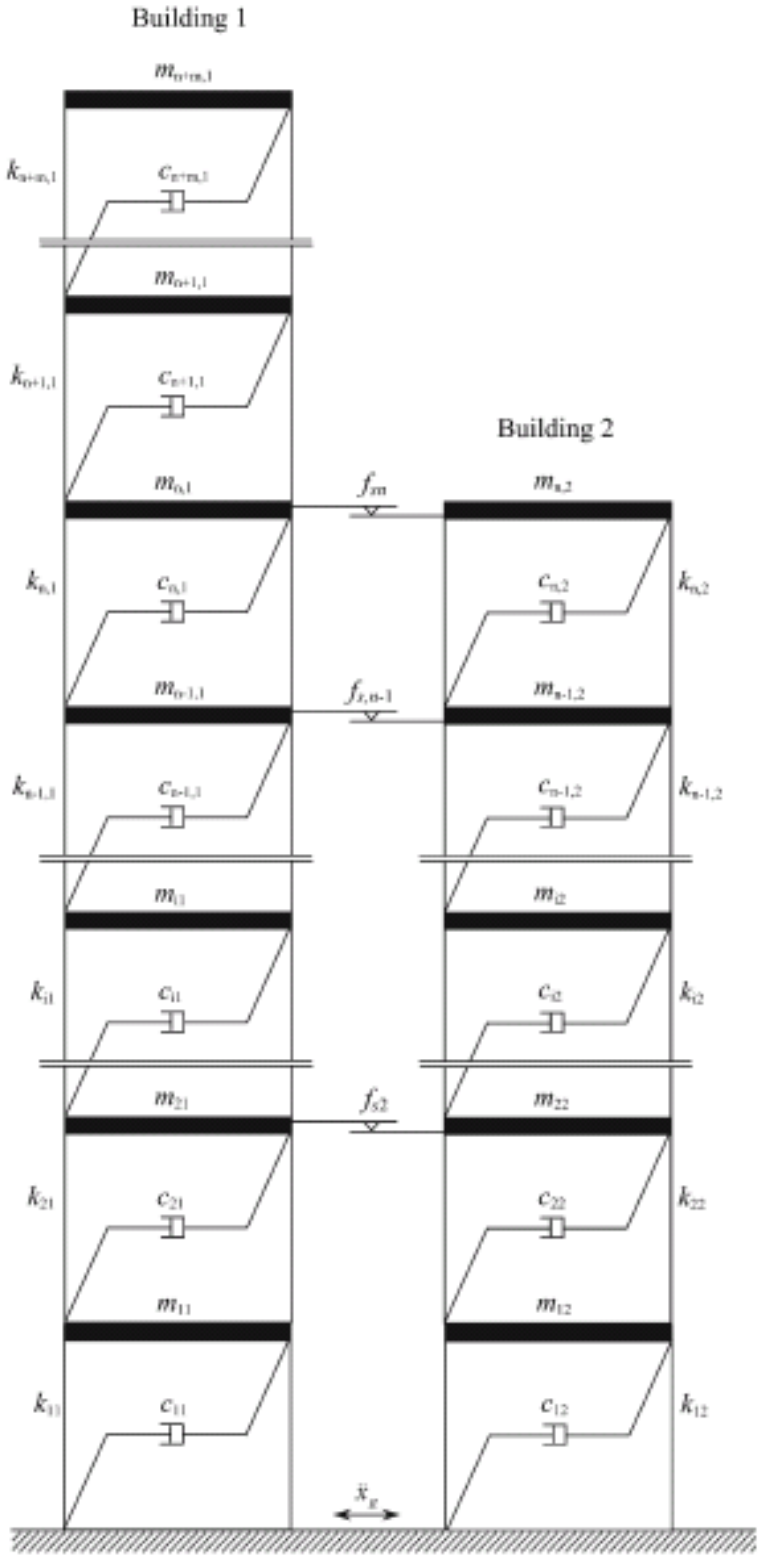

Figure 1.13 Structural Model of Two Adjacent Buildings Connected with Friction Dampers [21]

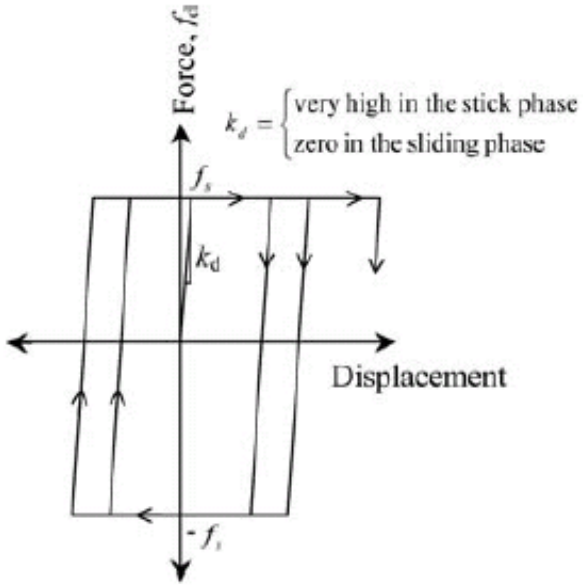

Figure 1.14 Displacement versus Damper Force [21]

1.7. Outline of the Thesis

In Chapter 2, shear building model with dry friction dampers is investigated and the equations of motion are derived.

In Chapter 3, solution methods for non-linear systems and description of nonlinear forces in terms of harmonic components are discussed. Moreover, frequency domain solution method is verified by comparing the results obtained from time marching solutions.

In Chapter 4, effect of parameters of dry friction damper utilized on a multistory building is investigated and different optimization studies are performed for different scenarios.

In Chapter 5, discussion, conclusion and future work are given.

CHAPTER 2

BUILDING MODEL WITH DRY FRICTION DAMPERS

2.1. Multistory Shear Building Model

As mentioned in Section 1.3.1. , shear building model is used in this thesis since orientation of the dampers is not investigated and response is studied only in one direction for optimization purposes.

In this thesis, the shear building model given in Figure 2.1 is used where the dampers are placed between the successive floors; however, alternative damper configurations are as well possible and in the following chapters, effect of the different damper configurations is also investigated.

2.1.1. Equations of Motion for a Multistory Building

Schematic representation of a n-story building model is given in Figure 2.1 for which the equations of motion can be given as follows;

$$\begin{aligned} &[M]\{\ddot{x}\}+[C]\{\dot{x}\}+[K]\{x\}+\{f_{NL}\}=\{f_{exc}\} \\ &\{f_{exc}\}=-[M]\ddot{x}_g \end{aligned} \tag{2.1}$$

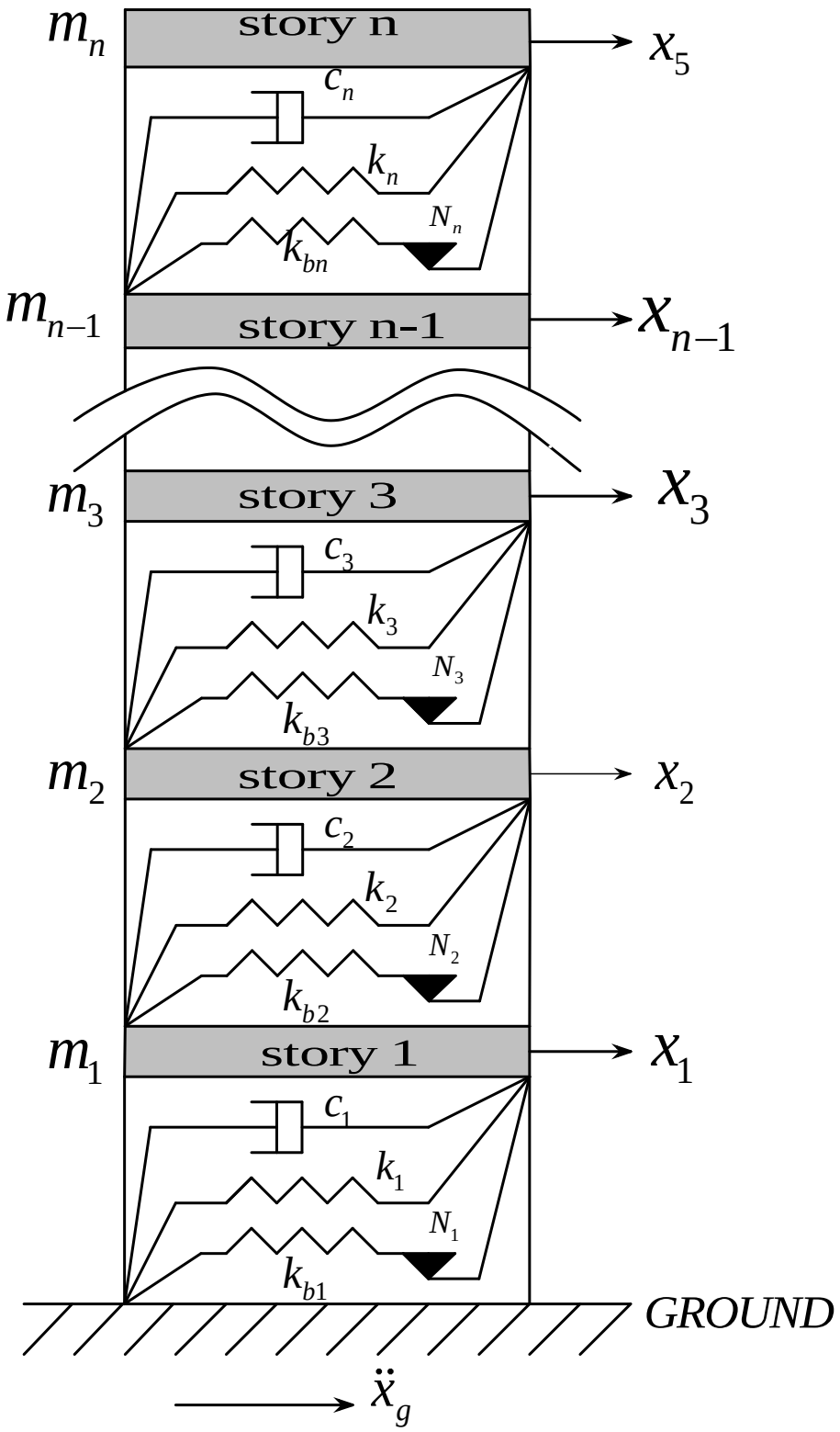

Figure 2.1 MDOF shear building model

In this equation, $[M]$, $[C]$ and $[K]$ represent mass, damping and stiffness matrices of the building and $\{x\}$, $\{\dot{x}\}$, $\{\ddot{x}\}$ are displacement, velocity and acceleration vectors of the stories, respectively, $\{f_{NL}\}$ is the nonlinear forcing vector consisting of the nonlinear forces due to friction dampers, $\{f_{exc}\}$ is the excitation vector, and $\ddot{x}_g$ is earthquake acceleration. The details of these matrices and vectors are given as;

$$[M] = diag(m_1, m_2, m_3 \cdots m_{n-1}, m_n), \tag{2.2}$$

$$[C] = \begin{bmatrix} c_1+c_2 & -c_2 & 0 & \cdots & \cdots & \cdots & 0 \\ -c_2 & c_2+c_3 & -c_3 & \cdots & \cdots & \cdots & \vdots \\ 0 & -c_3 & c_3+c_4 & \cdots & \cdots & \cdots & \vdots \\ \vdots & \cdots & -c_4 & \ddots & \cdots & \cdots & 0 \\ \vdots & \cdots & \cdots & 0 & -c_{n-1} & c_{n-1}+c_n & -c_n \\ 0 & \cdots & \cdots & \cdots & 0 & -c_n & c_n \end{bmatrix}, \tag{2.3}$$

$$[K] = \begin{bmatrix} k_1+k_2 & -k_2 & 0 & \cdots & \cdots & \cdots & 0 \\ -k_2 & k_2+k_3 & -k_3 & \cdots & \cdots & \cdots & \vdots \\ 0 & -k_3 & k_3+k_4 & \cdots & \cdots & \cdots & \vdots \\ \vdots & \cdots & -k_4 & \ddots & \cdots & \cdots & 0 \\ \vdots & \cdots & \cdots & 0 & -k_{n-1} & k_{n-1}+k_n & -k_n \\ 0 & \cdots & \cdots & \cdots & 0 & -k_n & k_n \end{bmatrix}, \tag{2.4}$$

$$\{x\} = \{x_1, x_2, x_3 \cdots x_{n-1}, x_n\}^T. \tag{2.5}$$

Details of nonlinear force vector, $\{f_{NL}\}$, is given in Section 3.2.2.

2.1.2. Dry Friction Model

As already mentioned before, due to its mathematical simplicity and success in predicting actual responses of the dampers, macro-slip friction model which is composed of a spring and a frictional contact with a slip load μN as shown in Figure 2.2, is used in this thesis. In this model, k_f, μ, N and x represent the contact stiffness of the damper, coefficient of friction, normal load acting across the contact surface and relative motion across the damper, respectively.

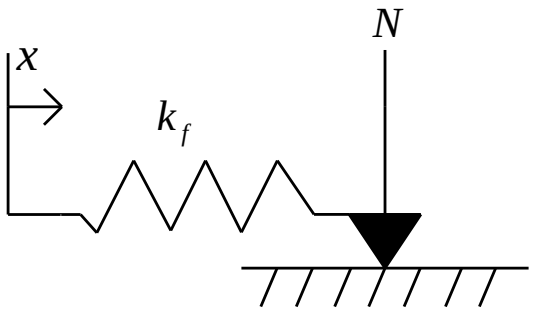

Figure 2.2 Macro-slip friction model

When the force on the spring is less than the slip load (force), μN, the damper is in stick state and the friction force is defined as;

$$F_f = k_f x . \tag{2.6}$$

Damper remains in stick state until the magnitude of the friction force reaches the slip force where further increase of the relative motion results in slip state. During the slip state, friction force equals to the slip force which can be expressed as;

$$F_f = \mu N . \tag{2.7}$$

The damper continues to slip until the relative velocity becomes zero (i.e. $\dot{x} = 0$) and at this point damper sticks again.

In the literature, frictional contact is idealized by perfectly plastic rigid models and modeled as a fictitious spring having infinite stiffness. However, in practice k_f may also be assumed to be a finite value due to the elasticity of the structure connected to the frictional contact.

While modeling the dry friction damper, flexibility of the elements that are used to support and connect the damper to the main structure should also be introduced as shown in Figure 2.3, where k_b represents the stiffness of the bracing. Stiffness of the damper assemblage, k_{bd}, can be given as follows;

$$\frac{1}{k_{bd}} = \frac{1}{\frac{1}{k_b} + \frac{1}{k_f}}. \tag{2.8}$$

Since $k_f \gg k_b$ Equation (2.8) reduces to ;

$$k_{bd} = k_b, \tag{2.9}$$

Therefore, dry friction damper is modeled with a spring of stiffness, k_b and the equations for the damper force are as follows;

$$F_d = \begin{cases} \mu N & \text{Positive Slip} \\ \mu N + k_b\left(x - A\right) & \text{Stick} \\ -\mu N & \text{Negative Slip} \\ -\mu N + k_b\left(x + A\right) & \text{Stick} \end{cases}, \tag{2.10}$$

where A is the amplitude of the relative displacement between the ends of the damper. The resulting hysteresis curve is given in Figure 2.4.

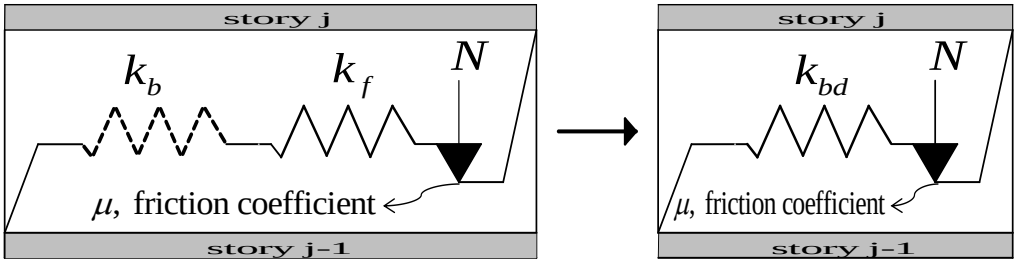

Figure 2.3 Modeling of a dry friction damper in series with a brace

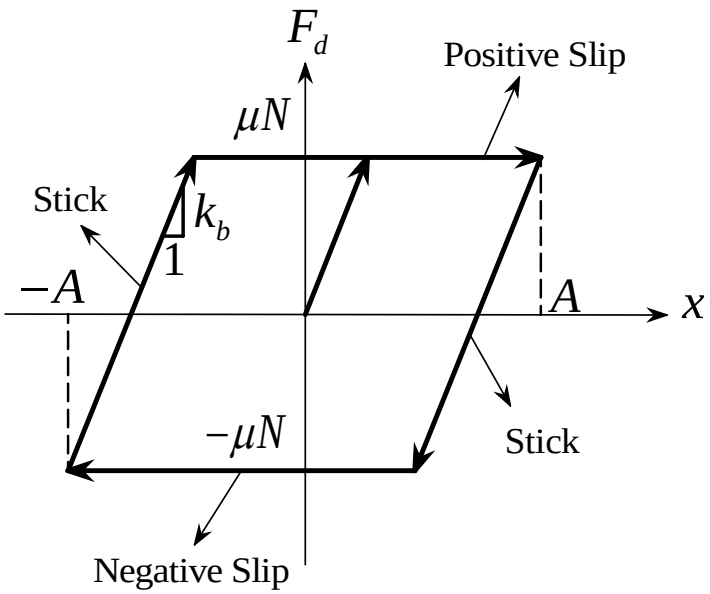

Figure 2.4 Hysteresis curve of dry friction damper

2.1.3. Calculation of Brace Stiffness

Brace stiffness is effective on reducing the response of the building during an earthquake together with the slip load. If it is high, it increases the overall rigidity of the structure; hence, results in decrease in vibration amplitudes of the building; however, this is not due to energy dissipation simply due to the increased structural rigidity. Material type and brace cross section area are some of the

physical factors that affect brace stiffness and most of the time it is not an adjustable parameter. Therefore, while optimizing the damper slip force, the effect of brace stiffness should also be considered.

High brace stiffness is a desirable characteristic to decrease the vibration amplitudes however, due to the physical constraints there is an upper limit. Therefore, it is not practical to consider high brace stiffness values in the analyses. Due to this reason, although effect of brace stiffness on displacement response is investigated in this thesis, brace stiffness is considered to be constant for the optimization of the dampers.

Tabeshpour et al. [22] mentioned that it is difficult to achieve values of k_b much greater than the story stiffness due to physical constraints. However, there exists several studies in the literature where values of k_b are much higher than story stiffness [17, 23, 24].

Hall [25] has indicated that, full moment connections are usually not employed for a braced frame and attachments of the beams and braces to a joint are often considered to be pinned. Using this approach, axial stiffness of a brace can be formulated as follows;

$$k_b = \frac{E_b A_b}{l_b}, \tag{2.11}$$

where E_b, A_b and l_b are elastic modulus, cross-sectional area and length of the brace, respectively.

2.2. Equations of Motion In Terms of Interstory Drift

In the literature, there are many different performance indexes to evaluate the improvement in the seismic performance of a building when dry friction dampers are installed. Some of these performance indexes can be listed as follows;

- Difference between the maximum story displacement before and after damper installation

- Difference between maximum relative displacement between two successive floors which is also called as interstory drift before and after damper installation

- Difference between the maximum story shear force before and after damper installation

- Ratio of dissipated energy to the earthquake input energy

Depending upon the chosen criteria, different solution methods may be used for the same problem. Since maximum displacement is always measured at the uppermost story at around the first natural frequency of the building as shown in Figure 2.5, the maximum story displacement is the easiest and most widely used performance criteria.

However, the reason behind the collapse of a building is mainly due to the high interstory drift between two successive stories. For this reason, during the optimization of the slip load of the dampers, the maximum interstory drift is investigated as the cost function in this thesis.

Opposite to the maximum displacement which is only related with the displacement of the uppermost story, interstory drift is the relative displacement between adjacent floors, therefore the maximum interstory drift does not have to be at the uppermost story as shown in Figure 2.6. Moreover, solution around only the first mode is not adequate since other modes in the frequency range of

earthquakes, may be more critical in terms of interstory drift. Therefore, interstory drift needs more computational effort compared to the determination of the maximum displacement; however, it is a more realistic performance criteria.

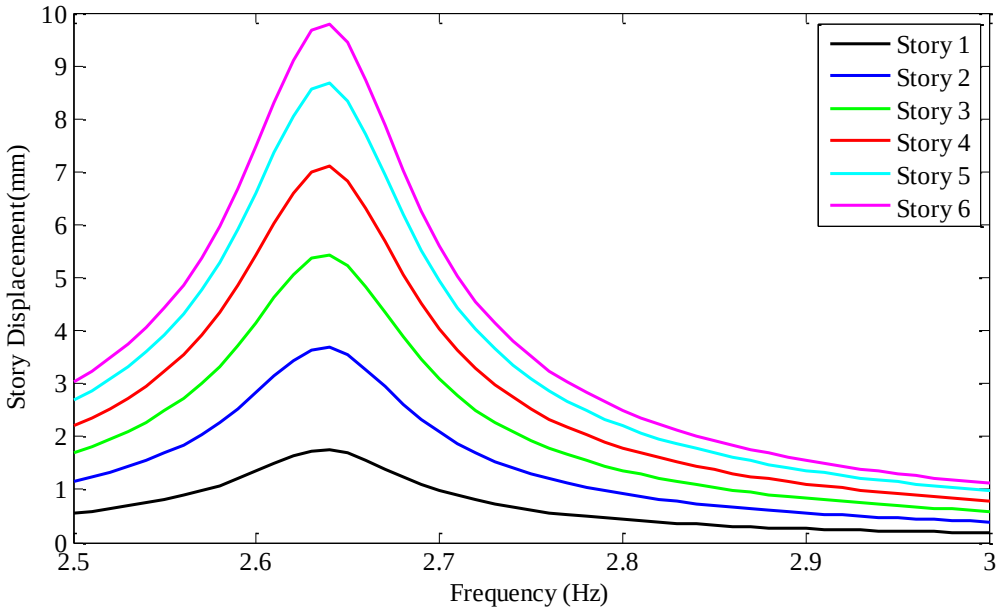

Figure 2.5 Story displacements with respect to the ground for a building without any damper

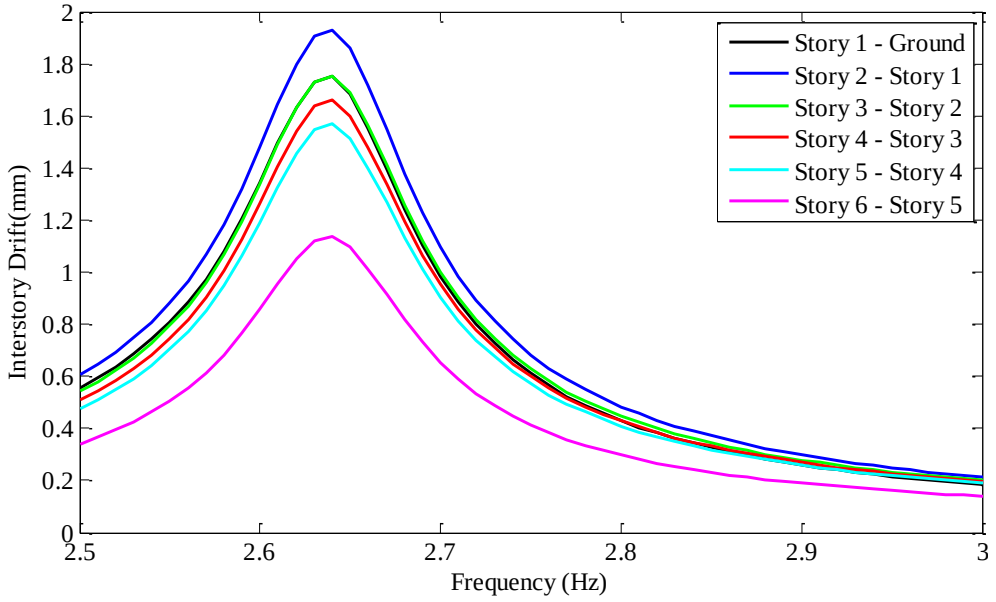

Figure 2.6 Interstory drifts for a building without any damper

In order to obtain the equations of motion in terms of interstory drift, Equation (2.1) should be rewritten by obtaining $\{x\}$, $\{\dot{x}\}$ and $\{\ddot{x}\}$ in terms of $\{y\}$, $\{\dot{y}\}$, $\{\ddot{y}\}$ which are interstory drift, interstory velocity and interstory acceleration vectors, respectively. The relation between interstory drift and displacement parameters are as follows;

$$\{y\} = \begin{bmatrix} x_1 \\ x_2 - x_1 \\ x_2 - x_1 \\ \vdots \\ x_n - x_{n-1} \end{bmatrix}, \tag{2.12}$$

$$\{\dot{y}\} = \begin{bmatrix} \dot{x}_1 \\ \dot{x}_2 - \dot{x}_1 \\ \dot{x}_2 - \dot{x}_1 \\ \vdots \\ \dot{x}_n - \dot{x}_{n-1} \end{bmatrix}, \tag{2.13}$$

$$\{\ddot{y}\} = \begin{bmatrix} \ddot{x}_1 \\ \ddot{x}_2 - \ddot{x}_1 \\ \ddot{x}_2 - \ddot{x}_1 \\ \vdots \\ \ddot{x}_n - \ddot{x}_{n-1} \end{bmatrix}. \tag{2.14}$$

For a three story building Equation (2.1) can be expanded as follows;

$$\begin{aligned} &M_{(1,1)}x_1 + C_{(1,1)}\dot{x}_1 + C_{(1,2)}\dot{x}_2 + C_{(1,3)}\dot{x}_3 + K_{(1,1)}x_1 + K_{(1,2)}x_2 + K_{(1,3)}x_3 + f_{NL_1} = f_{exc_1} \\ &M_{(2,2)}x_2 + C_{(2,1)}\dot{x}_1 + C_{(2,2)}\dot{x}_2 + C_{(2,3)}\dot{x}_3 + K_{(2,1)}x_1 + K_{(2,2)}x_2 + K_{(2,3)}x_3 + f_{NL_2} = f_{exc_2} \\ &M_{(3,3)}x_3 + C_{(3,1)}\dot{x}_1 + C_{(3,2)}\dot{x}_2 + C_{(3,3)}\dot{x}_3 + K_{(3,1)}x_1 + K_{(3,2)}x_2 + K_{(3,3)}x_3 + f_{NL_3} = f_{exc_3}. \end{aligned} \tag{2.15}$$

Equation (2.15) can be re-written in terms of drift parameters by changing variables as follows;

$$
\begin{aligned}
&M_{(1,1)}x_1 + \\
&C_{(1,1)}x_1 + C_{(1,2)}(\dot{x}_2 - \dot{x}_1) + C_{(1,2)}\dot{x}_1 + C_{(1,3)}(\dot{x}_3 - \dot{x}_2) + C_{(1,3)}(\dot{x}_2 - \dot{x}_1) + C_{(1,3)}\dot{x}_1 + \\
&K_{(1,1)}x_1 + K_{(1,2)}(x_2 - x_1) + K_{(1,2)}x_1 + K_{(1,3)}(x_3 - x_2) + K_{(1,3)}(x_2 - x_1) + K_{(1,3)}x_1 + f_{NL_1} = f_{exc_1} \\
&M_{(2,2)}(x_2 - x_1) + M_{(2,2)}x_1 + \\
&C_{(2,1)}\dot{x}_1 + C_{(2,2)}(\dot{x}_2 - \dot{x}_1) + C_{(2,2)}\dot{x}_1 + C_{(2,3)}(\dot{x}_3 - \dot{x}_2) + C_{(2,3)}(\dot{x}_2 - \dot{x}_1) + C_{(2,3)}\dot{x}_1 + \\
&K_{(2,1)}x_1 + K_{(2,2)}(x_2 - x_1) + K_{(2,2)}x_1 + K_{(2,3)}(x_3 - x_2) + K_{(2,3)}(x_2 - x_1) + K_{(2,3)}x_1 + f_{NL_2} = f_{exc_2} \\
&M_{(3,3)}(x_3 - x_2) + M_{(3,3)}(x_2 - x_1) + M_{(3,3)}x_1 + \\
&C_{(3,1)}\dot{x}_1 + C_{(3,2)}(\dot{x}_2 - \dot{x}_1) + C_{(3,2)}\dot{x}_1 + C_{(3,3)}(\dot{x}_3 - \dot{x}_2) + C_{(3,3)}(\dot{x}_2 - \dot{x}_1) + C_{(3,3)}\dot{x}_1 + \\
&K_{(3,1)}x_1 + K_{(3,2)}(x_2 - x_1) + K_{(3,2)}x_1 + K_{(3,3)}(x_3 - x_2) + K_{(3,3)}(x_2 - x_1) + K_{(3,3)}x_1 = f_{exc_3}.
\end{aligned}
\tag{2.16}
$$

If the terms are regrouped and displacement parameters are changed with interstory drift parameters, following equation is obtained;

$$
\begin{aligned}
&M_{(1,1)}y_1 + \\
&\left(C_{(1,1)} + C_{(1,2)} + C_{(1,3)}\right)\dot{y}_1 + \left(C_{(1,2)} + C_{(1,3)}\right)\dot{y}_2 + C_{(1,3)}\dot{y}_3 + \\
&\left(K_{(1,1)} + K_{(1,2)} + K_{(1,3)}\right)y_1 + \left(K_{(1,2)} + K_{(1,3)}\right)y_2 + K_{(1,3)}y_3 + f_{NL_1} = f_{exc_1} \\
&M_{(2,2)}y_1 + M_{(2,2)}y_2 + \\
&\left(C_{(2,1)} + C_{(2,2)} + C_{(2,3)}\right)\dot{y}_1 + \left(C_{(2,2)} + C_{(2,3)}\right)\dot{y}_2 + C_{(2,3)}\dot{y}_3 + \\
&\left(K_{(2,1)} + K_{(2,2)} + K_{(2,3)}\right)y_1 + \left(K_{(2,2)} + K_{(2,3)}\right)y_2 + K_{(2,3)}y_3 + f_{NL_2} = f_{exc_2} \\
&M_{(3,3)}y_1 + M_{(3,3)}y_2 + M_{(3,3)}y_3 \\
&\left(C_{(3,1)} + C_{(3,2)} + C_{(3,3)}\right)\dot{y}_1 + \left(C_{(3,2)} + C_{(3,3)}\right)\dot{y}_2 + C_{(3,3)}\dot{y}_3 + \\
&\left(K_{(3,1)} + K_{(3,2)} + K_{(3,3)}\right)y_1 + \left(K_{(3,2)} + K_{(3,3)}\right)y_2 + K_{(3,3)}y_3 + f_{NL_3} = f_{exc_3}
\end{aligned}
\tag{2.17}
$$

Using Equation (2.17), mass, damping and stiffness matrices of the $n-story$ building for interstory drift parameters can be written as follows;

$$\left[M^{drift}\right]=\begin{bmatrix} m_1 & 0 & 0 & \dots & 0 \\ m_2 & m_2 & 0 & \dots & 0 \\ \vdots & \vdots & \vdots & \vdots & \vdots \\ m_n & m_n & m_n & m_n & m_n \end{bmatrix} \tag{2.18}$$

$$\left[C^{drift}\right]=\begin{bmatrix} C_{1,1}+C_{1,2}+\cdots+C_{1,n} & C_{1,2}+\cdots+C_{1,n} & \dots & C_{1,n} \\ C_{2,1}+C_{2,2}+\cdots+C_{2,n} & C_{2,2}+\cdots+C_{2,n} & \dots & C_{2,n} \\ \vdots & \vdots & \vdots & \vdots \\ C_{n,1}+C_{n,2}+\cdots+C_{n,n} & C_{n,2}+\cdots+C_{n,n} & \dots & C_{n,n} \end{bmatrix} \tag{2.19}$$

$$\left[K^{drift}\right]=\begin{bmatrix} K_{1,1}+K_{1,2}+\cdots+K_{1,n} & K_{1,2}+\cdots+K_{1,n} & \dots & K_{1,n} \\ K_{2,1}+K_{2,2}+\cdots+K_{2,n} & K_{2,2}+\cdots+K_{2,n} & \dots & K_{2,n} \\ \vdots & \vdots & \vdots & \vdots \\ K_{n,1}+K_{n,2}+\cdots+K_{n,n} & K_{n,2}+\cdots+K_{n,n} & \dots & K_{n,n} \end{bmatrix} \tag{2.20}$$

After obtaining these matrices, equation of motion in terms of interstory drift parameters is given as follows;

$$\left[M^{drift}\right]\{\ddot{y}\}+\left[C^{drift}\right]\{\dot{y}\}+\left[K^{drift}\right]\{y\}+\{f_{NL}\}=\{f_{exc}\}. \tag{2.21}$$

It should be noted, the nonlinear force vector is a function of the relative displacements between the stories where friction dampers are placed, and in order to calculate them interstory drift can be directly used.

CHAPTER 3

FREQUENCY DOMAIN SOLUTION METHOD

3.1. Comparison of Frequency and Time Domain Solutions

Especially when the number of degrees of freedom of a system increases and a wide frequency interval is the scope of interest, then frequency domain solutions are very advantageous over time domain solution methods since they require less computation time and effort.

Moreover, it is very difficult to determine the most unfavorable ground motion for the building in time domain as mentioned before. When these advantages are considered, frequency domain solution seems to be more preferable compared to time domain solution.

However if it is required to get the transient solution, i.e. steady + unsteady response under a seismic ground motion, time domain solution should be utilized. It should be also noted that frequency domain solution can only deal with periodic excitations whereas any type of excitation can be considered by time domain methods .

3.2. Frequency Domain Solution of Nonlinear Vibratory Systems

For frequency domain solution, $\{f_{exc}\}$ is assumed to be a sinusoidal function as follows;

$$\{f_{exc}\} = \mathrm{Im}\left(\{F\}e^{i\varphi}\right), \tag{3.1}$$

where $\varphi = \omega t$, $\{F\}$ and ω are the complex vector of amplitudes of external forces and excitation frequency, respectively. Assuming that the structure also vibrates harmonically, the response can be expressed as follows;

$$\{x\} = \mathrm{Im}\left(\{X\}e^{i\varphi}\right), \tag{3.2}$$

where $\{X\}$ is the complex vector of displacement amplitudes.

Nonlinear forces are also periodic due to periodic relative displacement and can be expressed as;

$$\{f_{NL}\} = \mathrm{Im}\left(\{F_{NL}\}e^{i\varphi}\right), \tag{3.3}$$

where $\{F_{NL}\}$ is the complex vector of the amplitudes of nonlinear force vector, $\{f_{NL}\}$.

Then, substituting Equations (3.1), (3.2) and (3.3) into the Equation (2.1), the following equation is obtained:

$$\left[[K]-\omega^2[M]+i\omega[C]\right]\{X\}+\{F_{NL}\}=\{F\}. \tag{3.4}$$

If nonlinear forces do not exist in the system, then Equation (3.4) reduces to;

$$\left[[K]-\omega^2[M]+i\omega[C]\right]\{X\}=\{F\}. \tag{3.5}$$

Then, $\{X\}$ can be calculated as follows;

$$\{X\}=\left[[K]-\omega^2[M]+i\omega[C]\right]^{-1}\{F\}. \tag{3.6}$$

3.2.1. Describing Function Method

Using "Describing Function Method", complex vector of the amplitudes of nonlinear force vector, $\{F_{NL}\}$, can be written in terms of $\{X\}$ as follows;

$$\{F_{NL}\}=[\Delta(X)]\{X\}, \tag{3.7}$$

where $[\Delta(X)]$ is called as generalized quasi-linear matrix.

Tanrikulu et al. [26], has expressed nonlinear force, $\{f_{NL}\}$, in their study as follows;

The k[th] element of $\{f_{NL}\}$ can be expressed as;

$$f_{NL_k}=\sum_{j=1}^{n} f_{NL_{kj}}\ , \tag{3.8}$$

where n is the total degrees of freedom and $f_{NL_{kj}}$ represents the nonlinear restoring force element acting between k and j for $k \neq j$. If $k = j$, it represents the force element acting between coordinate k and the ground. $f_{NL_{kj}}$ is a function of relative displacement and its derivatives;

$$
\begin{aligned}
& f_{NL_{kj}}(z_{kj}, \dot{z}_{kj}, \ddot{z}_{kj} \ldots) \\
& z_{kj} = x_k - x_j \text{ for } k \neq j \\
& z_{kj} = x_k \text{ for } k = j.
\end{aligned} \tag{3.9}
$$

As given in reference [13], elements of the generalized quasi-linear matrix, $[\Delta(X)]$, can be calculated as follows;

$$
\Delta(X)_{kk} = v_{kk} + \sum_{\substack{j=1 \\ j \neq k}}^{n} v_{kj} \quad \text{and} \quad \Delta(X)_{kj} = -v_{kj} \tag{3.10}
$$

where v_{kj} is the single harmonic input describing function and can be described as the equivalent linear complex stiffness for the nonlinear force $f_{NL_{kj}}$, in this thesis it is the friction force, acting between the k^{th} and j^{th} coordinates. v_{kj} and v_{kk} can be defined as follows;

$$
\begin{aligned}
v_{kj} &= \frac{i}{\pi \left\| x_k - x_j \right\|} \int_0^{2\pi} f_{NL_{kj}} e^{-i\varphi} d\varphi \quad \text{for k} \neq \text{j} \\
v_{kk} &= \frac{i}{\pi \left\| x_k \right\|} \int_0^{2\pi} f_{NL_{kj}} e^{-i\varphi} d\varphi
\end{aligned} \quad . \tag{3.11}
$$

Using Equation (3.7), Equation (3.4) can be written as follows;

$$
\left[[K] - \omega^2 [M] + i\omega [C] + [\Delta(X)] \right] \{X\} = \{F\}. \tag{3.12}
$$

An iterative nonlinear equation solver is required to calculate $\{X\}$ from Equation (3.12).

In this study, only the fundamental harmonic terms are considered as suggested in reference [27], since in the working range of dry friction dampers higher-harmonic terms are smaller compared to the fundamental harmonic term. However, as

indicated by Ciğeroğlu and Özguven [13], it is also possible to include higher harmonics into the calculations by following a very similar approach if required.

More details on "Describing Function Method" can be found in references [13] and [26].

3.2.2. Describing Functions for Dry Friction Damper

In Section 2.1.2. , modeling of dry friction dampers has been investigated and corresponding hysteresis curve is shown in Figure 2.4. In this section, generalized quasi-linear matrix of non-linear dry friction element will be obtained using the describing functions method.

In Equation (2.10), friction force across the damper is expressed as a piecewise function. Therefore, in order to determine which equation is valid at which condition and calculate the integral given in Equation (3.11), the points at which the damper changes state (stick or slip) should be identified. To determine these points, assume a sinusoidal relative displacement at the damper end as follows;

$$x = A\sin(\beta), \tag{3.13}$$

where A is the amplitude of the displacement and β is equal to;

$$\beta = \omega t + \gamma, \tag{3.14}$$

where γ is the phase angle of the damper with respect to the excitation frequency ω.

For one dimensional motion with constant normal load, the damper goes into the stick state when the motion reverses its direction . This condition can be formulated as follows;

$$\dot{x} = \frac{d}{dt}\left(A\sin\left(\beta\right)\right) = 0, \tag{3.15}$$

which is satisfied at two points;

$$\beta_1 = \pi/2 \quad \text{or} \quad \beta_3 = 3\pi/2 \tag{3.16}$$

The damper remains in stick condition until the force reaches to the slip force. Therefore, the point at which the damper goes into slip state from stick phase can be calculated by equating the force on the spring to the slip load which results in the following condition ;

$$\pm\mu N + k_b\left(A\sin\left(\beta\right) - A\sin\left(\beta_1\right)\right) = \mp\mu N, \tag{3.17}$$

where β is the point at which the damper goes from stick to slip state and positive and negative signs at the right hand side correspond to the positive slip and negative slip, respectively. By solving β from Equation (3.16), the following result for positive and negative slip is obtained;

$$\beta = \sin^{-1}\left(1 \pm \frac{2\mu N}{k_b A}\right). \tag{3.18}$$

From Equation (3.17) the angle from stick to positive slip state can be obtained as follows;

$$\beta(t)_2 = \sin^{-1}\left(1 - \frac{2\mu N}{k_b A}\right). \tag{3.19}$$

Similarly, the angle from stick to negative slip is given as follows;

$$\beta(t)_4 = \beta(t)_2 + \pi. \tag{3.20}$$

These angles are shown on the hysteresis diagram which is given in Figure 3.1.

After finding the points at which the damper changes state, damper force can be written as follows;

$$F_d = \begin{cases} \mu N & \beta(t)_2 + \pi \le \beta(t) < \dfrac{\pi}{2} \\ \mu N + k_b\left(A\sin\left(\beta(t)\right) - A\right) & \dfrac{\pi}{2} \le \beta(t) < \beta(t)_2 \\ -\mu N & \beta(t)_2 \le \beta(t) < \dfrac{3\pi}{2} \\ -\mu N + k_b\left(A\sin\left(\beta(t)\right) + A\right) & \dfrac{3\pi}{2} \le \beta(t) < \beta(t)_2 + \pi \end{cases}, \qquad (3.21)$$

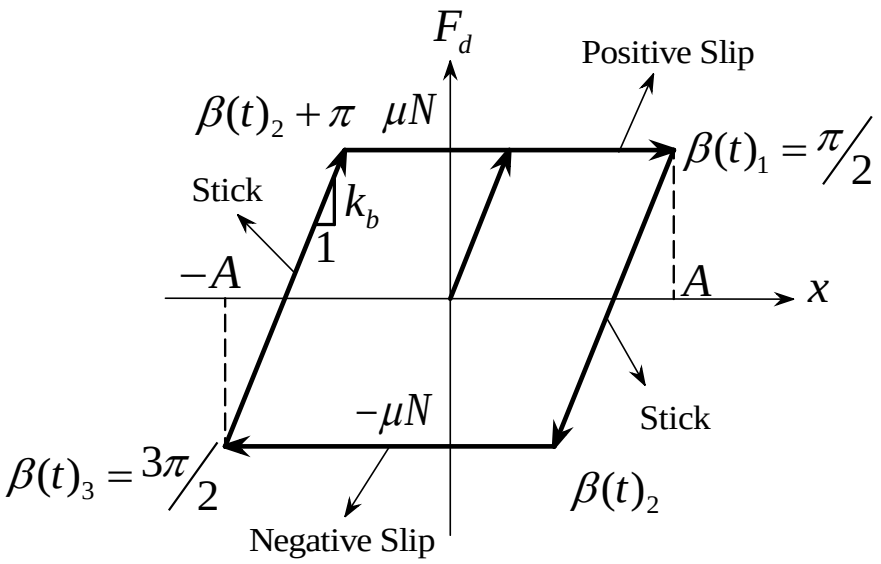

Figure 3.1 Hysteresis diagram of dry friction damper and transition points

From reference [13], imaginary and real parts of the describing function for dry friction damper can be written as;

$$\left.\begin{aligned} \upsilon_{im} &= -\frac{4\mu N(\mu N - Ak_b)}{\pi k_b A^2} \\ \upsilon_{re} &= \frac{1}{\pi}\left(\frac{2\mu N}{A} - k_b\right)\sqrt{1-\left(\frac{k_b A - 2\mu N}{k_b A}\right)^2} + k_b\frac{\varphi}{\pi} - \frac{k_b}{2} \end{aligned}\right\} \text{for } k_b A > \mu N$$

$$\left.\begin{aligned} \upsilon_{im} &= 0 \\ \upsilon_{re} &= k_b \end{aligned}\right\} \text{for } k_b A \le \mu N \qquad , (3.22)$$

where A is the steady-state vibration amplitude and φ is equal to;

$$\varphi = \pi - \sin^{-1}\left(\frac{-\delta}{A}\right), \tag{3.23}$$

and δ denotes the intersection of the hysteresis curve with the x-axis and can be defined as follows;

$$\delta = A - \frac{\mu N}{k_b}. \tag{3.24}$$

3.2.3. Solution of Resulting Nonlinear Equations

Since $[\Delta(X)]$ is displacement dependent, an iterative method is required to solve Equation (3.12). In this thesis Newton's method, details of which are given below, is utilized for this purpose.

Equation (3.12) can be expressed as a residual vector as follows;

$$\{R(\{X\},\omega)\} = \left[[K] - \omega^2[M] + i\omega[C] + [\Delta(X)]\right]\{X\} - \{F\} = \{0\}. \tag{3.25}$$

Using Newton's method the following iterative formula can be written for the solution of Equation (3.25);

$$\{X\}_{k+1} = \{X\}_k - \left[\frac{\partial\{R(\{X\},\omega)\}}{\partial\{X\}}\right]^{-1}\Bigg|_{\{X\}_k,\omega} \{R(\{X\}_k,\omega)\}, \qquad (3.26)$$

where k is the iteration number and $\left[\partial\{R(\{X\},\omega)\}/\partial\{X\}\right]$ is the Jacobian matrix and should be calculated either analytically or numerically. It can be expressed as follows;

$$\left[\frac{\partial\{R(\{X\},\omega)\}}{\partial\{X\}}\right] = \left[[K] - \omega^2[M] + i\omega[C]\right] + \frac{\partial}{\partial\{X\}}\left[\left[\Delta(\{X\})\right]\{X\}\right]. \qquad (3.27)$$

Iterative formula given in Equation (3.26) is applied successively until a pre-defined error tolerance, either on the relative difference between $\{X\}_{k+1}$ and $\{X\}_k$ or on the value of the residual vector $\{R(\{X_{k+1}\},\omega)\}$ or on both, is satisfied.

Speed and convergence of the Newton's Method depend on the closeness of the initial guess to the real solution. Therefore, a good initial guess is very important and to increase the quality of the initial guess, a first order predictor can be used [28].

3.2.4. Path Following and Homotopy Continuation Method

In the nonlinear vibration analysis, usually nonlinear frequency response function is investigated. To obtain the frequency displacement curve a path should be followed and there are several methods for this purpose. In this thesis, homotopy continuation method is utilized.

Equation (3.25) can be separated as follows;

$$\{R(\{X\},\omega)\} = L(\{X\},\omega) + h * N(\{X\},\omega) = \{0\}, \qquad (3.28)$$

where $L(\{X\},\omega)$ is the linear part, $N(\{X\},\omega)$ is the nonlinear part and h is a multiplying factor of the nonlinear part. If h is assumed to be zero, Equation (3.28) can be easily solved since the system becomes linear. Increasing h from 0 to 1 with certain Δh increments, the nonlinear problem defined in Equation (3.28) can be solved considering the initial guess for each step as the solution obtained in the previous increment;

$$
\begin{array}{llll}
h = h_{i-1} \Delta h_i \quad i = 2,...,K & & & \\
i = 1 \rightarrow & \text{initial guess is } \{X\}_{linear} & \rightarrow & \text{solution is } \{X\}_1 \\
i = 2 \rightarrow & \text{initial guess is } \{X\}_1 & \rightarrow & \text{solution is } \{X\}_2 \\
i = 3 \rightarrow & \text{initial guess is } \{X\}_2 & \rightarrow & \text{solution is } \{X\}_3 \\
\vdots & \vdots & \vdots & \vdots \\
i = K \rightarrow & \text{initial guess is } \{X\}_{K-1} & \rightarrow & \text{solution is } \{X\}_K
\end{array}
\quad , \quad (3.29)
$$

where $\{X\}_K$ is the solution of Equation (3.25). In order to obtain good initial guesses for the next step, determination of Δh is important. In case the nonlinear function changes too much for a certain increment, value of Δh can be altered adaptively to ensure the convergence of the solution.

In this thesis Δh is adjusted according to the following formula [29];

$$\Delta h_k = \Delta h_{k-1} \sqrt{\frac{n_{norm}^{iter}}{n_{k-1}^{iter}}} \, , \qquad (3.30)$$

where Δh_k and Δh_{k-1} are the increment at the k^{th} and $(k-1)^{th}$ solution points respectively, n_{k-1}^{iter} is the number of iterations at the $(k-1)^{th}$ solution point and n_{norm}^{iter} is the nominal value of iteration number which is predefined.

3.2.4.1. Predictor - Corrector for Path Following Methods

As mentioned in Section 3.2. , initial guess is very important for Newton's method in order to prevent divergence and/or enhance faster converge. For this purpose, a first order predictor is used in this thesis.

A tangent vector to the solution curve can be obtained as by differentiating Equation (3.25) with respect to the ω;

$$\frac{dR\left(\{X\},\omega\right)}{d\omega}=\frac{\partial R\left(\{X\},\omega\right)}{\partial x}\frac{\partial\{X\}}{\partial\omega}+\frac{\partial R\left(\{X\},\omega\right)}{\partial\omega}=\{0\}. \tag{3.31}$$

Then the tangent vector can be calculated as follows;

$$\frac{\partial\{X\}}{\partial\omega}=-\left(\frac{\partial R\left(\{X\},\omega\right)}{\partial x}\right)^{-1}\frac{\partial R\left(\{X\},\omega\right)}{\partial\omega}. \tag{3.32}$$

If the solution is expanded at the at the next frequency step using first order Taylor series, initial guess for the next iteration can be calculated as follows;

$$\begin{aligned}\{X\}\big|_{\omega_{k+1}}&=\{X_k\}\big|_{\omega_k}+\frac{\partial\{X_k\}}{\partial\omega}\delta\omega\\ \{X\}\big|_{\omega_{k+1}}&=\{X_k\}\big|_{\omega_k}-\left(\left(\frac{\partial R\left(\{X_k\},\omega_k\right)}{\partial x}\right)^{-1}\frac{\partial R\left(\{X_k\},\omega_k\right)}{\partial\omega}\right)\delta\omega\end{aligned}, \tag{3.33}$$

where $\omega_{k+1}=\omega_k+\delta\omega$. Homotopy continuation method with tangent predictor is illustrated in Figure 3.2. where superscript (0) means the initial guess for each step.

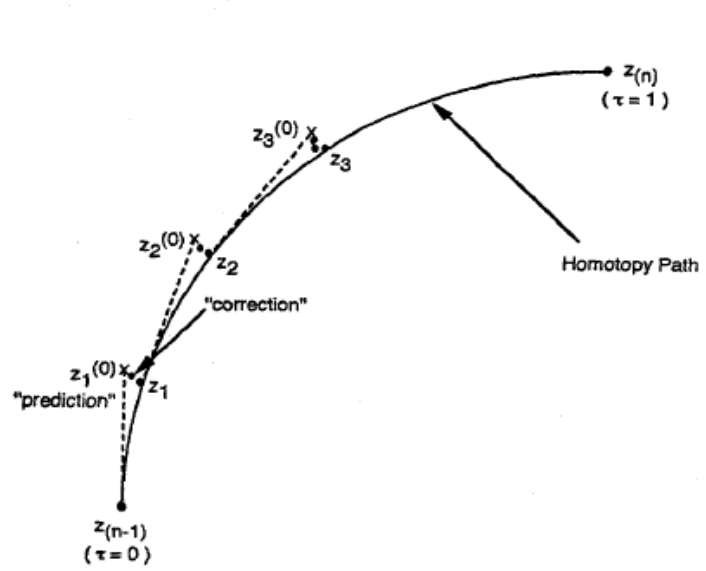

Figure 3.2 Homotopy continuation method with initial guess predictor [30]

3.2.5. Direct Determination of Resonance Frequencies and Resonance Amplitudes for a Nonlinear System

Frequency response curve or the so-called "tracking curve" is important to observe the response of a system at the interested frequency range and using this curve harmonic response can be determined at any frequency. However, if only determination of the maximum vibration amplitude at the interested frequency range is important and it is the only design criterion; it is sufficient to determine the maximum response level and the corresponding resonance frequency rather than the whole frequency response curve.

As Petrov [31] mentioned in his study, resonance forced response levels are conventionally determined by calculation of the response amplitudes over a frequency range where the resonance regimes are expected and finding the maximum amplitude point at this frequency range. In his study, he developed a method for the direct parametric analysis of resonance regimes for the nonlinear systems.

In this thesis, based on Petrov's study a new method is developed for optimization of the damper parameters that has never been used in the design of dry friction dampers used in seismic protection of buildings. Using this method, response levels are only calculated at resonance frequencies rather than calculating at each frequency in the interested frequency range. This method has two main advantages;

- For each damper parameter numerous forced response calculations are required and sometimes it may take quite a long time to calculate the response levels at each frequency. This especially brings difficulty in optimization of large systems. However, in this method since only the vibration amplitude at the resonance frequency is determined, the nonlinear equation of motion is only solved at a single frequency value.
- In conventional methods, exact determination of the resonance frequency is highly dependent on the frequency increment used. Although smaller increments give a more accurate result, the required calculation time increases and using a higher frequency increment may result in missing the actual resonance frequency and loss of precision. However with the method explained here, resonance frequency and the corresponding maximum response can be calculated accurately.

According to the desired performance index type, residual vector, $\left\{R\left(\{X\},\omega\right)\right\}$, can be obtained either for displacements with respect to the ground or for interstory drifts and this method can be applied for both types of performance indices.

3.2.5.1. Resonance Frequency Determination

Using Equation (3.25), harmonic response of a nonlinear system can be calculated at a defined frequency. In order to determine a resonance frequency, ω_{res} , it should be also treated as an unknown value

Since frequency became a new unknown value, a new equation is required to find the resonance frequency and the maximum vibration amplitude at this frequency; however, it is not possible to obtain a single resonance frequency for all degrees of freedom (DOFs). Therefore, the DOF at which the maximum response level is required should be identified first. The equation for the determination of the maximum response of the q^{th} DOF can be written as follows

$$r\left(\{X\},\omega\right)=\frac{1}{2}\frac{\partial}{\partial\omega}\left(\left(X_{re_q}\right)^2+\left(X_{im_q}\right)^2\right)=\{X\}^T I_{jk}\frac{\partial\{X\}}{\partial\omega}=0, \qquad (3.34)$$

where q is the number of the selected DOF and I_{jk} is a diagonal matrix which has the only two unity values at the diagonals which correspond to real and imaginary parts of coefficients of the q^{th} DOF.

3.2.5.2. Solving Equations of Motion at Resonance Frequency

In order to calculate ω_{res} and $\{X_{res}\}$, Equation (3.25) and Equation (3.34) should be solved simultaneously. For this purpose, the combined residual vector for the resonance regime can be written as follows;

$$\left\{R^{res}\left(\{Q\}\right)\right\}=\begin{Bmatrix}\left\{R\left(\{X\},\omega\right)\right\}\\ r\left(\{X\},\omega\right)\end{Bmatrix}=0, \qquad (3.35)$$

where the vector of unknowns for the new set of equations defined by Equation (3.35) can be given as follows;

$$\{Q\} = \begin{Bmatrix} \{X\} \\ \omega \end{Bmatrix}. \tag{3.36}$$

Using Newton's method, the following iterative formula can be written for the solution of Equation (3.35);

$$\{Q\}_{k+1} = \{Q\}_k - \left[\frac{\partial \left\{ R^{res}\left(\{Q\}\right) \right\}}{\partial \{Q\}} \right]^{-1} \Bigg|_{\{Q\}=\{Q\}_k} \left\{ R^{res}\left(\{Q\}_k\right) \right\}. \tag{3.37}$$

The new Jacobian matrix, $\dfrac{\partial \left\{ R^{res}\left(\{Q\}\right) \right\}}{\partial \{Q\}}$, can be defined as follows;

$$\frac{\partial \left\{ R^{res}\left(\{Q\}\right) \right\}}{\partial \{Q\}} = \begin{bmatrix} \left[\dfrac{\partial \left\{ R\left(\{X\},\omega\right) \right\}}{\partial \{X\}} \right] & \left\{ \dfrac{\partial \left\{ R\left(\{X\},\omega\right) \right\}}{\partial \omega} \right\} \\ \dfrac{\partial r\left(\{X\},\omega\right)}{\partial \{X\}} & \dfrac{\partial r\left(\{X\},\omega\right)}{\partial \omega} \end{bmatrix}. \tag{3.38}$$

To calculate $\dfrac{\partial r\left(\{X\},\omega\right)}{\partial \{X\}}$ and $\dfrac{\partial r\left(\{X\},\omega\right)}{\partial \omega}$, Equation (3.34) can be differentiated with respect to $\{X\}$ and ω;

$$\begin{aligned} \frac{\partial r\left(\{X\},\omega\right)}{\partial \{X\}} &= I_{jk} \frac{\partial \{X\}}{\partial \omega} + \{X\}^T I_{jk} \frac{\partial}{\partial \{X\}} \left(\frac{\partial \{X\}}{\partial \omega} \right) \\ \frac{\partial r\left(\{X\},\omega\right)}{\partial \omega} &= \{X\}^T I_{jk} \frac{\partial}{\partial \omega} \left(\frac{\partial \{X\}}{\partial \omega} \right) \end{aligned} \tag{3.39}$$

,

and $\frac{\partial\{X\}}{\partial\omega}$ can be calculated by taking full derivative of Equation (3.25) with respect to ω as follows;

$$\left[\frac{\partial\left\{R\left(\{X\},\omega\right)\right\}}{\partial\{X\}}\right]\frac{\partial\{X\}}{\partial\omega}+\frac{\partial\left\{R\left(\{X\},\omega\right)\right\}}{\partial\omega}=0$$
$$\frac{\partial\{X\}}{\partial\omega}=-\left[\frac{\partial\left\{R\left(\{X\},\omega\right)\right\}}{\partial\{X\}}\right]^{-1}\frac{\partial\left\{R\left(\{X\},\omega\right)\right\}}{\partial\omega} \quad (3.40)$$

3.2.5.3. Initial Guess Determination

For the method proposed in Section 3.2.5. , it is difficult to find a good initial guess since there may be a big difference between resonance displacement amplitudes for a linear and a nonlinear system due to the damper parameters. In this section a method will be discussed to overcome this difficulty.

For a SDOF system, phase shift can be calculated as follows;

$$\phi=a\tan\left(\frac{2\zeta r}{1-r^2}\right),\quad r=\frac{\omega}{\omega_n} \quad (3.41)$$

where ζ is the damping ratio and r is the ratio of harmonic force frequency over the undamped natural frequency.

For the low damping ratio, damped natural frequency of the system has a similar value to the undamped natural frequency of the system. For such cases, if a frequency is selected around the undamped resonance region, r approaches to 1 and ϕ approaches to $\pm\pi/2$. Since ϕ is around $\pm\pi/2$, the real part of the complex displacement, X_{re}, approaches to zero around the resonance. Equation (3.28) can

now be solved for ω and imaginary part of displacement, X_{im}, since X_{re} is known to be 0.

For a SDOF system, Equation (3.25) can be re-written as follows;

$$R(X,\omega)=\left(k-\omega^2\cdot m+i\omega\cdot c+\Delta(X)\right)X-F=0; \qquad (3.42)$$

however, since $\Delta(X)$, X and F are complex terms, real and imaginary parts should be solved simultaneously as follows;

$$\begin{bmatrix} k-\omega^2\cdot m+\Delta(X)_{re} & -\omega\cdot c-\Delta(X)_{im} \\ \omega c+\Delta(X)_{im} & k-\omega^2\cdot m+\Delta(X)_{re} \end{bmatrix}\begin{Bmatrix} X_{re} \\ X_{im} \end{Bmatrix}-\begin{Bmatrix} F_{re} \\ F_{im} \end{Bmatrix}=\{0\}. \qquad (3.43)$$

As explained before, by assuming X_{re} to be 0, Equation (3.43) can be solved for X_{re} and ω. The response and frequency determined from this method can be used as an initial guess to the Equation (3.35). The method can also be applied to MDOF systems in a similar manner.

However in some cases natural frequency of the nonlinear system is not close to the undamped natural frequency of the system then r does not approach to 1 although ω is selected around the undamped resonance region. Hence, the solution cannot be found with the above proposed method. At this time, response of the linear system at the natural frequency should be used as the initial guess for the solution of Equation (3.35) and small increments should be used at the homotopy continuation method.

Both the undamped case and the full stuck case are linear systems and responses can be calculated by simple matrix inversion or through modal analysis. For the full stuck case, the friction dampers act as paralel springs connected between the stories since there is no slip; therefore, $[K]$ should be updated in order to include the brace stiffnesses.

From the solution of the full stuck case, required slip force in order to satisfy no slip condition for the dampers, can be calculated by multiplying the brace stiffness with the maximum damper displacement. Then, it should be determined whether the no damper response or the full stuck response should be used as an initial guess according to the closeness of the given slip forces to the full stuck case slip forces. By this way, further decrease in computation time is obtained and the risk of divergence is eliminated.

If the full stuck response is used as an initial guess, in Equation (3.28) the homotopy parameter, h, should be decreased from h_{stuck} to 1 with certain Δh increments where h_{stuck} is defined as follows;

$$h_{stuck} = \frac{\max\left(\{PS_{stuck}\}\right)}{\min\left(\{PS\}\right)}. \tag{3.44}$$

3.2.6. Comparison of Calculation Times for the Determination of Maximum Interstory Drift

In this section, calculation times will be compared to determine the maximum interstory drifts using tracking curve method and homotopy method with direct determination of resonance frequencies. For this purpose, a 6-story building with 6 identical dampers is investigated and the maximum nonlinear vibratory response is calculated for different slip loads and bracing stiffnesses by using two different methods.

In the first method, frequency response is calculated at the interested frequency range as usually done in the literature and the maximum response is found out by looking at these results. In the second method the direct determination of resonance frequencies with homotopy continuation method, presented in Section 3.2.5. , is utilized to determine the maximum response.

Each case is solved ten times using the both methods to compare the required times for determining the maximum response. The computational advantage of direct determination of the maximum vibration amplitude can be seen from Table 3.1.

Calculation time is especially important for optimization studies since the cost function is calculated numerous times. Moreover, more accurate results can be obtained with direct determination of the resonance point since the accuracy of the classical method depends on the frequency increment. In this analysis, 0.01 Hz is used as frequency increment and the calculations are done on a laptop computer with Intel® i7 - 1.73 GHz CPU and 6 GB RAM.

Table 3.1 Comparison of the direct resonance frequency calculation method and the curve tracking method

		HOMOTOPY METHOD		**DETERMINATION FROM TRACKING CURVE**			
Normalized Bracing Stiffness	Normalized Slip Load	Maximum Interstory Drift(mm)	Time (s)	Maximum Interstory Drift(mm)	Time (s)	**Interstory Drift Accuracy (%)**	**Time Ratio**
0,1	0,05	20,84	0,6	20,55	3,9	**1,39**	**6,50**
0,1	1	8,82	0,9	8,80	2,3	**0,29**	**2,56**
0,2	0,05	20,80	0,6	20,48	5,0	**1,56**	**8,33**
0,2	1	4,73	0,6	4,72	3,1	**0,13**	**5,17**
0,5	0,05	20,78	0,6	20,42	6,3	**1,73**	**10,55**
0,5	1	2,80	0,5	2,80	2,6	**0,00**	**5,20**
2	0,05	20,78	1,2	20,39	8,8	**1,88**	**7,33**
2	1	0,80	1	0,80	4,1	**0,00**	**4,10**
5	0,05	20,77	1,1	20,37	11,4	**1,94**	**10,36**
5	1	0,32	0,9	0,32	11,0	**0,00**	**12,23**

3.3. Time Domain Solution of Nonlinear Vibratory Systems and Verification of the Frequency Domain Method

In order to verify the results of frequency domain solution, time domain analysis has also been performed on a single story building. Equation of motion is solved using "ode45" function of MATLAB. Time domain analyses have been conducted at certain frequencies to obtain the frequency response curve.

At the beginning of each time step of time domain solution, dry friction damper is assumed to be at stick state and a solution is found by solving Equation (2.1). After finding the solution, this assumption is checked and if it is correct, the next time-step is solved but if it is incorrect, same time step is solved by considering the damper at slip state and damper force is calculated according to this assumption. By studying the value of the relative velocity between the ends of the spring, it can be determined whether the damper is at positive slip or negative slip state.

3.3.1. Verification of the Frequency Domain Method

In this section, the verification of the suggested frequency domain solution method is demonstrated by comparing the results with time marching methods. For this reason, a single story building, shown in Figure 3.3, equipped with a dry friction damper connected between the ground and the floor is investigated under a harmonic ground acceleration. In order to have a scale for the parameters used in this thesis, the stiffness and the slip load of the damper is normalized as follows;

$$SR = \frac{k_{b1}}{k_1}, \quad PS = \frac{F_s}{m_1 g} 100, \tag{3.45}$$

where SR and PS demonstrates the stiffness ratio and the percentage slip load, respectively and g is gravitational acceleration. The response of the SDOF system is studied by using sinusoidal ground acceleration, $\ddot{x}_g$, with an amplitude of 0.2 m/s^2 where SR is kept as constant at 0.2 and PS is varied between 0.7 and 6.

The model parameters of the SDOF system are given as follows;

$$m = 5000\text{kg},\ k = 805000\text{N/m},\ c = 1280\text{Ns/m} \tag{3.46}$$

Figure 3.4 shows the comparison of displacement values of the building calculated by using the frequency domain solution and time domain simulation where $PS = 0$ is the case corresponding to no damper. When the results are compared, it is seen that the values are in excellent agreement although single harmonic solution is used in the harmonic balance method.

3.3.2. Comparison of Optimization Results Utilizing Frequency and Time Domain Solutions

As mentioned before, it is difficult to find the most undesirable motion for a building in time domain since the ground excitation during an earthquake is totally random. Therefore, optimizing the dampers for a specific earthquake may not give good results for another earthquake.

In this section, slip force of a dry friction damper installed at a single story building is optimized to decrease the maximum displacement according to the 1999 BOLU Earthquake both in time and frequency domains. Then the response of the building with the optimized damper is investigated under different earthquakes in time domain and results are compared.

The model parameters of the SDOF system are given as follows;

$$m = 5102\text{kg},\ k = 805700\text{N/m},\ c = 1285.7\text{Ns/m} \qquad (3.47)$$

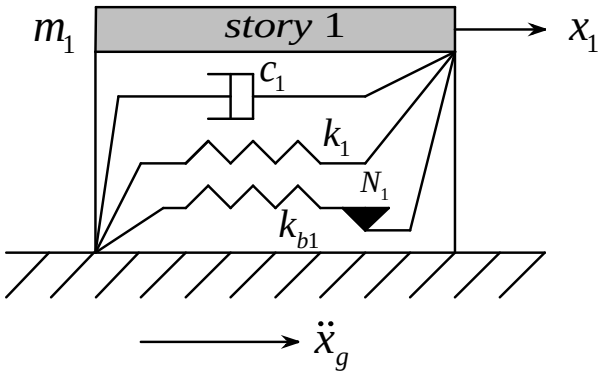

Figure 3.3 SDOF shear building model

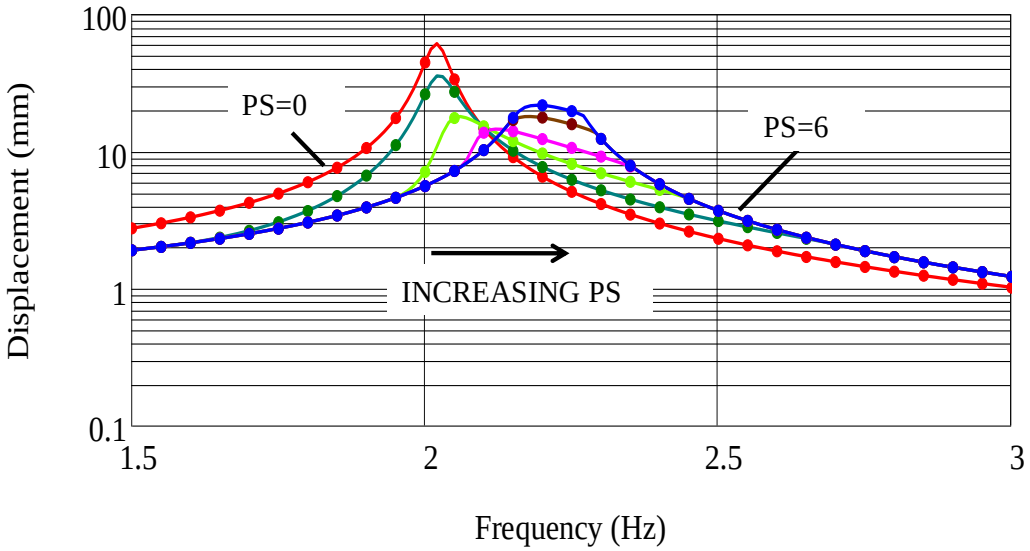

Figure 3.4 Comparison of frequency domain (solid lines) and time domain (dots) solutions. PS= 0, 0.7, 1.5, 2.5, 4.5 and 6.

In Figure 3.5, earthquake ground acceleration in east-west direction of 1999 Bolu Earthquake measured at Bolu city center is given and in Figure 3.6 frequency response function (FRF) of this ground acceleration is shown. In earthquake engineering *gal* is used as the acceleration unit and is equal to 1 cm/s^2. Graphs of

other earthquake ground accelerations and FRF of these ground accelerations are given in Appendix B.

When the slip force of the friction damper is optimized to minimize the maximum displacement according to the time record history of 1999 Bolu Earthquake, optimum PS value is found as 3.96. However, when the same optimization is done in frequency domain with a constant harmonic ground acceleration which has a magnitude of $0.067\,\mathrm{m/s^2}$ optimum PS value is found as 0.85.

In this analysis, maximum value of the FRF data has been chosen as the constant harmonic ground acceleration magnitude. For this purpose, some other techniques can be developed but in the literature there is no information related to this issue, since frequency domain optimization is a new concept for optimization of dry friction dampers installed on buildings.

Maximum displacement responses of the investigated system with these two dampers to different earthquakes using time marching method are given at Table 3.2. When the results are compared for Bolu earthquake, it is seen that damper optimized in frequency domain is not as effective as the damper optimized in time domain due to the fact that in time domain solution, damper is optimized specifically for this earthquake. However, the damper optimized in frequency domain performs a better performance for other earthquakes since frequency domain optimization is a more general approach .

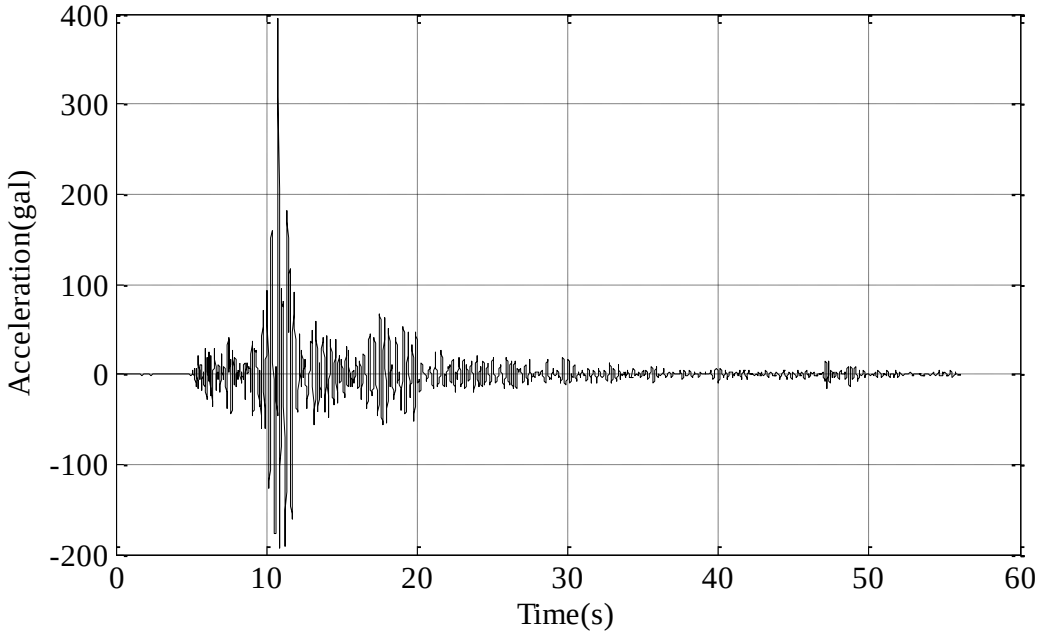

Figure 3.5 Time history record of 1999 Bolu Earthquake (EW direction)

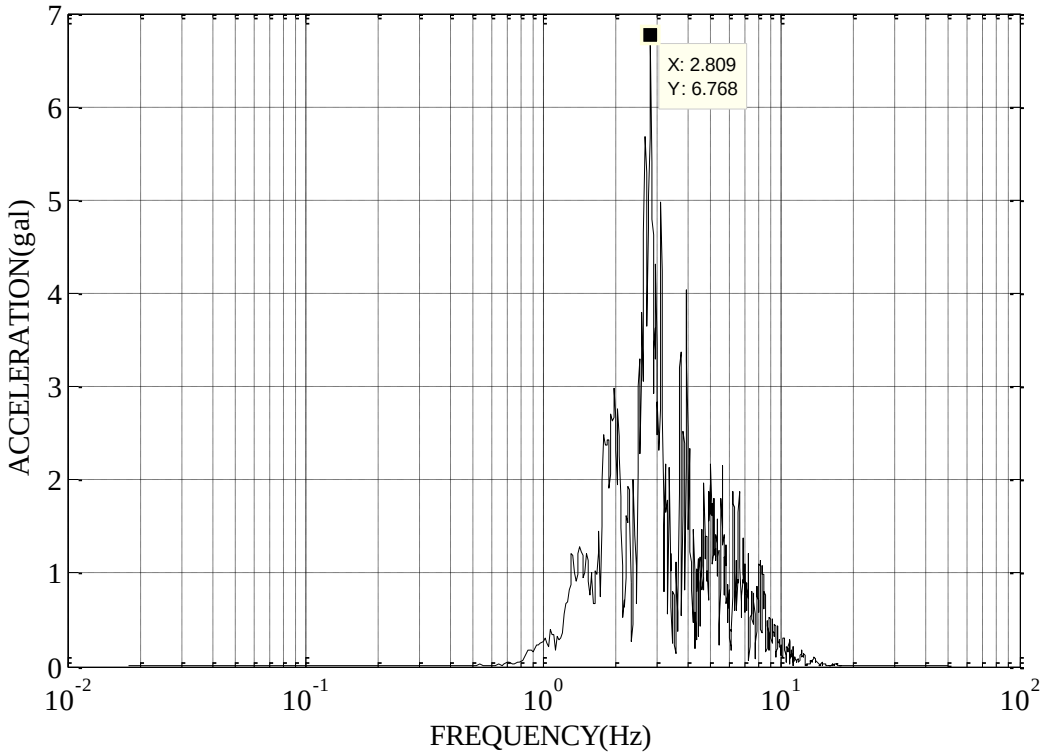

Figure 3.6 FFT of 1999 Bolu Earthquake (E-W direction)

Table 3.2 Maximum displacement responses of a single story building with different dampers under different earthquakes

EARTHQUAKE NAME	MAX. DISPLACEMENT WITHOUT DAMPER (MM)	MAX. DISPLACEMENT WITH OPT. DAMPER IN FREQUENCY DOMAIN (MM)	**REDUCTION %**	MAX. DISPLACEMENT WITH OPT. DAMPER IN TIME DOMAIN (MM)	**REDUCTION %**
BOLU, 1990	43,47	36,39	**16,29**	34,91	**19,69**
ERZINCAN, 1992	3,95	3,36	**14,94**	3,91	**1,01**
DENIZLI, 1976	29,90	25,18	**15,79**	25,63	**14,28**
AFYON, 2002	9,60	3,52	**63,33**	4,39	**54,27**

CHAPTER 4

RESULTS AND CASE STUDIES

4.1. Effect of Dry Friction Damper Parameters on the Displacement of a Single Story Building

As already mentioned before, bracing stiffness and slip load are two main parameters that determine the characteristics and energy dissipation capacity of a damper. In this section, the effect of brace stiffness and slip load on vibration amplitude of a building is demonstrated with a simple analysis by using a single story model. For this reason, the same building investigated in Section 3.3. is investigated under a sinusoidal ground acceleration which has a magnitude of $0.2\ \text{m/s}^2$.

The response of the SDOF system is studied by varying PS and SR from 0 to 10 although it is difficult to achieve values of SR much greater than 1.

Figure 4.1, Figure 4.2 and Figure 4.3 show the effect of PS on the displacement amplitude and resonance frequency of the building when SR is kept constant at 0.2. As already mentioned before, $PS = 0$ is the case corresponding to no damper.

As can be seen from Figure 4.1, there is an optimum point of PS which results in minimum displacement amplitude. It should also be noted that, for high values of PS, damper cannot slip and the system behaves like a linear one with an equivalent stiffness of $k_1 + k_{b_1}$ and the resonance frequency of the building becomes identical to the stuck case resonance frequency.

Figure 4.4, Figure 4.5 and Figure 4.6 show the effect of SR on the displacement amplitude and the resonance frequency of the building when PS is kept constant at 2. In this analysis, $SR = 0$ is the case corresponding to no damper. From these graphs, it is observed that, the maximum displacement amplitude decreases and the resonance frequency increases with increasing SR.

Effect of SR and PS on the maximum displacement is as well demonstrated on a 3-D graph given in Figure 4.7. From this figure, it can be seen that optimum PS is a function of SR.

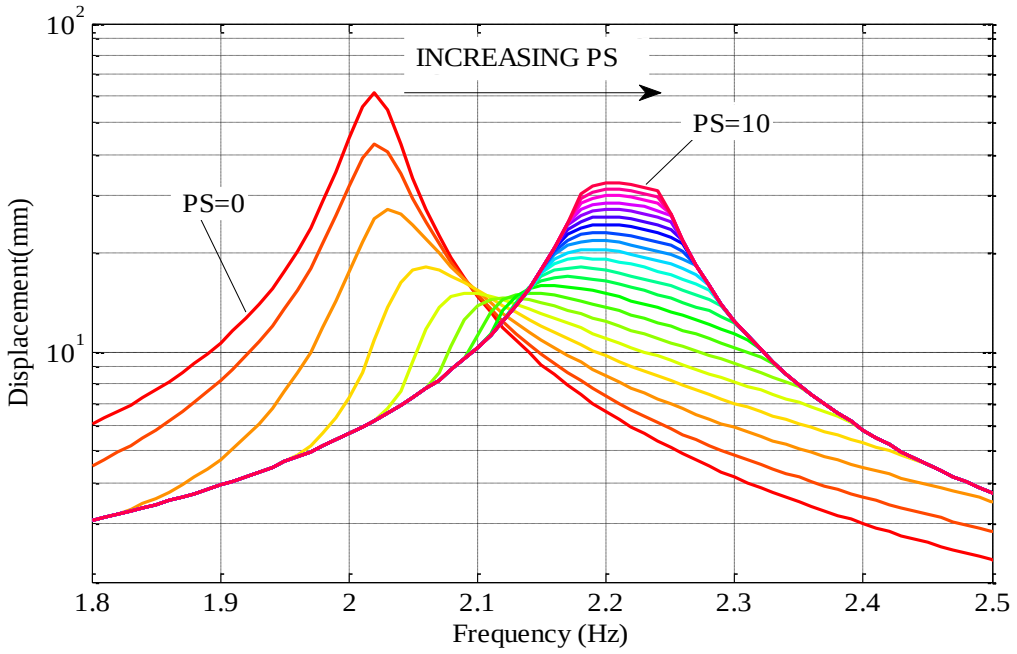

Figure 4.1 Frequency-displacement curve for SR=0.2 and PS values as 0, 0.5, 1, 1.5,...,10

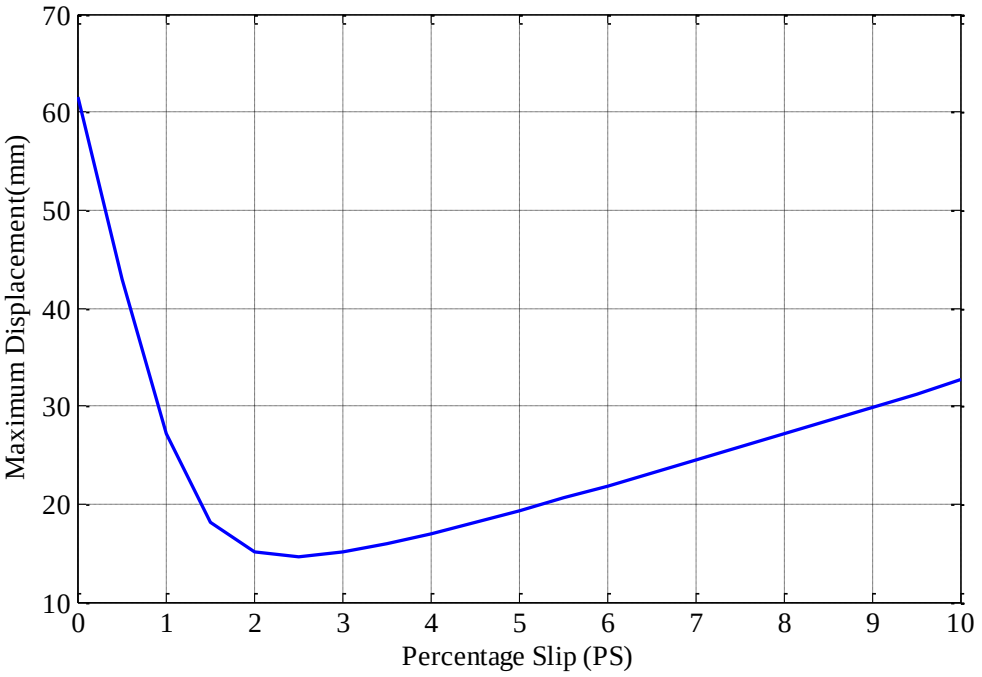

Figure 4.2 Maximum displacement versus PS curve for SR=0.2

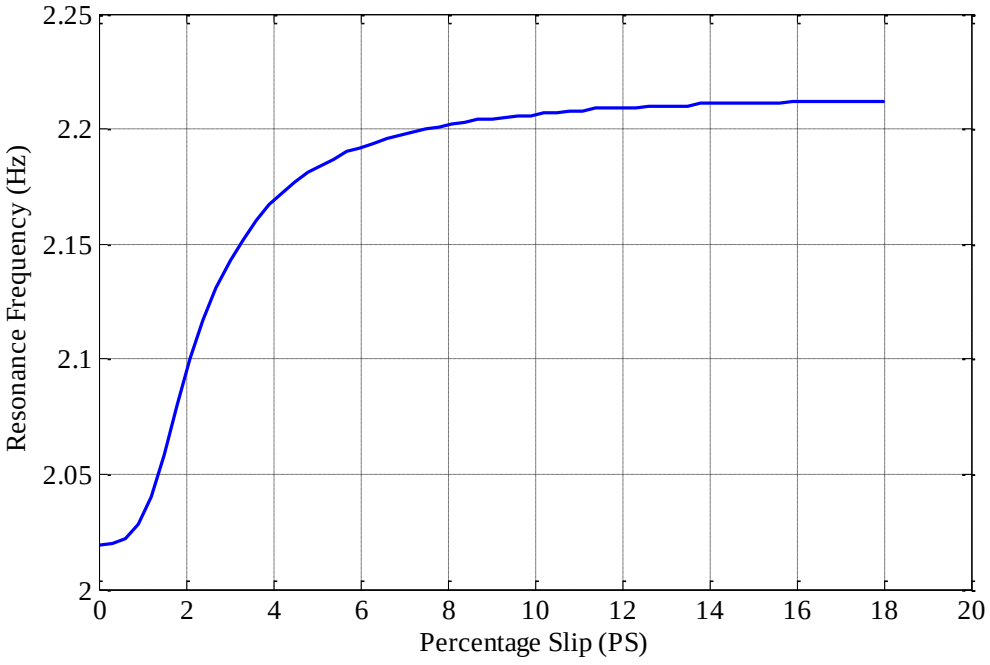

Figure 4.3 Resonance frequency versus PS curve for SR=0.2

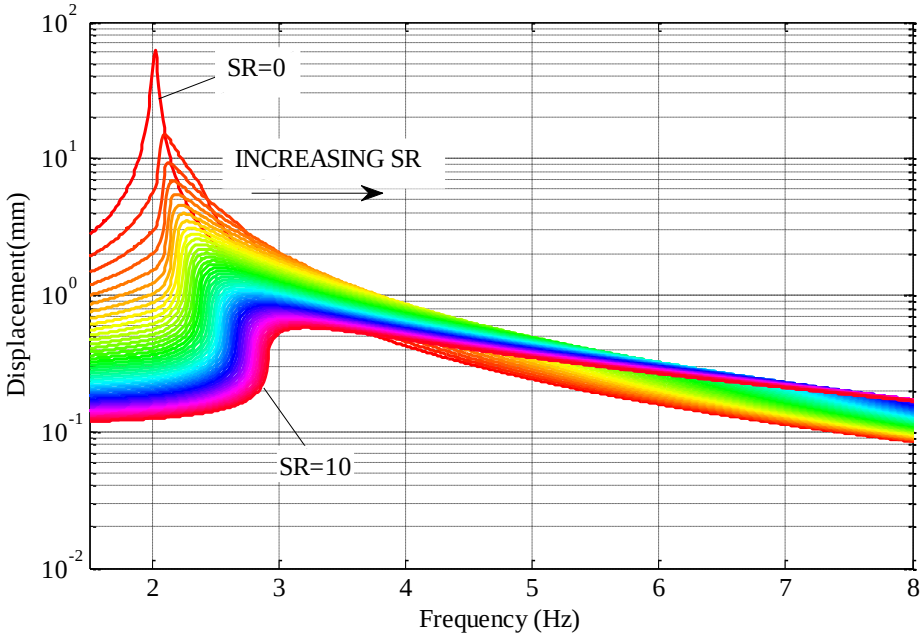

Figure 4.4 Frequency-displacement curve for PS=2 and SR values as 0, 0.2, 0.4, 0.6,...,10

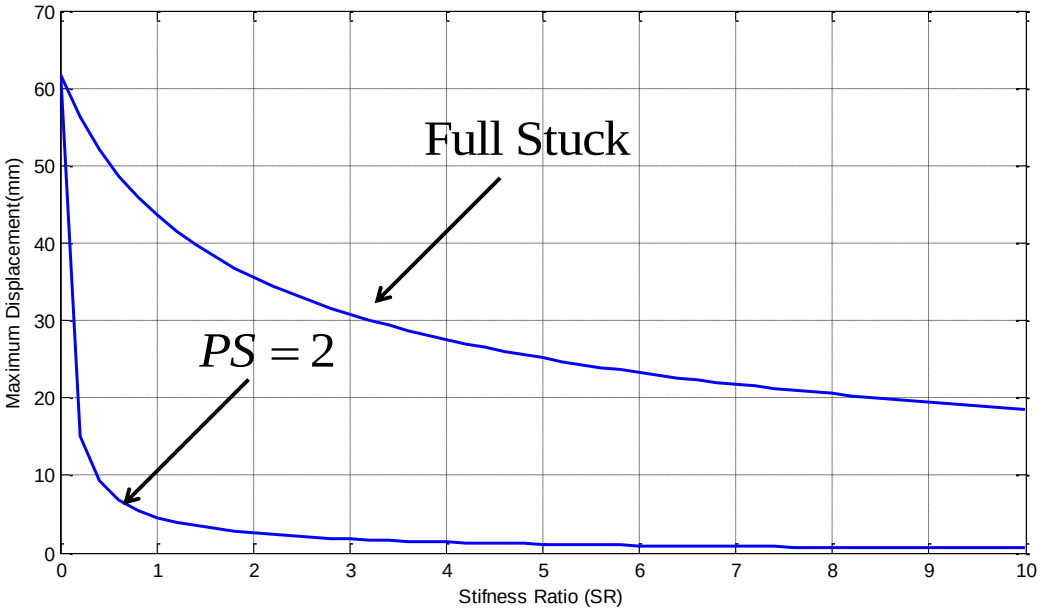

Figure 4.5 Maximum displacement versus SR curve for PS=2

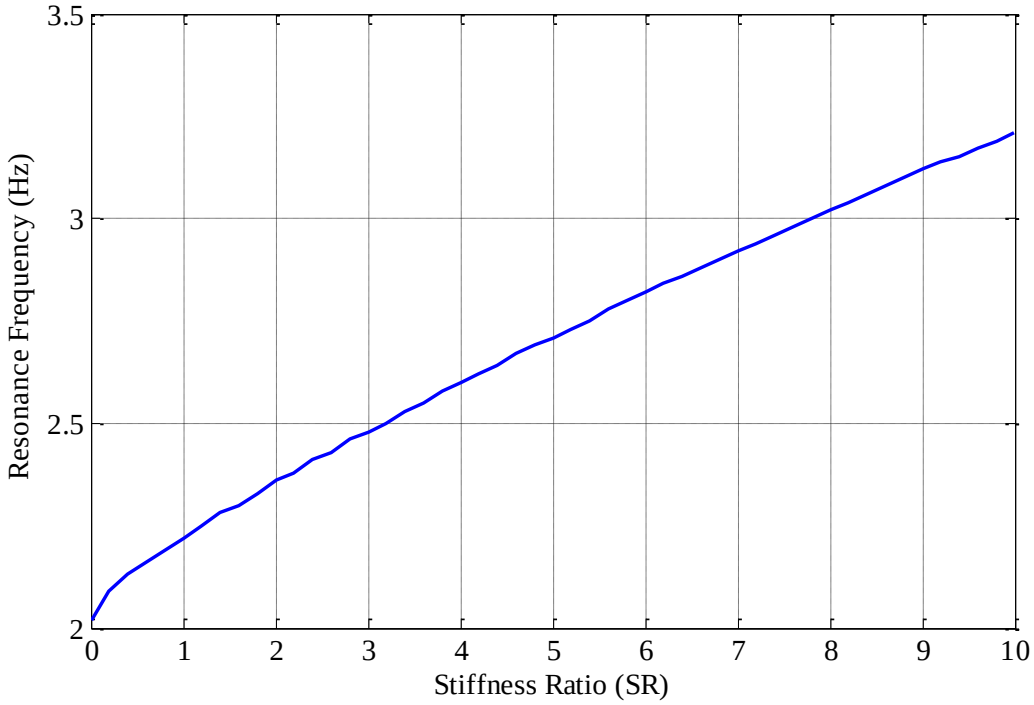

Figure 4.6 Resonance frequency versus SR curve for PS=2

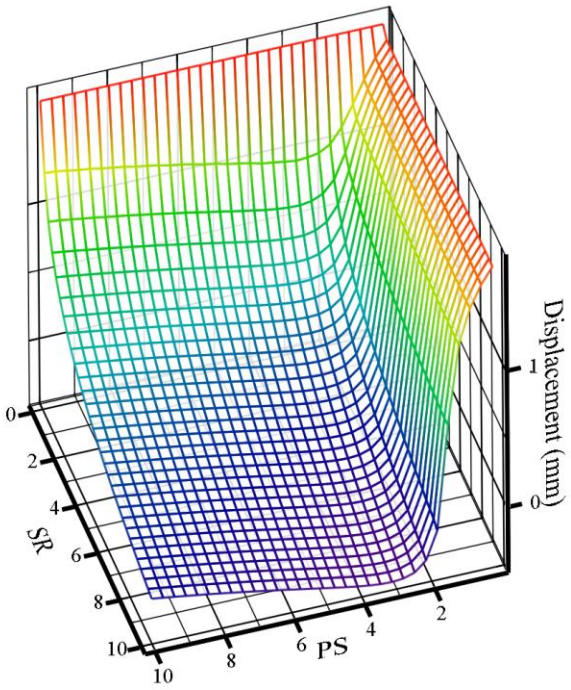

Figure 4.7 Effect of PS and SR on maximum displacement

4.2. Effect of Dry Friction Damper Parameters on the Energy Dissipation Capacity of a Dry Friction Damper

The energy dissipated by the dry friction damper per cycle can be calculated as follows by using the general definition of mechanical work;

$$E_d = \int F_d dx, \tag{4.1}$$

where F_d is the damper force as given in Equation (3.21) and x is the position vector. For a sinusoidal relative displacement at the damper as given in Equation (3.13), Equation (4.1) can be calculated as follows;

$$E_d = A\int_0^{2\pi} F_d \cos(\beta) d\beta \tag{4.2}$$

where A is the is the amplitude of the relative displacement at the damper as mentioned before.

If the damper remains at stick state all through the cycle;

$$\begin{aligned} F_d &= k_b A \sin(\beta) \\ E_d &= k_b A^2 \int_0^{2\pi} \sin(\beta)\cos(\beta) d\beta = 0 \end{aligned}. \tag{4.3}$$

For such a case, displacement magnitude along the building will decrease due to the increased rigidity due to the stiffness of the integrated brace, but not due to the energy dissipated by the dry friction damper.

However, if slip case also occurs on the damper, to be able to calculate the dissipated energy, piecewise integral should be calculated using the damper force given in Equation (3.21). Using Equations (3.21) and (4.2), damped energy per cycle can be calculated as follows;

$$E_d = A\int_{\beta_2+\pi}^{\pi/2} \mu N\cos(\beta)\,d\beta + A\int_{\pi/2}^{\beta_2}\left[\mu N + k_b\left(A\sin(\beta)-A\right)\right]\cos(\beta)\,d\beta -$$
$$A\int_{\beta_2}^{3\pi/2} \mu N\cos(\beta)\,d\beta + A\int_{3\pi/2}^{\beta_2+\pi}\left[-\mu N + k_b\left(A\sin(\beta)+A\right)\right]\cos(\beta)\,d\beta \qquad (4.4)$$
$$E_d = 4A\mu N\left(1-\frac{2\mu N}{k_b A}\right)$$

To investigate the effects of the dry friction damper parameters on the energy dissipation capacity, the same building investigated in Section 3.3. is used under a sinusoidal ground acceleration which has a magnitude of $0.2\ \text{m/s}^2$.

The amount of the dissipated energy by the dry friction damper is studied by varying PS and SR from 0 to 10 as performed in Section 4.2.

Figure 4.8 shows the effect of PS on the dissipated energy from the friction damper in one cycle when SR is kept constant at 0.2. It is observed that as PS increases, the frequency range of energy dissipation decreases. For the case considered here, the maximum energy dissipation per cycle occurs when PS is very small or very large. Since energy dissipation is equal to the friction force multiplied by displacement, in the former case, this results in large vibration amplitudes due to low PS; whereas, low vibration amplitudes occur in the latter case. From Figure 4.1, optimum PS is found out to be 2 for minimum displacement and for this case natural frequency has been determined as 2.1 Hz. Studying Figure 4.8, it is seen that for PS value of 2 satisfies the maximum energy dissipation per cycle at 2.1 Hz.

Figure 4.9 shows the effect of SR on the dissipated energy from the friction damper in one cycle when PS is kept constant at 2. From Figure 4.5, it has been determined that the maximum displacement of the building decreases with the increasing SR. However, in Figure 4.9 , it is seen that dissipated energy by the damper decreases with the increasing SR as well. Therefore, the decrease in the response is not due to friction damping but it is mainly due to the increased rigidity with the effect of the brace that connects the damper to the building.

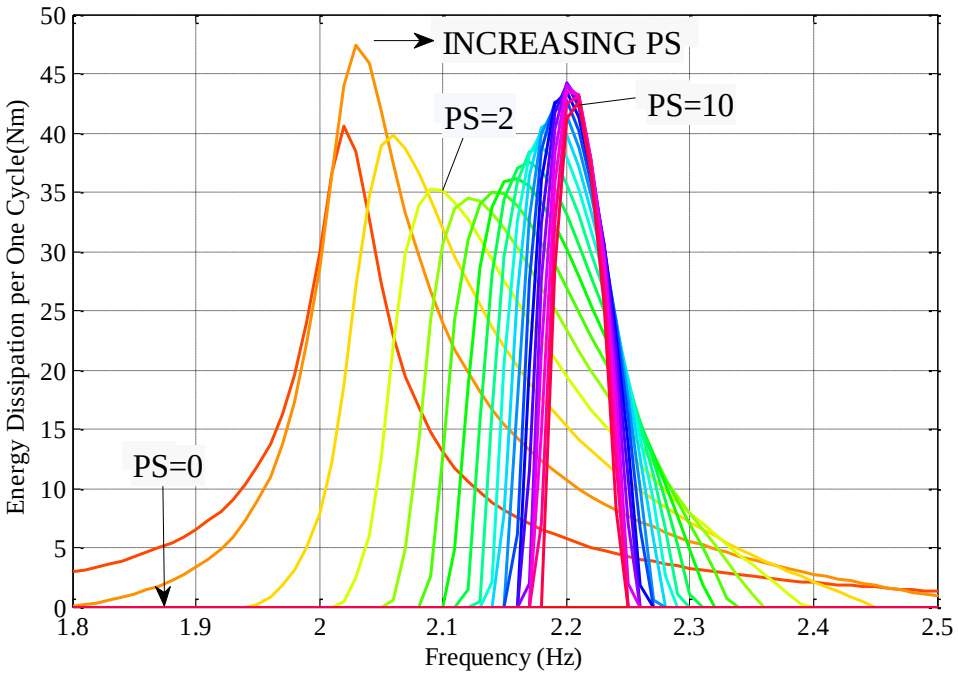

Figure 4.8 Frequency - dissipated energy curve for SR=0.2 and PS values as 0, 0.5, 1, 1.5,...,10

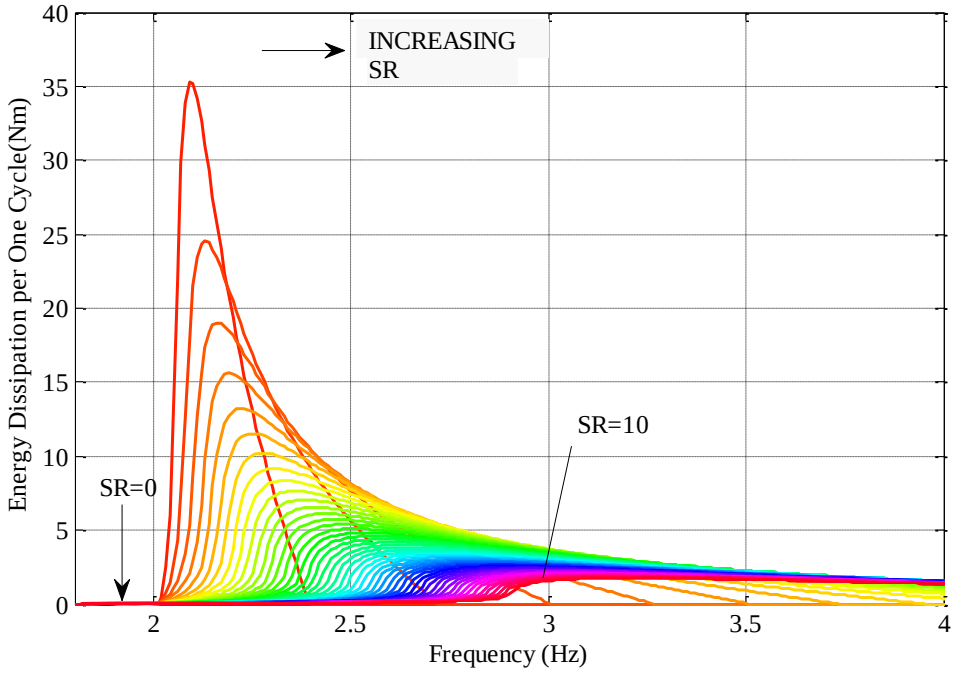

Figure 4.9 Frequency - dissipated energy curve for PS=2 and SR values as 0, 0.2, 0.4, 0.6,...,10

4.3. Results for Multistory Building

Up to now all of the results are given for a single story building which is easier to solve. In the following analyses, effects of SR and PS are studied, optimization studies are performed for different scenarios and effect of different damper configurations are investigated on a multistory building under harmonic excitation.

Structural parameters of the 6-story shear building model used during the analyses are given in Table 4.1 and illustrated in Figure 2.1. These building parameters are obtained from reference [32].

Table 4.1 Structural properties of the 6 story building model

Floor Masses (kg)	**Stiffness Coefficients (kN/m)**	**Damping Coefficients (kNs/m)**
$m_1 = 50000$	$k_1 = 74000$	$c_1 = 120$
$m_2 = 50000$	$k_2 = 66000$	$c_2 = 90$
$m_3 = 50000$	$k_3 = 56000$	$c_3 = 75$
$m_4 = 50000$	$k_4 = 44000$	$c_4 = 65$
$m_5 = 50000$	$k_5 = 31000$	$c_5 = 45$
$m_6 = 50000$	$k_6 = 16000$	$c_6 = 32$

Before studying the effects of damper parameters, no damper case and full stuck case are investigated. As can be seen from Figure 4.10, the maximum interstory drift for the building without any damper is 24.4 mm at 1.25 Hz and it is measured between the 5^{th} and the 6^{th} story. For the building with full stuck dampers maximum inter-story drift is 22.3 mm at 1.38 Hz and it is again measured between the 5^{th} and the 6^{th} story as shown in Figure 4.11.

4.3.1. Effect of Dry Friction Dampers on the Displacement and Interstory Drift

In this section, effect of the bracing stiffness and slip load of the damper on displacement and interstory drift will be shown on a multi-story building. For this reason the 6-story building is investigated under a sinusoidal ground acceleration which has a magnitude of 0.067 m/s^2. For a multistory building, the stiffness and the slip load of each damper are normalized as follows;

$$SR_q = \frac{k_{bq}}{k_q}, \quad PS_q = \frac{F_{sq}}{W}100, \tag{4.5}$$

where q is the story number and W is the building weight.

The response of the system is studied by varying PS and SR from 0 to 10 and it is assumed that all of the dampers have the same properties, i.e. slip forces and bracing stiffnesses are the same for all the dampers.

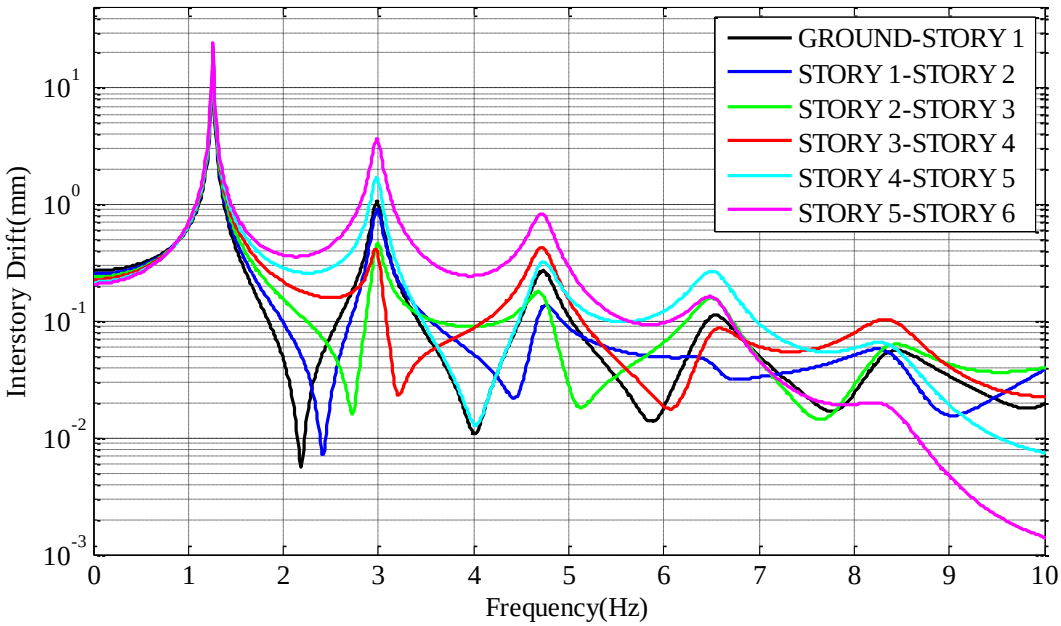

Figure 4.10 Interstory drift plot (no damper)

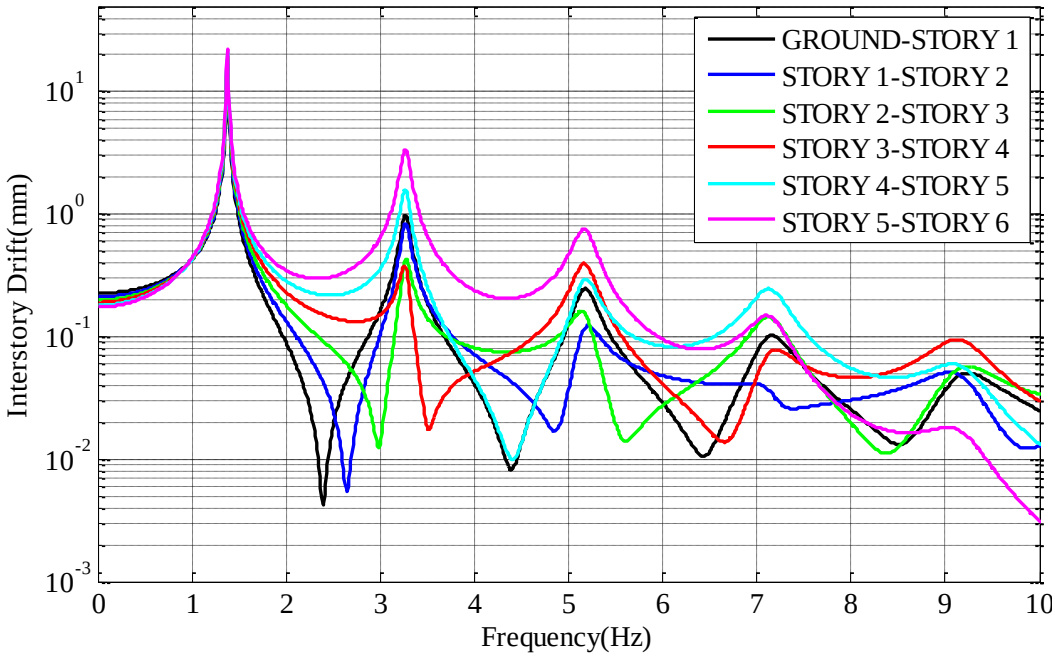

Figure 4.11 Interstory drift plot (full stuck)

Figure 4.12 and Figure 4.14 show the effect of PS on the displacement of the 6th story relative to the ground as a function of frequency when SR is kept constant at 0.5. Since the maximum displacement is measured at the 6th story, plots for the other stories are not shown.

Figure 4.14 - Figure 4.19 show the effect of PS on the interstory drift when SR is kept constant at 0.5. Figure 4.20 and Figure 4.21 show that, there exist optimum PS values which result in the minimum displacement and interstory drift.

Figure 4.22 shows the effect of the SR on the 6th story displacement relative to the ground with respect to frequency when PS is kept constant at 1.7.

Figure 4.23-Figure 4.28 show the effect of the SR on the interstory drift when PS is kept constant at 1.7. Figure 4.29 and Figure 4.30 show that, the maximum displacement with respect to the ground and interstory drift decreases with increasing SR. In Figure 4.21, the curve that shows the maximum interstory drift between 5th and 6th stories is broken around PS=1 region and looks different from the other curves. At this region, second natural frequency of the building is more critical compared with the first natural frequency and that is the reason for this broken region.

From Figure 4.31 maximum story displacements of the building can be seen for different PS values when SR is kept constant at 0.5 and from Figure 4.32 maximum story displacements of the building can be seen for different SR values when PS is kept constant as 1.7.

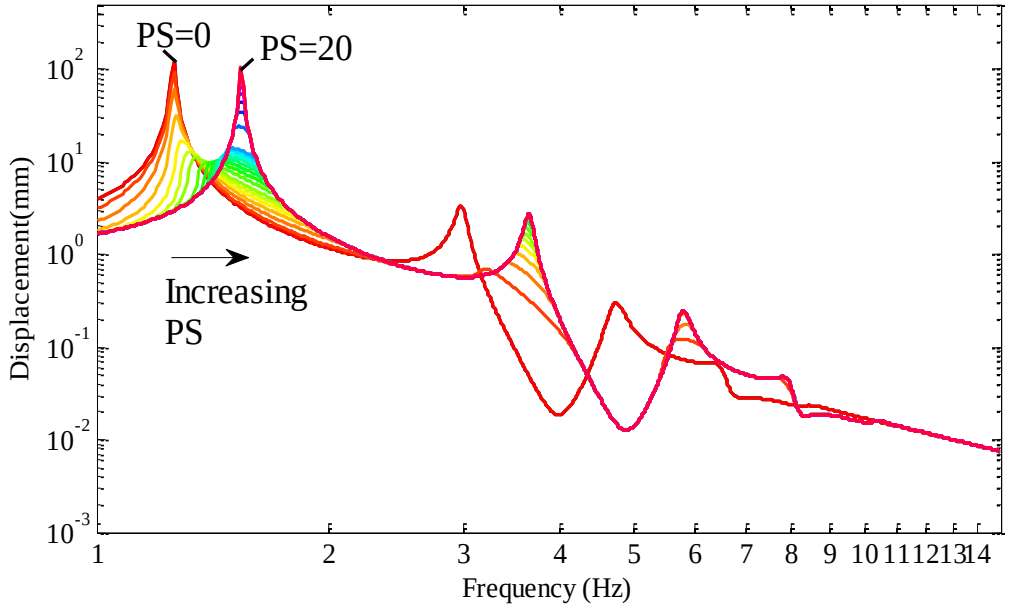

Figure 4.12 Frequency - displacement curve of the 6th story for SR=0.5 and PS values between 0 and 20

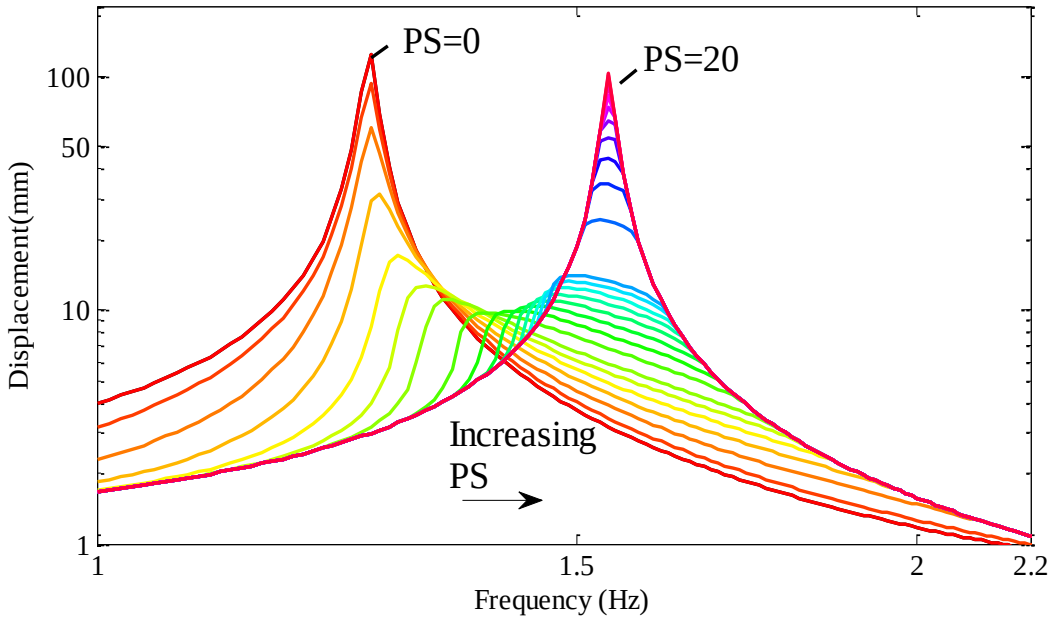

Figure 4.13 Frequency - displacement curve of the 6th story around the first mode for SR=0.5 and PS values between 0 and 20

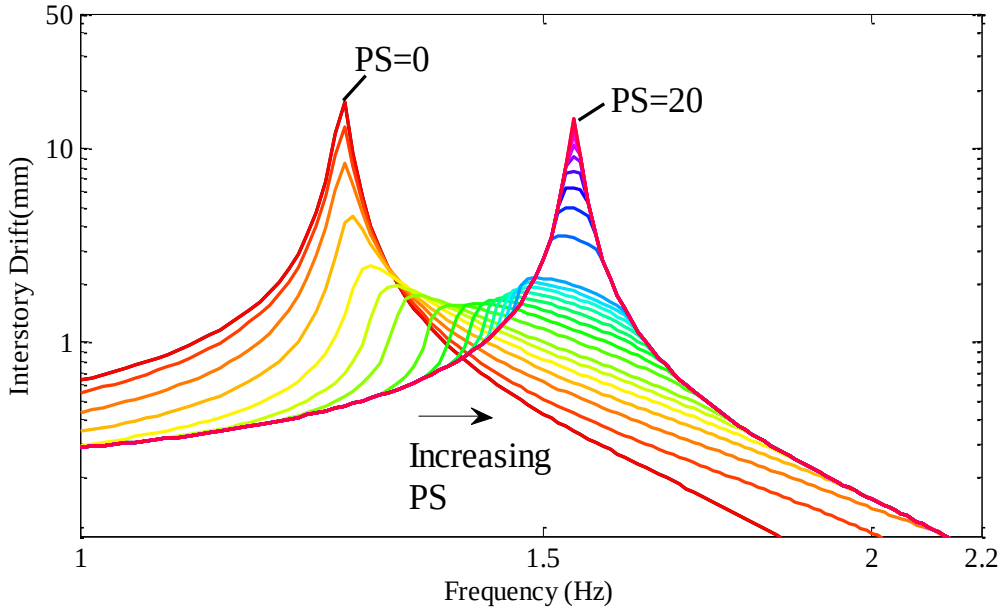

Figure 4.14 Frequency - interstory drift curve between ground and 1st story around the first mode for SR=0.5 and PS values between 0 and 20

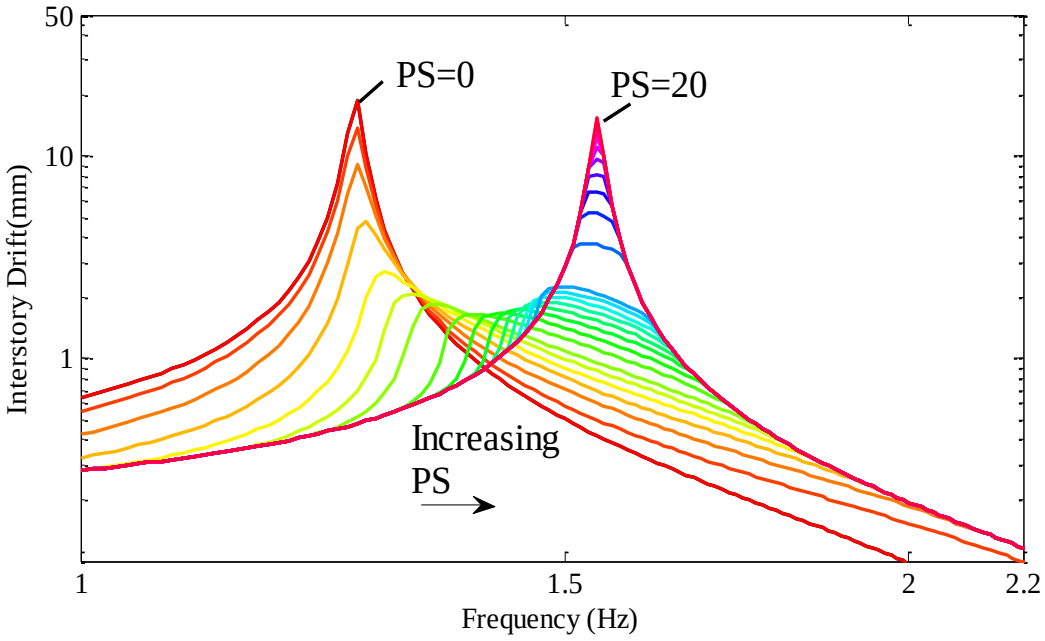

Figure 4.15 Frequency - interstory drift curve between 1st and 2nd story around the first mode for SR=0.5 and PS values between 0 and 20

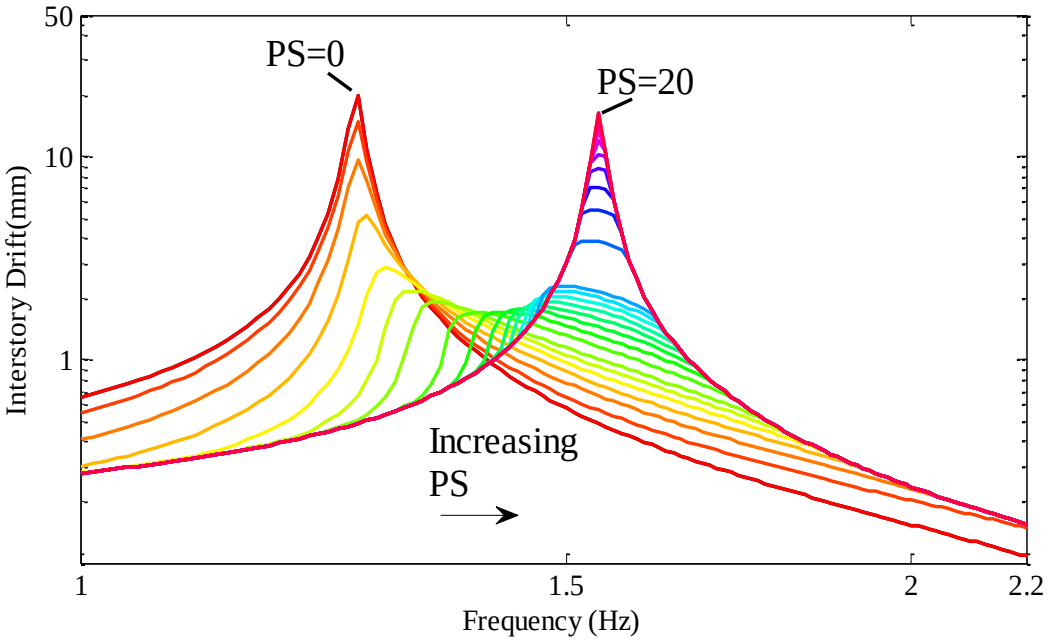

Figure 4.16 Frequency - interstory drift curve between 2nd and 3rd story around the first mode for SR=0.5 and PS values between 0 and 20

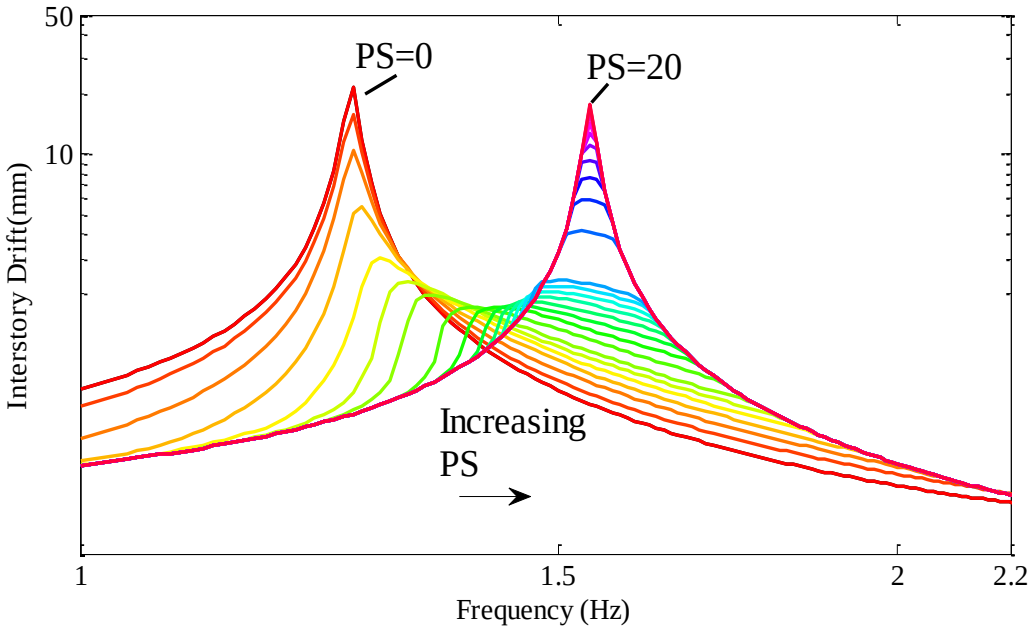

Figure 4.17 Frequency - interstory drift curve between 3rd and 4th story around the first mode for SR=0.5 and PS values between 0 and 20

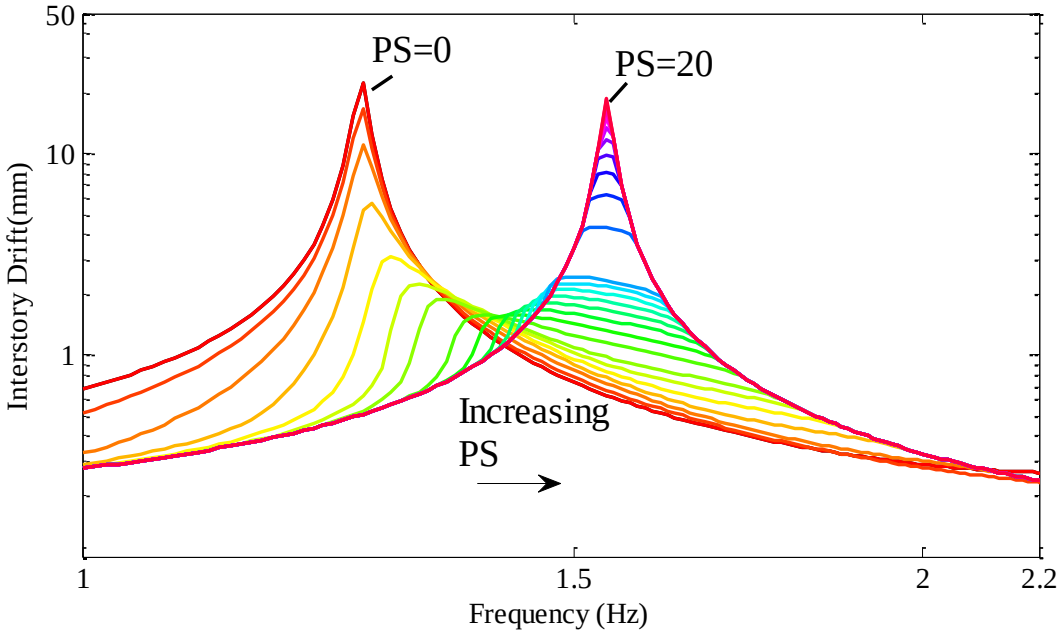

Figure 4.18 Frequency - interstory drift curve between 4th and 5th story around the first mode for SR=0.5 and PS values between 0 and 20

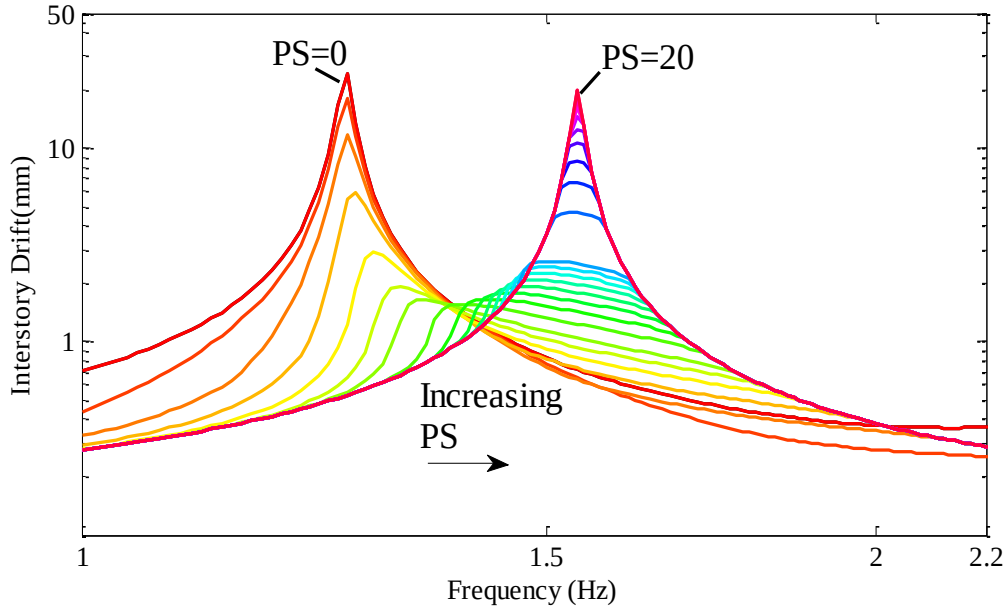

Figure 4.19 Frequency - interstory drift curve between 5th and 6h story around the first mode for SR=0.5 and PS values between 0 and 20

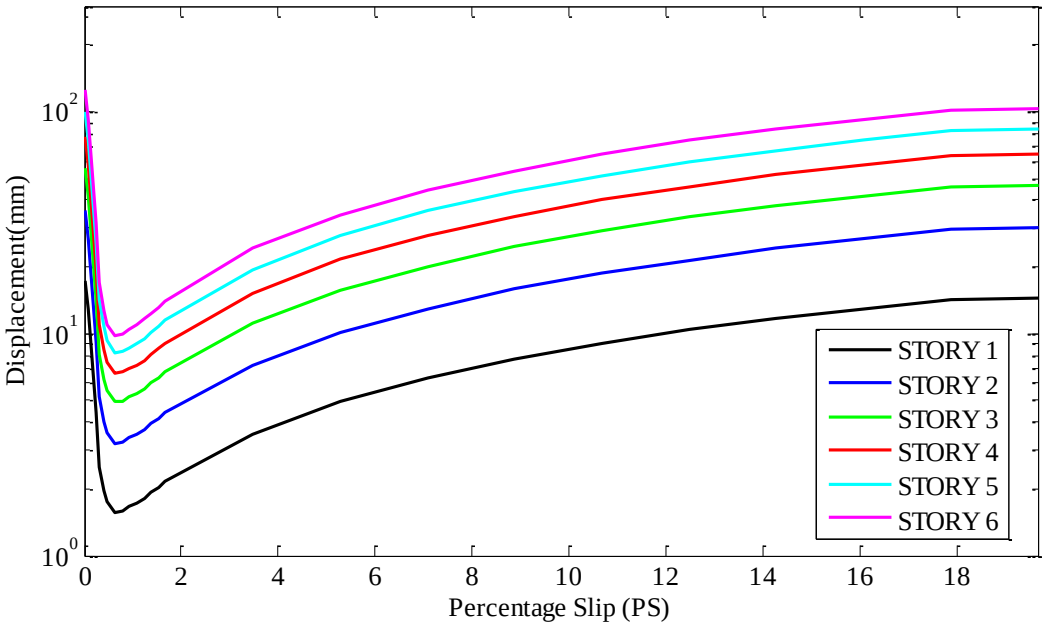

Figure 4.20 Maximum story displacements versus PS curves for SR=0.5

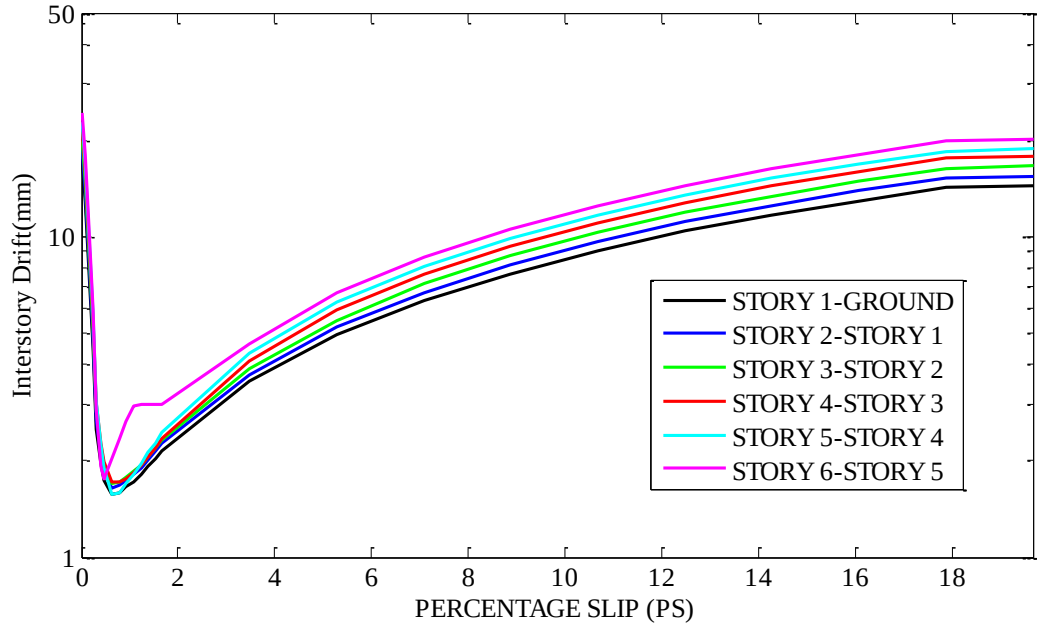

Figure 4.21 Maximum interstory drifts versus PS curves for SR=0.5

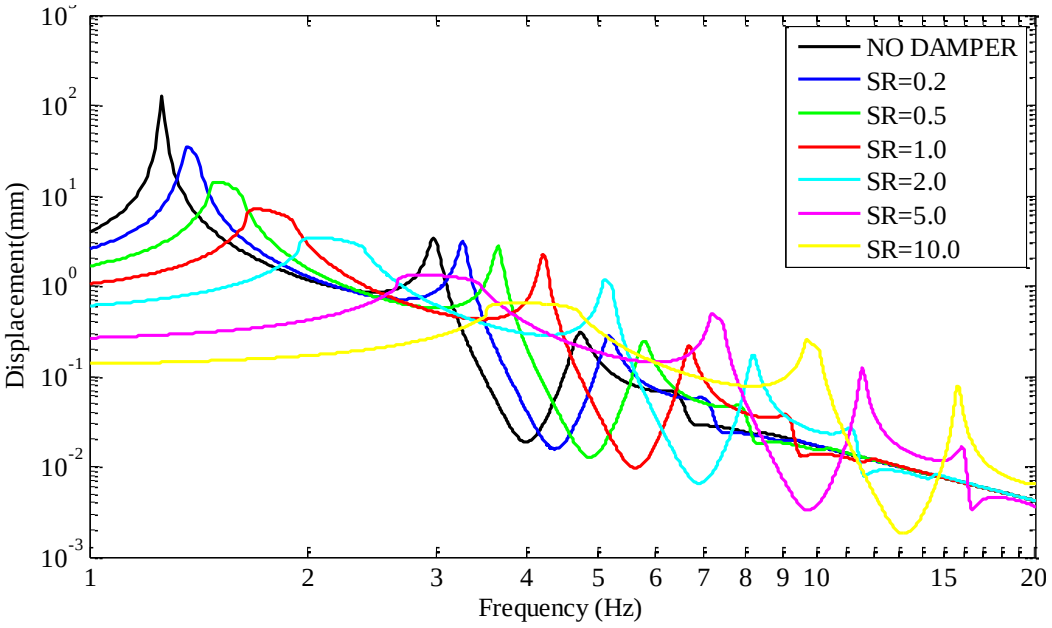

Figure 4.22 Frequency - displacement curve of the 6th story for PS=1.7 and SR values between 0 and 10

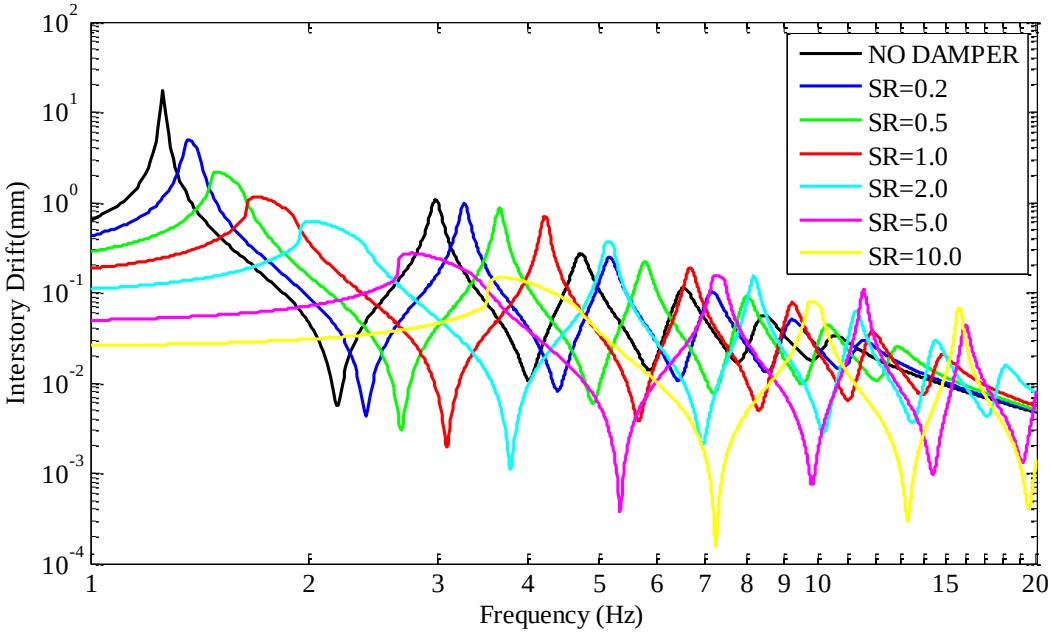

Figure 4.23 Frequency - interstory drift curve between ground and 1st story for PS=1.7 and SR values between 0 and 10

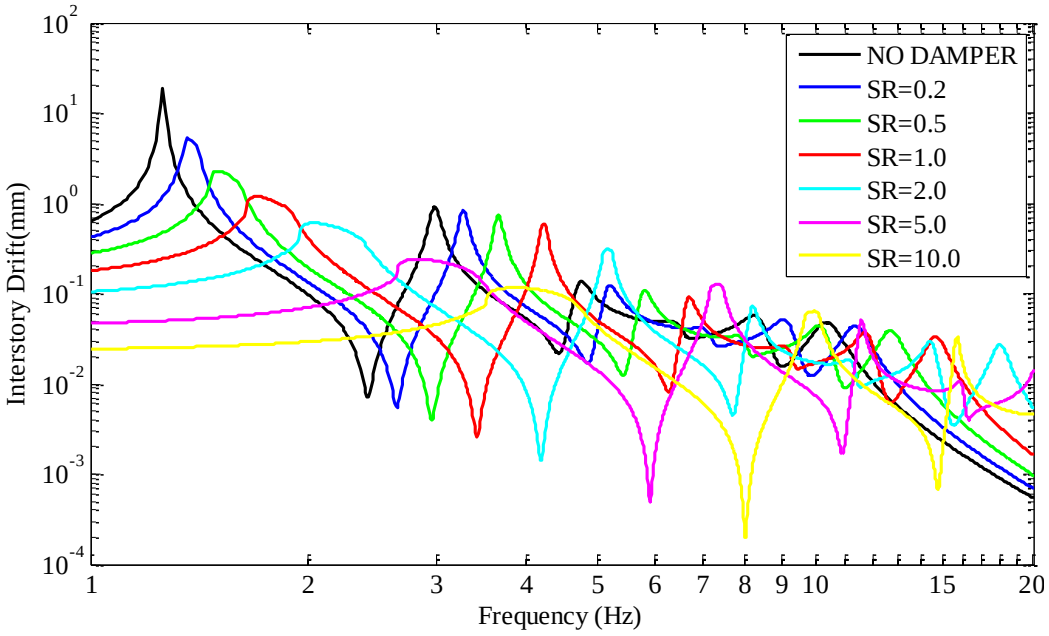

Figure 4.24 Frequency - interstory drift curve between 1st story and 2nd story for PS=1.7 and SR values between 0 and 10

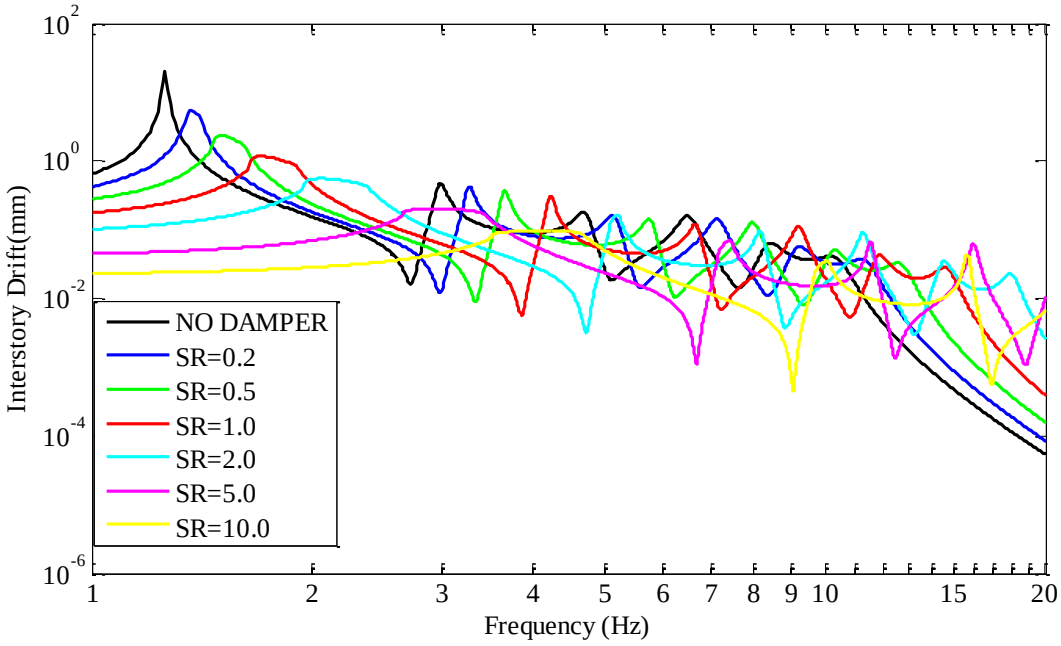

Figure 4.25 Frequency - interstory drift curve between 2nd story and 3rd story for PS=1.7 and SR values between 0 and 10

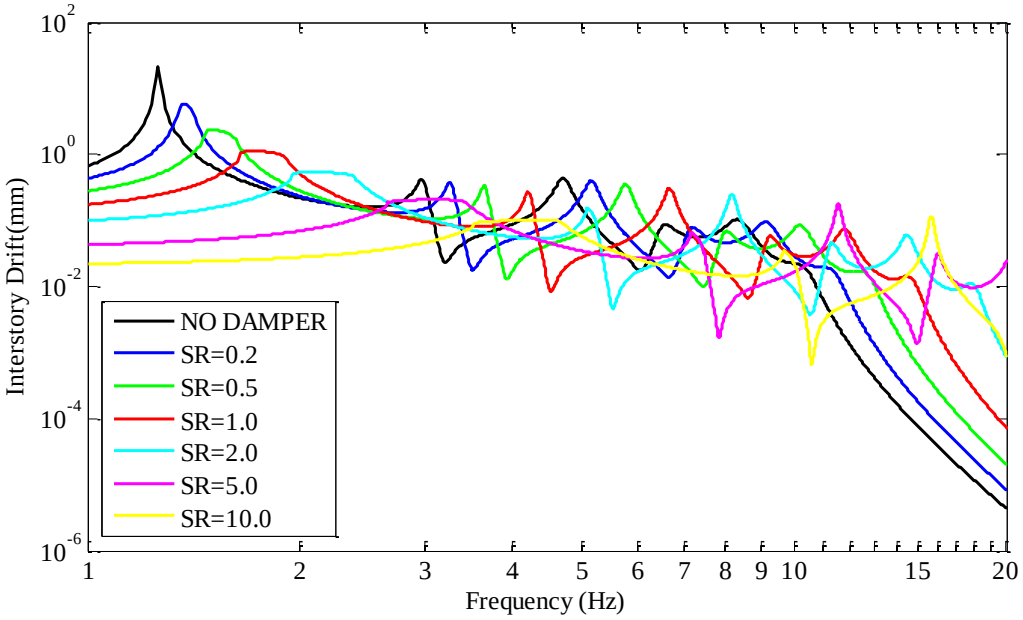

Figure 4.26 Frequency - interstory drift curve between 3rd story and 4th story for PS=1.7 and SR values between 0 and 10

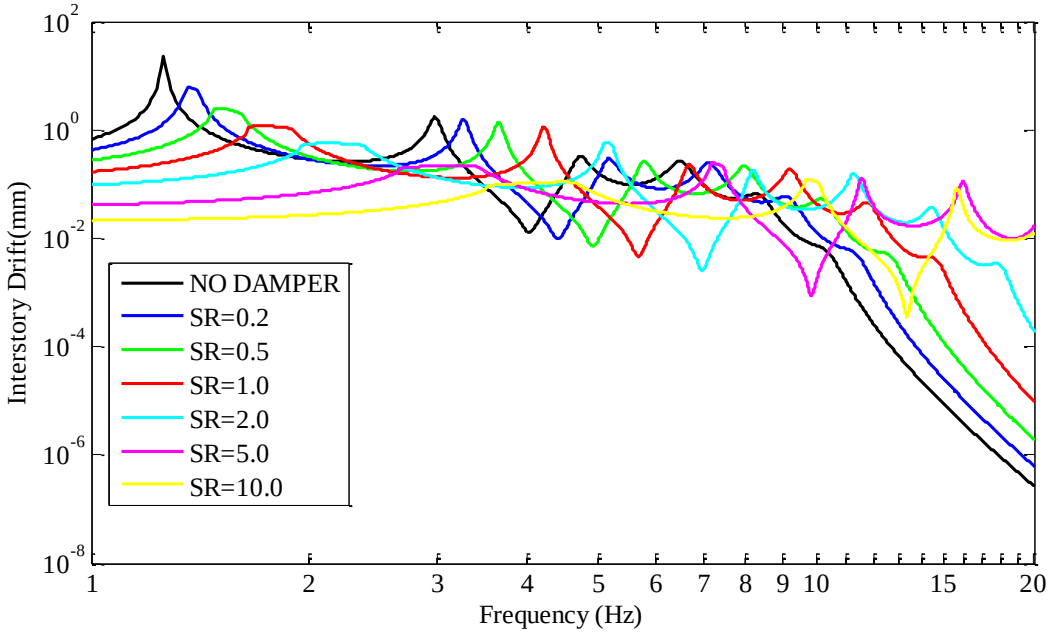

Figure 4.27 Frequency - interstory drift curve between 4th story and 5th story for PS=1.7 and SR values between 0 and 10

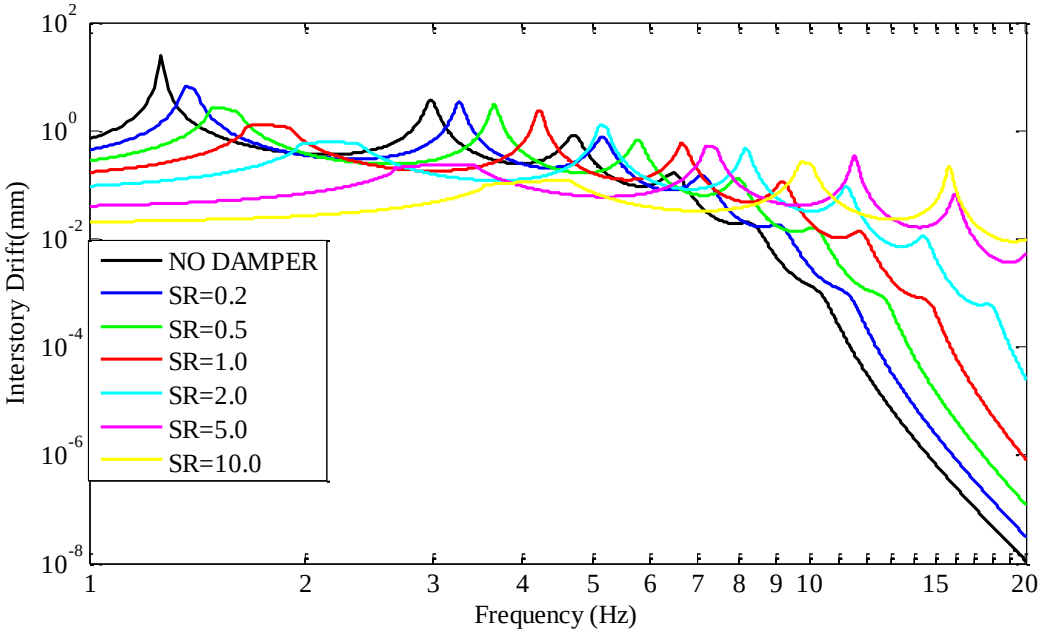

Figure 4.28 Frequency - interstory drift curve between 5th story and 6th story for PS=1.7 and SR values between 0 and 10

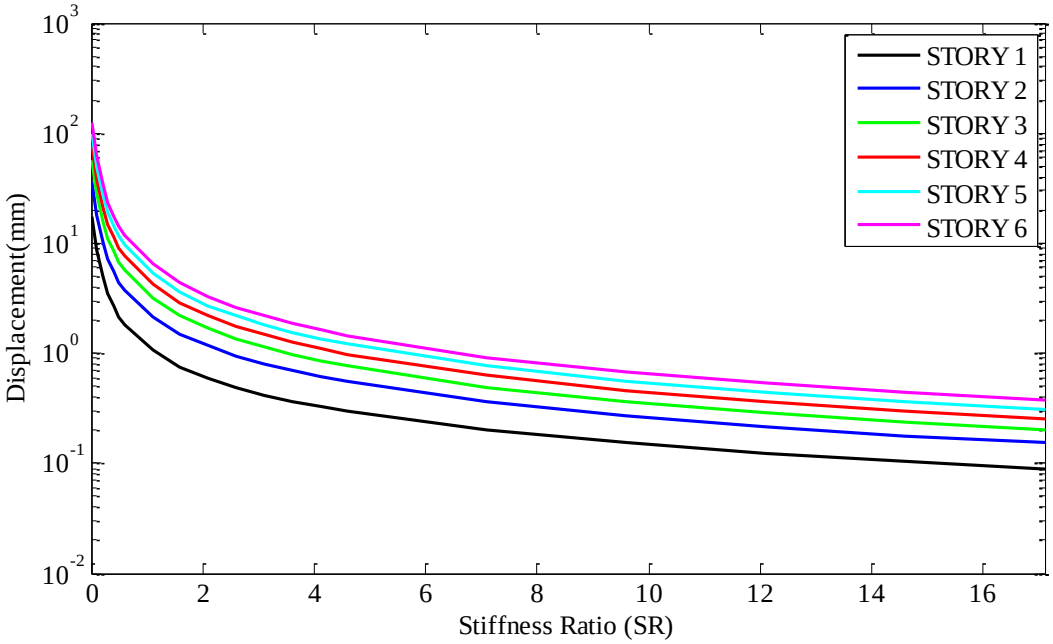

Figure 4.29 Maximum story displacement versus SR curves for PS=1.7

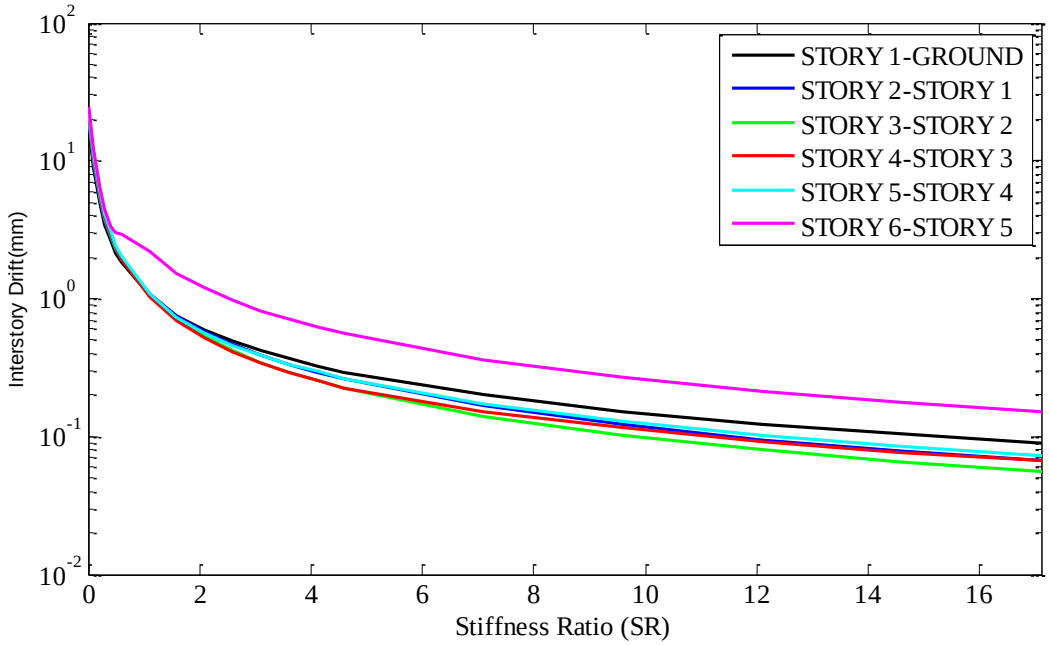

Figure 4.30 Maximum interstory drift versus SR curves for PS=1.7

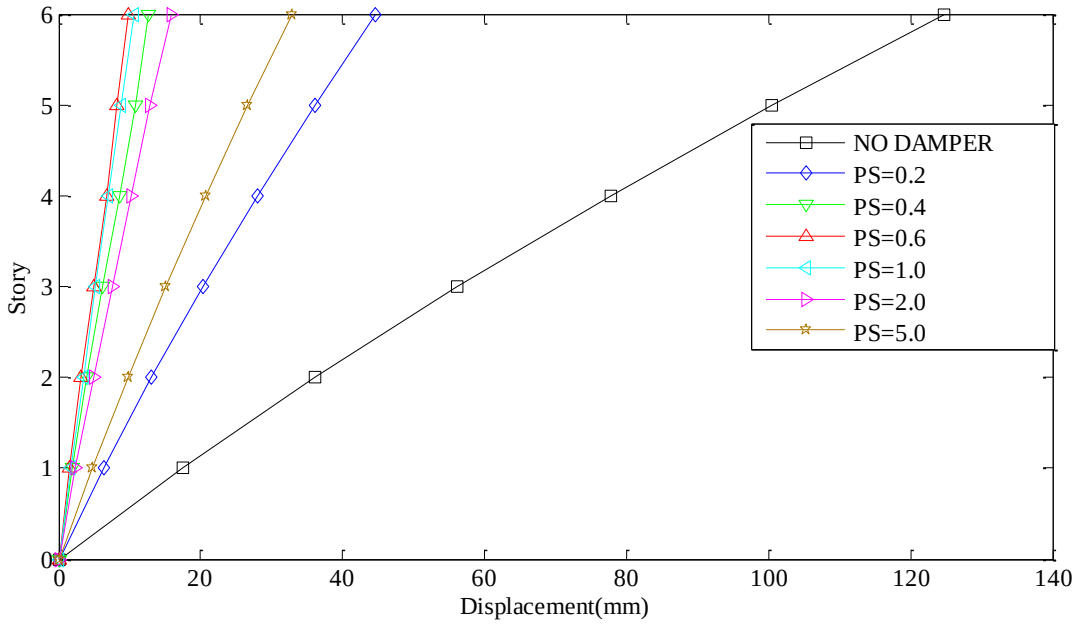

Figure 4.31 Maximum story displacements wrt the ground for SR=0.5 and PS values between 0 and 5

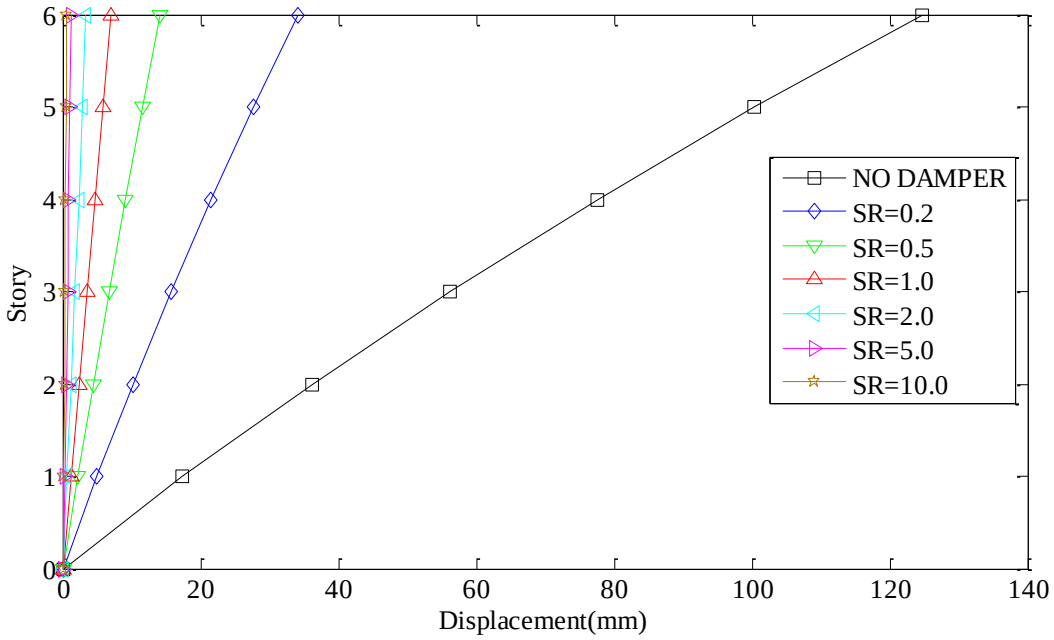

Figure 4.32 Maximum story displacements wrt the ground for PS=1.7 and SR values between 0 and 10

4.4. Optimization Studies on a Multistory Building having Friction Dampers only at Adjacent Stories

In this part of the thesis, slip force optimization of the dampers is investigated on a 6-story building under sinusoidal ground acceleration which has a magnitude of 0.067 m/s^2. Since the bracing stiffness is not an easily adjustable parameter, *SR* is kept constant as 0.2 during these studies and the same building model is used given in Section 4.3. and damper configuration is shown in Figure 4.33.

In these studies optimization is carried out on the slip load of the dampers and their places whereas the cost function is defined as the minimization of the maximum interstory drift in the frequency range of 0 Hz-15 Hz.

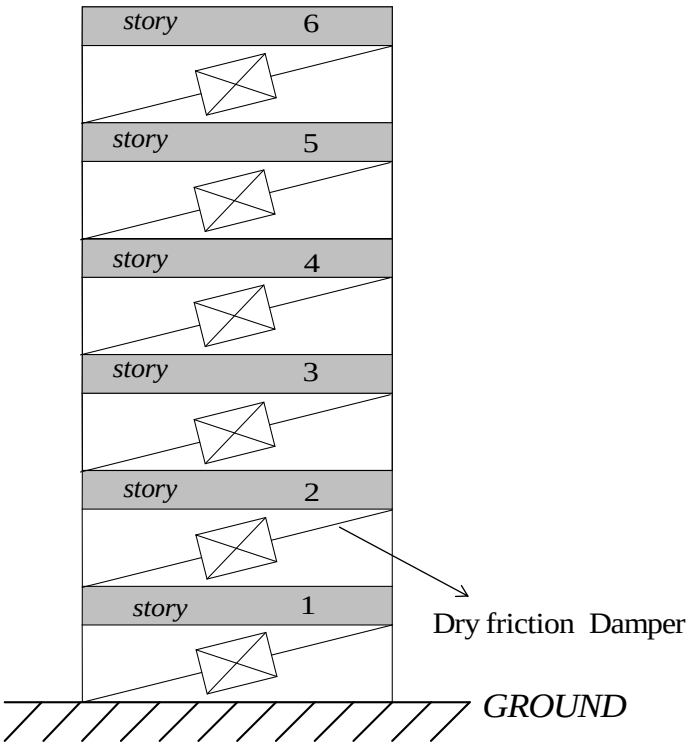

Figure 4.33 Shear building model having friction dampers only at adjacent stories

In real life one of the main objectives of the optimal damper design is to minimize the cost of the damper system. For this purpose, some optimization scenarios are also investigated such as decreasing the number of dampers or using identical dampers.

During the optimization studies, it is not required to get the full frequency displacement curve since the cost function only deals with the maximum interstory drift. For this reason, equations of motion are written in terms of drift parameters as investigated in Section 2.2. and the equations of motion are solved using the method described in Section 3.2.5. and homotopy continuation method by directly determining the resonance amplitudes.

During the optimizations, a hybrid optimization method is utilized in MATLAB® which applies "Genetic Algorithm" at first and then uses "fmincon", a gradient based optimization, in order to enhance the results further.

At the end of each case study, optimization results are verified by changing the optimum PS values of the dampers between 0% and 400% and showing minimum interstory drift occurs at the determined optimum PS value. In the verification graphs, maximum interstory drift values for different PS values are normalized with respect to the optimum value.

Moreover, at the end of each case study response of the building with optimized friction dampers is investigated for different earthquake acceleration magnitudes to see the effect of the optimized dampers under different design earthquakes. In these graphs, ground acceleration is changed between 0% and 400% of the initial design earthquake ground acceleration magnitude, i.e. 0.067 m/s^2, and for each design earthquake, maximum interstory drift value is normalized as follows;

$$Y_{norm} = \frac{\max\left(\left\{Y_{damped}\right\}\right)}{\max\left(\left\{Y_{undamped}\right\}\right)}, \tag{4.6}$$

where $\left\{Y_{damped}\right\}$ and $\left\{Y_{undamped}\right\}$ is the complex vector of interstory drift amplitudes calculated for building with optimized dampers and undamped case respectively.

4.4.1. Case Study 1 - Optimization with 6 Identical Dampers

In this case study, installation of 6 identical dampers is investigated.

At the end of the optimization, optimum value for PS is obtained as 0.5631 and the maximum interstory drift at 1.26 Hz is reduced to 3.92 mm as shown in Table 4.2 and Figure 4.34.

Figure 4.35 shows the verification of the results. It can be concluded that similar to the single story building, a correct choice of PS values should be different than

the optimum values determined. Since the slope of Figure 4.35 at the right of the optimum value is less than the slope at the left of the optimum value, a *PS* value slightly larger than the optimum value, i.e. 0.5631, should be used in the design. Figure 4.36 shows the response of the building with optimum dampers for different design earthquake ground acceleration magnitudes and it can be concluded that at any earthquake ground acceleration value around the design value, the optimized dampers have a very good performance and decreases the building response drastically.

Table 4.2 Results of case study 1

Damper Location	**Opt. PS Value**
Ground - 1st Story	0.5631
1st Story - 2nd Story	0.5631
2nd Story - 3rd Story	0.5631
3rd Story - 4th Story	0.5631
4th Story - 5th Story	0.5631
5th Story - 6th Story	0.5631
Maximum Interstory Drift (mm)	**3.92**
Reduction for Maximum Interstory Drift (%)	**83.93**

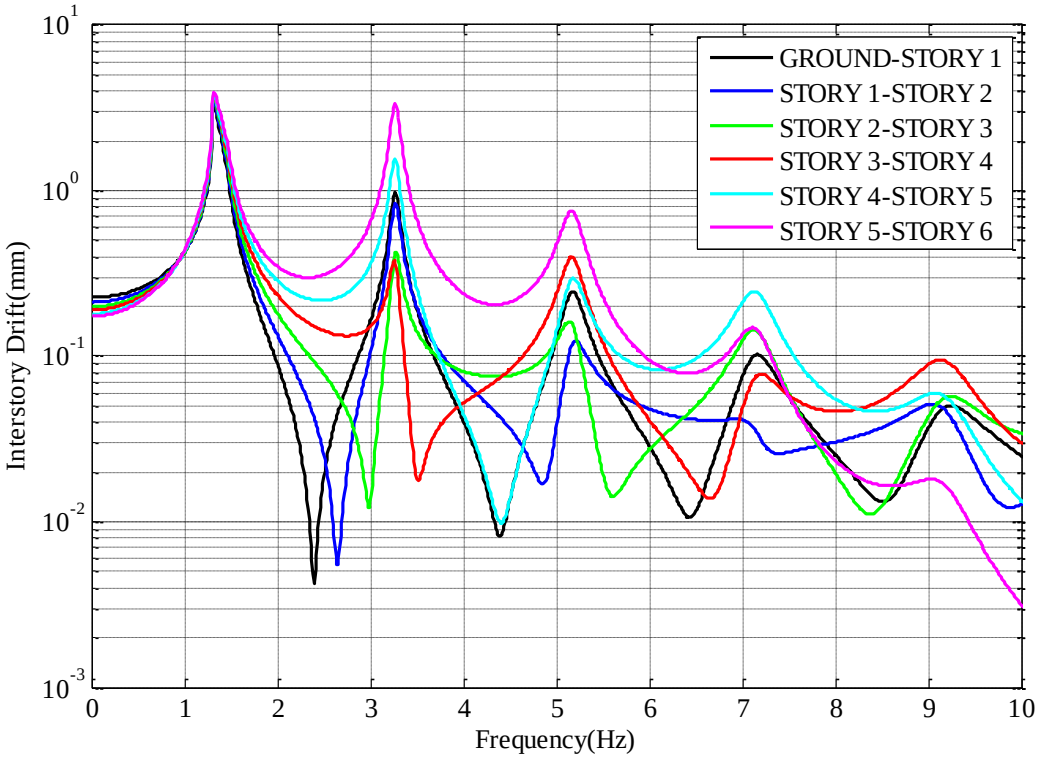

Figure 4.34 Interstory drift plot - Case study 1

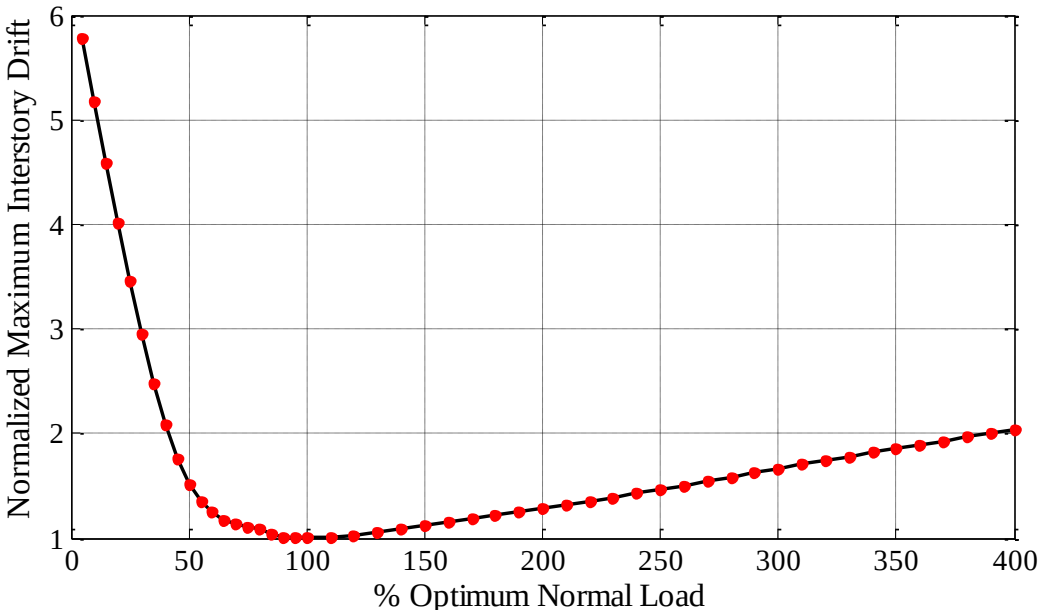

Figure 4.35 Verification plot - Case study 1

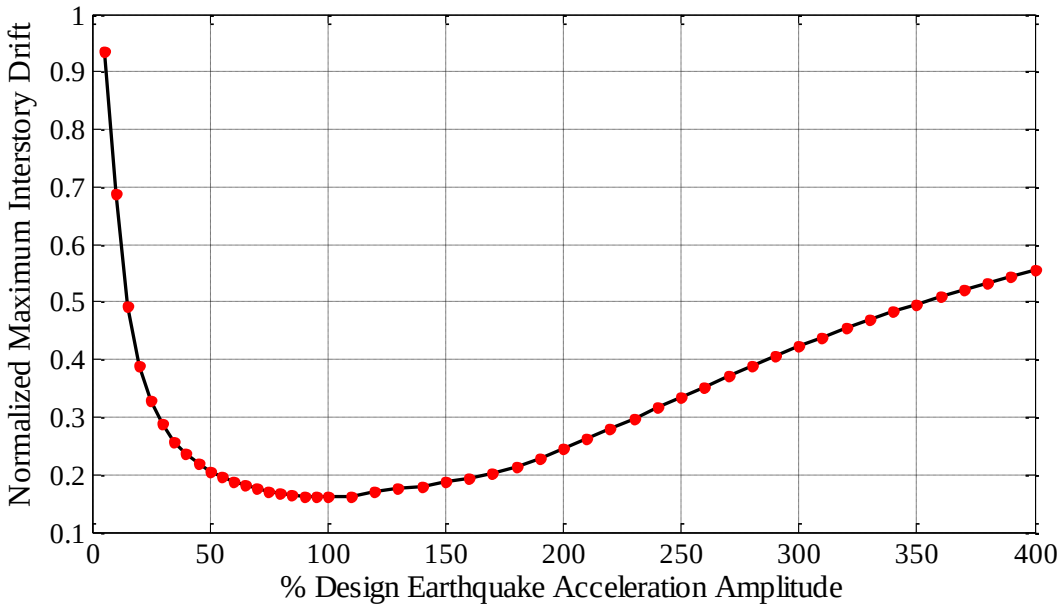

Figure 4.36 Response of the building for different design earthquake ground acceleration magnitudes - Case study 1

4.4.2. Case Study 2 - Optimization with 6 Different Dampers

In this case study, installation of 6 different dampers is investigated and the optimum PS values for all the dampers are determined.

Results of the optimization are given in Table 4.3 and the maximum interstory drift at 1.32 Hz is reduced to 3.71mm as shown in Figure 4.37

Figure 4.38 shows the verification of the results. Since the slope of Figure 4.38 at the right of the optimum value is less than the slope at the left of the optimum value, PS values slightly larger than the optimum values should be used in the design. Figure 4.39 shows the response of the building with optimum dampers for different design earthquake ground acceleration magnitudes and it can be concluded that at any earthquake ground acceleration value around the design

earthquake ground acceleration, the optimized dampers have a very good performance and decreases the building response drastically.

Table 4.3 Results of case study 2

Damper Location	**Opt. PS Value**
Ground - 1st Story	0.6767
1st Story - 2nd Story	0.6443
2nd Story - 3rd Story	0.5832
3rd Story - 4th Story	0.4922
4th Story - 5th Story	0.3912
5th Story - 6th Story	0.3279
Maximum Interstory Drift (mm)	**3.71**
Reduction for Maximum Interstory Drift (%)	**84.80**

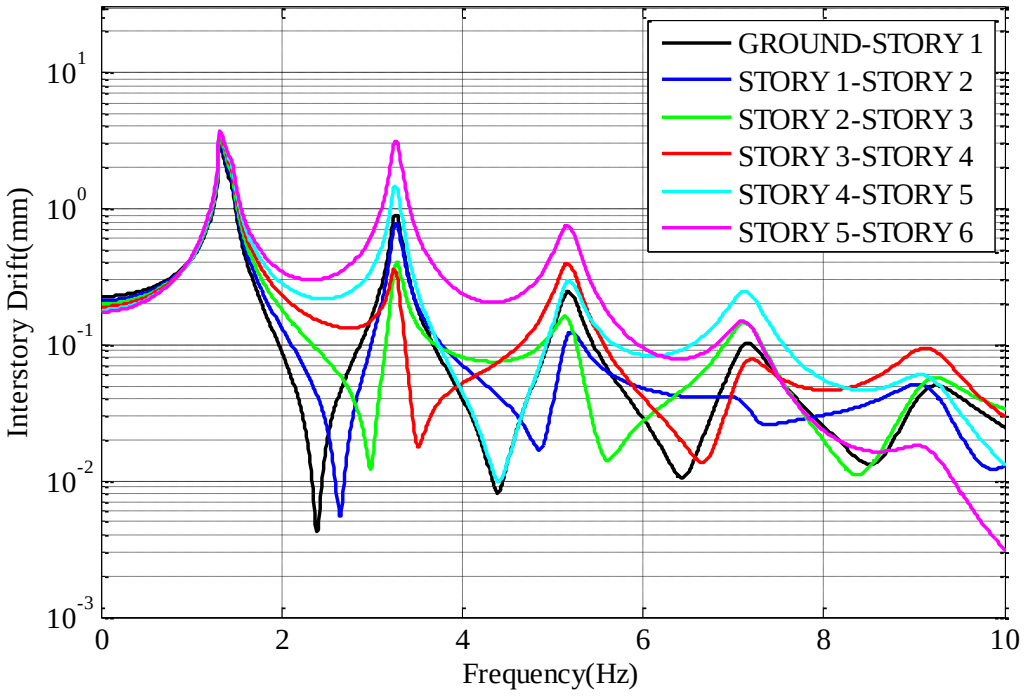

Figure 4.37 Interstory drift plot - Case study 2

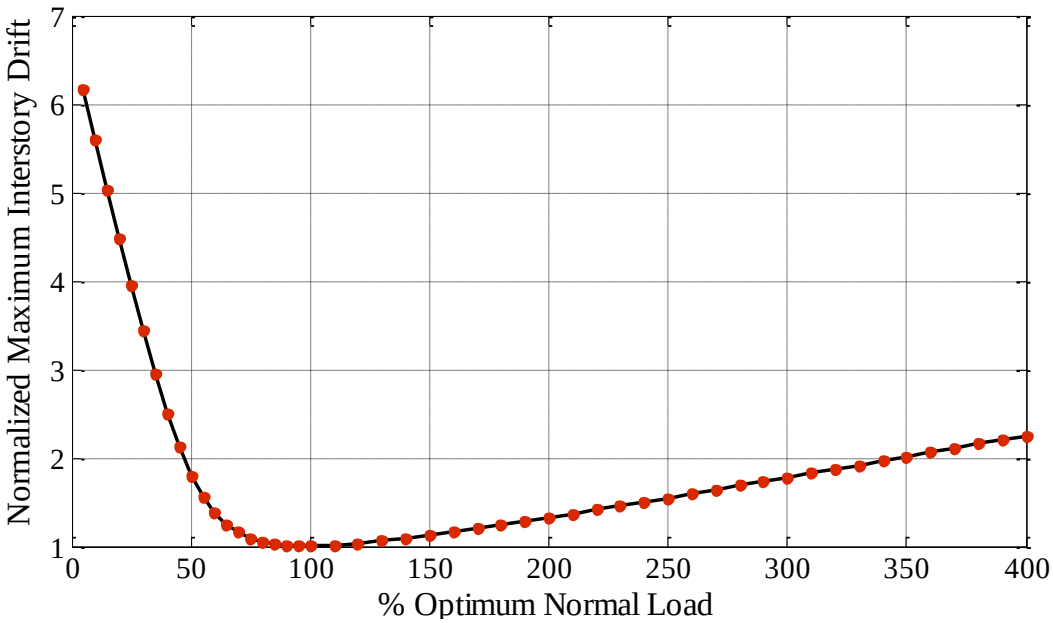

Figure 4.38 Verification plot - Case study 2

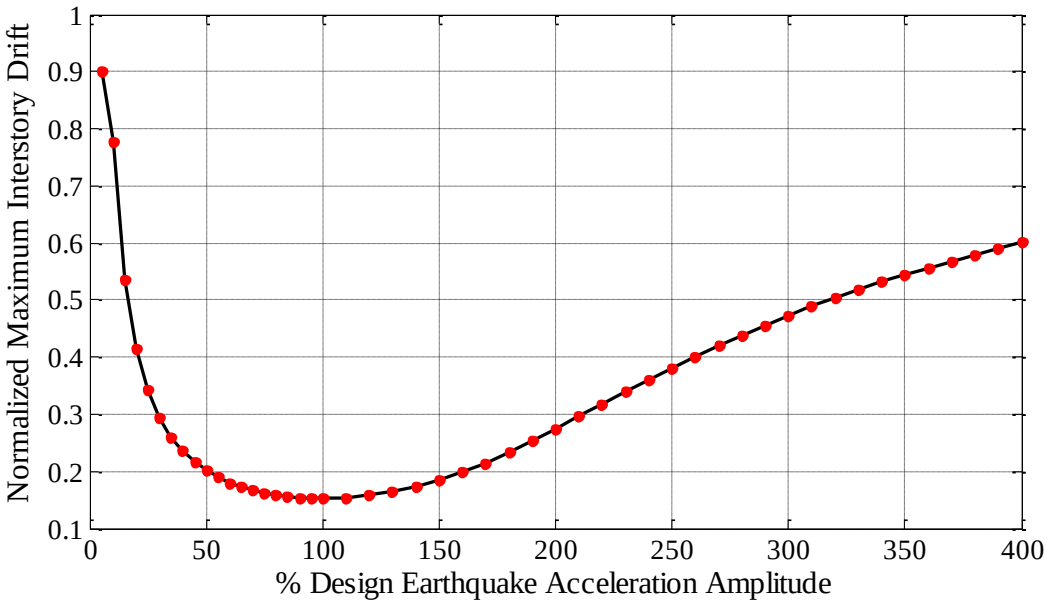

Figure 4.39 Response of the building for different design earthquake ground acceleration magnitudes - Case study 2

4.4.3. Case Study 3 - Optimization with 5 Identical Dampers

In this case study, installation of 5 identical dampers is investigated. It is a rather complex optimization problem since the placement of the dampers should also be optimized together with the PS values.

At the end of the optimization, the optimum value for *PS* is obtained as 0.6517 and the location of no dry friction damper is determined to be between ground and 1st story. The maximum interstory drift at 1.31 Hz is reduced to 4.82 mm as shown in Table 4.4 and Figure 4.40.

Figure 4.41 shows the verification of the results. Since the slope of Figure 4.41 at the right of the optimum value is less than the slope at the left of the optimum value, PS value slightly larger than the optimum value, i.e. 0.6517, should be used in the design. Figure 4.42 shows the response of the building with optimum dampers for different design earthquake ground acceleration magnitudes and it can be concluded that at any earthquake ground acceleration value around the design earthquake ground acceleration, the optimized dampers have a very good performance and decreases the building response drastically.

Table 4.4 Results of case study 3

Damper Location	**Opt. PS Value**
Ground - 1st Story	X
1st Story - 2nd Story	0.6517
2nd Story - 3rd Story	0.6517
3rd Story - 4th Story	0.6517
4th Story - 5th Story	0.6517
5th Story - 6th Story	0.6517
Maximum Interstory Drift (mm)	**4.82**
Reduction for Maximum Interstory Drift (%)	**80.25**

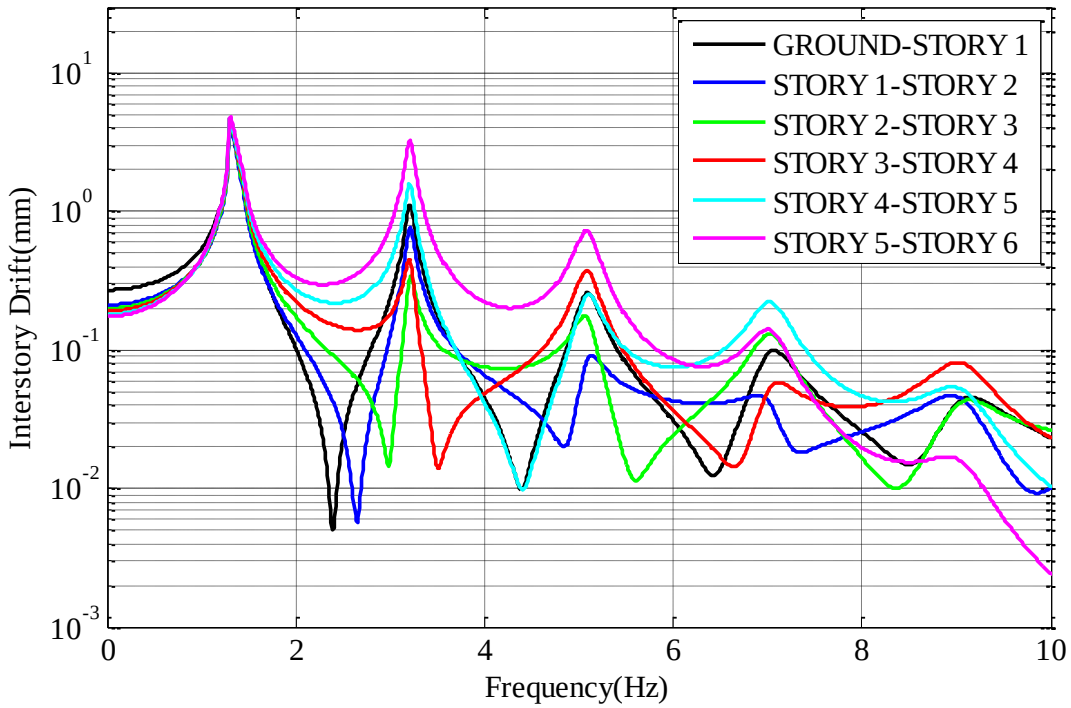

Figure 4.40 Interstory drift plot - Case study 3

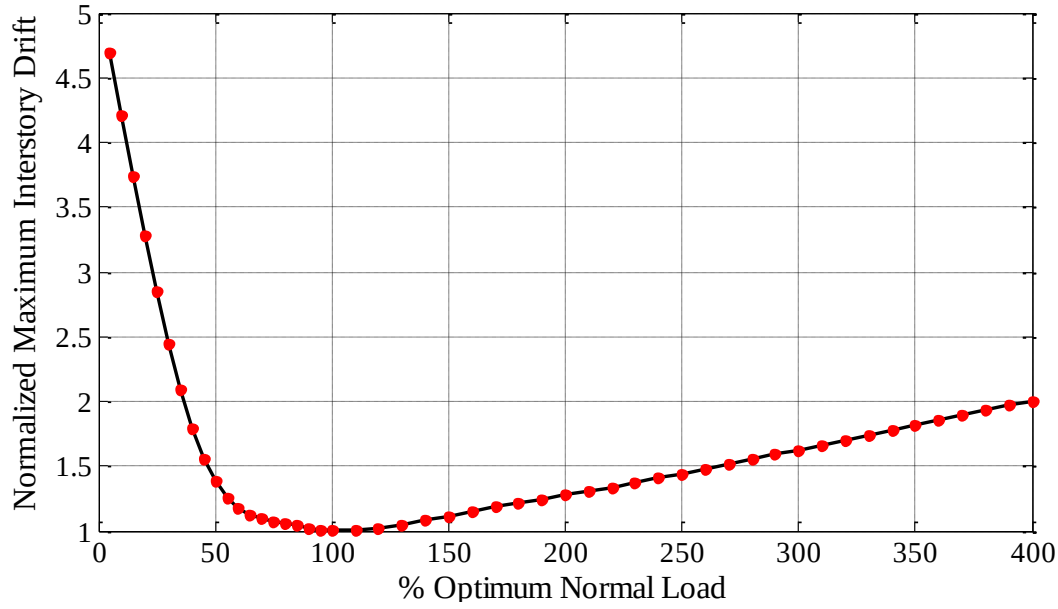

Figure 4.41 Verification plot - Case study 3

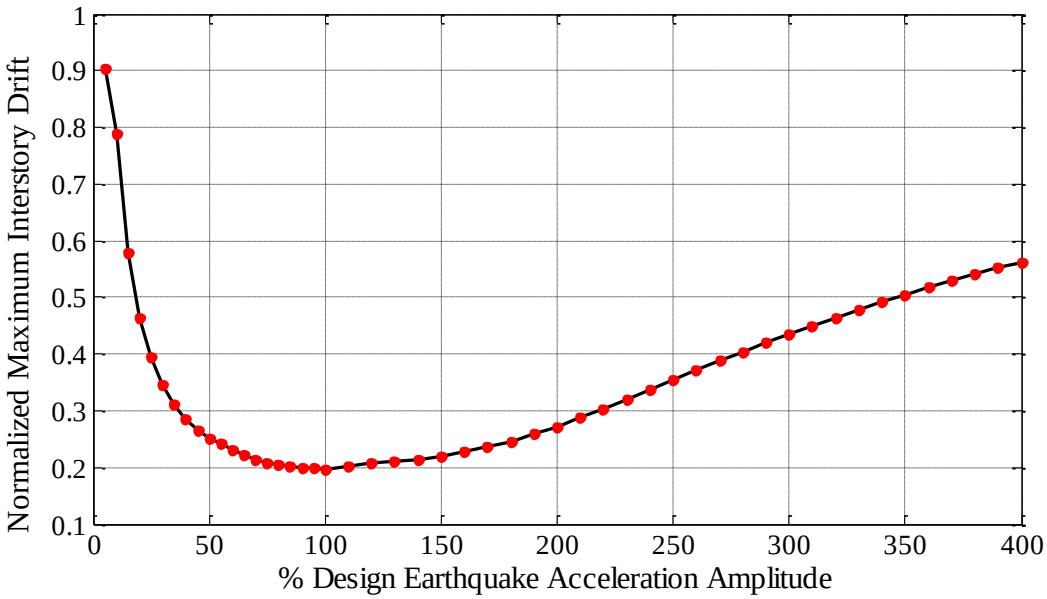

Figure 4.42 Response of the building for different design earthquake ground acceleration magnitudes - Case study 3

4.4.4. Case Study 4 - Optimization with 5 Different Dampers

In this case study, installation of 5 different dampers is investigated and the optimum PS values of all the dampers and locations are determined.

Results of the optimization are given in Table 4.5 and the maximum interstory drift at 1.3 Hz is reduced to 4.54 mm as shown in Figure 4.43.

Figure 4.44 shows the verification of the results. Since the slope of Figure 4.44 at the right of the optimum value is less than the slope at the left of the optimum value, PS values slightly larger than the optimum values should be used in the design. Figure 4.45 shows the response of the building with optimum dampers for different design earthquake ground acceleration magnitudes and it can be concluded that at any earthquake ground acceleration value around the design

earthquake ground acceleration, the optimized dampers have a very good performance and decreases the building response drastically.

Table 4.5 Results of case study 4

Damper Location	**Opt. PS Value**
Ground - 1st Story	X
1st Story - 2nd Story	0.7814
2nd Story - 3rd Story	0.706
3rd Story - 4th Story	0.5922
4th Story - 5th Story	0.4591
5th Story - 6th Story	0.3834
Maximum Interstory Drift (mm)	**4.54**
Reduction for Maximum Interstory Drift (%)	**81.39**

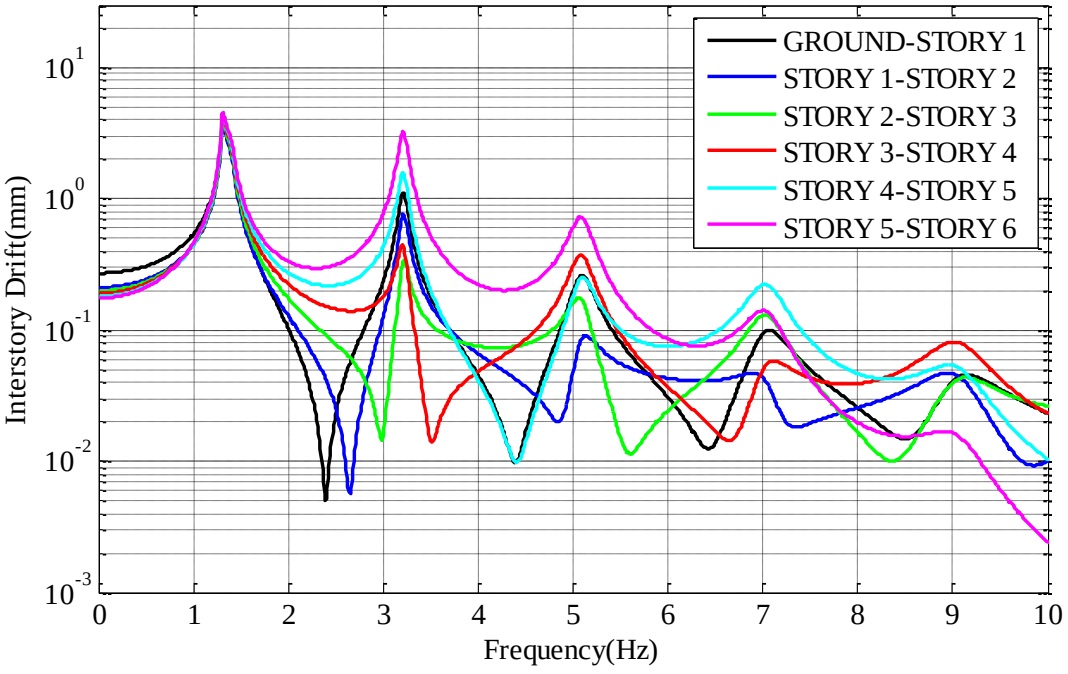

Figure 4.43 Interstory drift plot - Case study 4

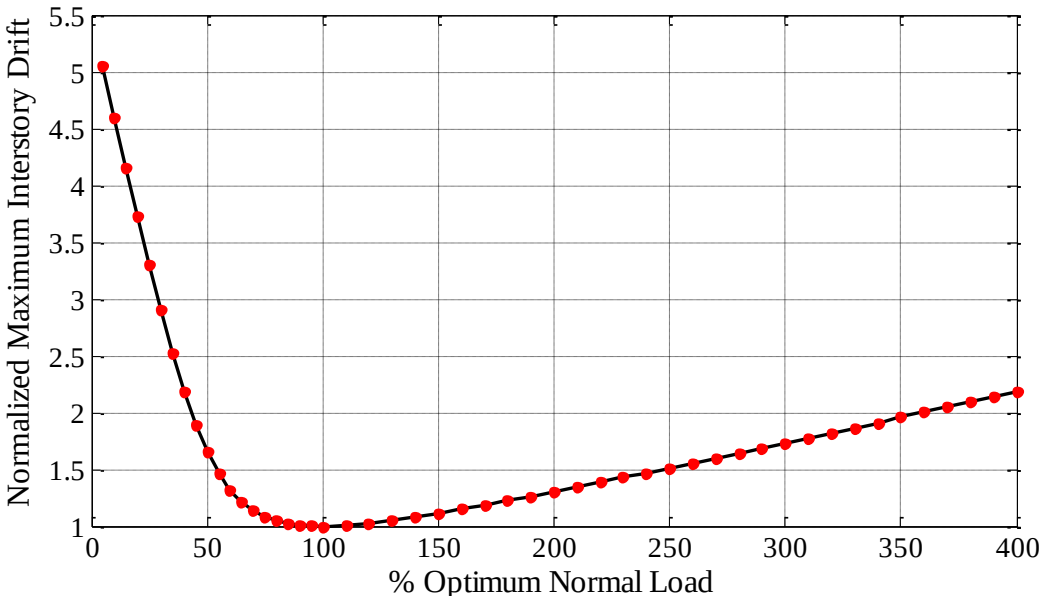

Figure 4.44 Verification plot - Case study 4

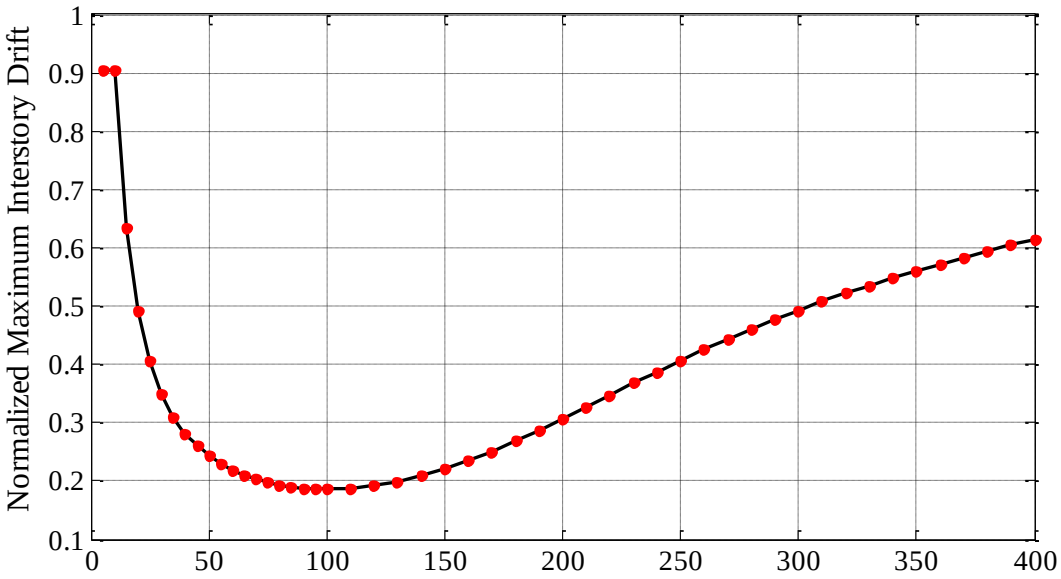

Figure 4.45 Response of the building for different design earthquake ground acceleration magnitudes - Case study 4

4.4.5. Case Study 5 - Optimization with 3 Identical Dampers

In this case study, installation of 3 identical dampers is investigated.

At the end of the optimization process, the optimum value for *PS* is obtained as 0.9116 and the optimum damper locations are determined as the first three stories. The maximum interstory drift at 1.29 Hz is reduced to 6.7 mm as shown in Table 4.6 and Figure 4.46.

Figure 4.47 shows the verification of the results. Since the slope of Figure 4.47 at the right of the optimum value is less than the slope at the left of the optimum value, *PS* value slightly larger than the optimum value, i.e. 0.9116, should be used in the design. Figure 4.48 shows the response of the building with optimum dampers for different design earthquake ground acceleration magnitudes and it can be concluded that at any earthquake ground acceleration value around the design earthquake ground acceleration, the optimized dampers have a very good performance and decreases the building response drastically.

Table 4.6 Results of case study 5

Damper Location	**Opt. PS Value**
Ground - 1st Story	0.9116
1st Story - 2nd Story	0.9116
2nd Story - 3rd Story	0.9116
3rd Story - 4th Story	X
4th Story - 5th Story	X
5th Story - 6th Story	X
Maximum Interstory Drift (mm)	**6.7**
Reduction for Maximum Interstory Drift (%)	**72.54**

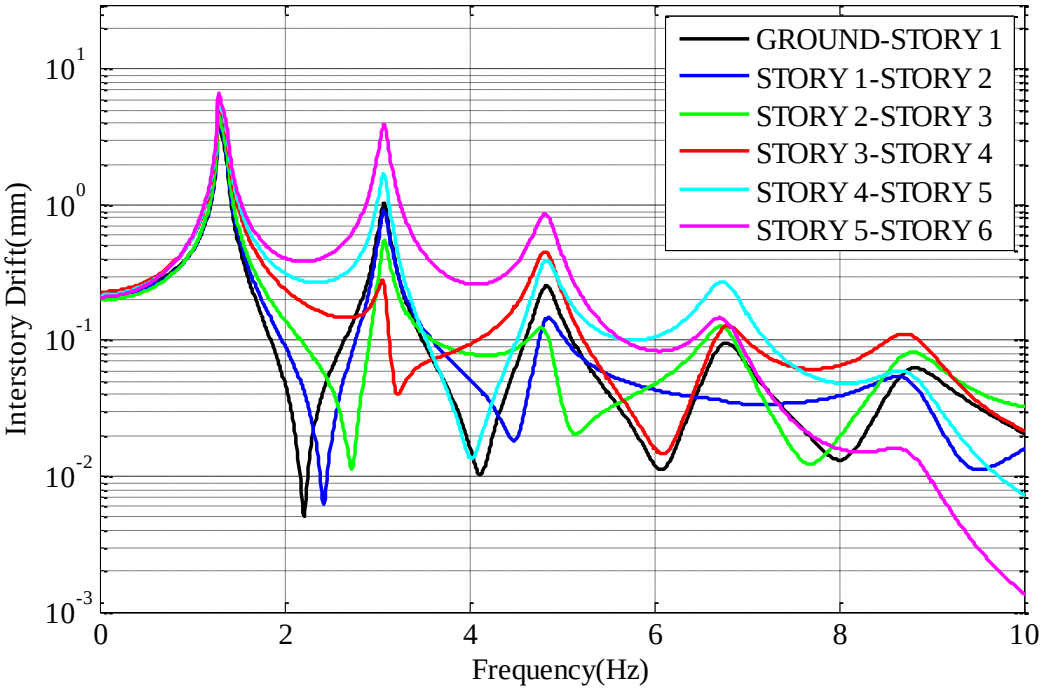

Figure 4.46 Interstory drift plot - Case study 5

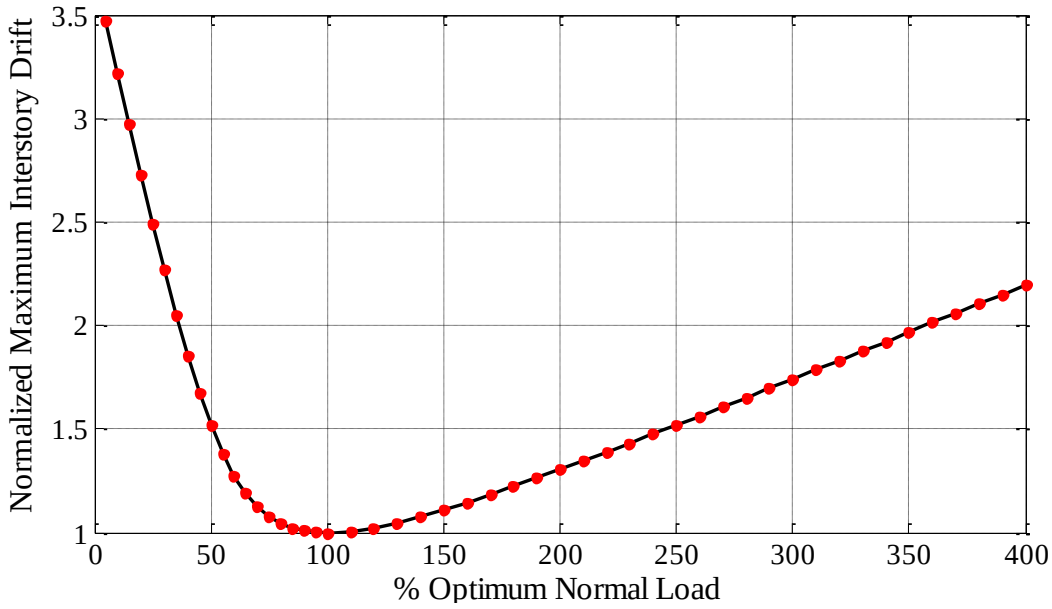

Figure 4.47 Verification plot - Case study 5

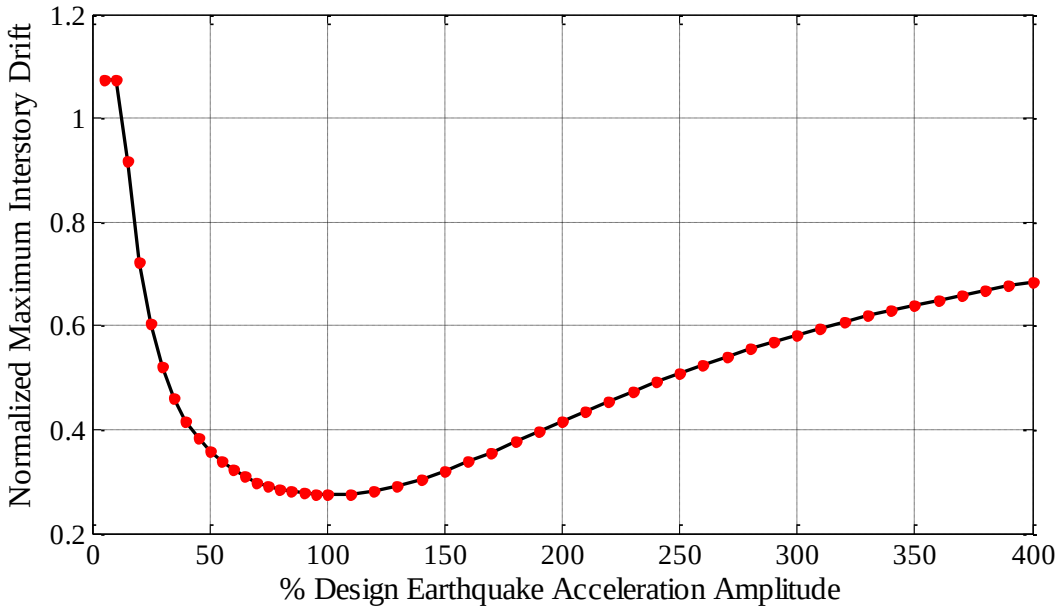

Figure 4.48 Response of the building for different design earthquake ground acceleration magnitudes - Case study 5

4.4.6. Case Study 6 - Optimization with 3 Different Dampers

In this case study, installation of 3 different dampers is investigated and the optimum PS values of all the dampers and their locations are determined.

Results of the optimization are given in Table 4.7 and the maximum interstory drift at 1.29 Hz is reduced to 6.68 mm as shown in Figure 4.49.

Figure 4.50 shows the verification of the results. Since the slope of Figure 4.50 at the right of the optimum value is less than the slope at the left of the optimum value, PS values slightly larger than the optimum values should be used in the design. Figure 4.51 shows the response of the building with optimum dampers for different design earthquake ground acceleration magnitudes and it can be concluded that at any earthquake ground acceleration value around the design earthquake ground acceleration, the optimized dampers have a very good performance and decreases the building response drastically.

Table 4.7 Results of case study 6

Damper Location	**Opt. PS Value**
Ground - 1st Story	0.9678
1st Story - 2nd Story	0.9278
2nd Story - 3rd Story	0.8477
3rd Story - 4th Story	X
4th Story - 5th Story	X
5th Story - 6th Story	X
Maximum Interstory Drift (mm)	**6.68**
Reduction for Maximum Interstory Drift (%)	**72.62**

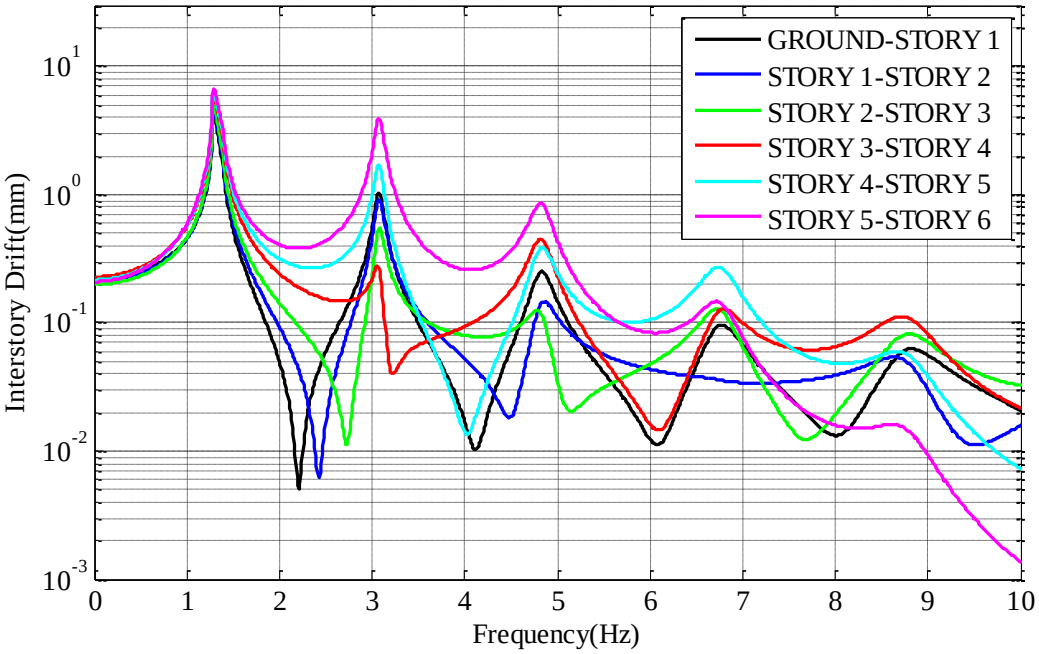

Figure 4.49 Interstory drift plot - Case study 6

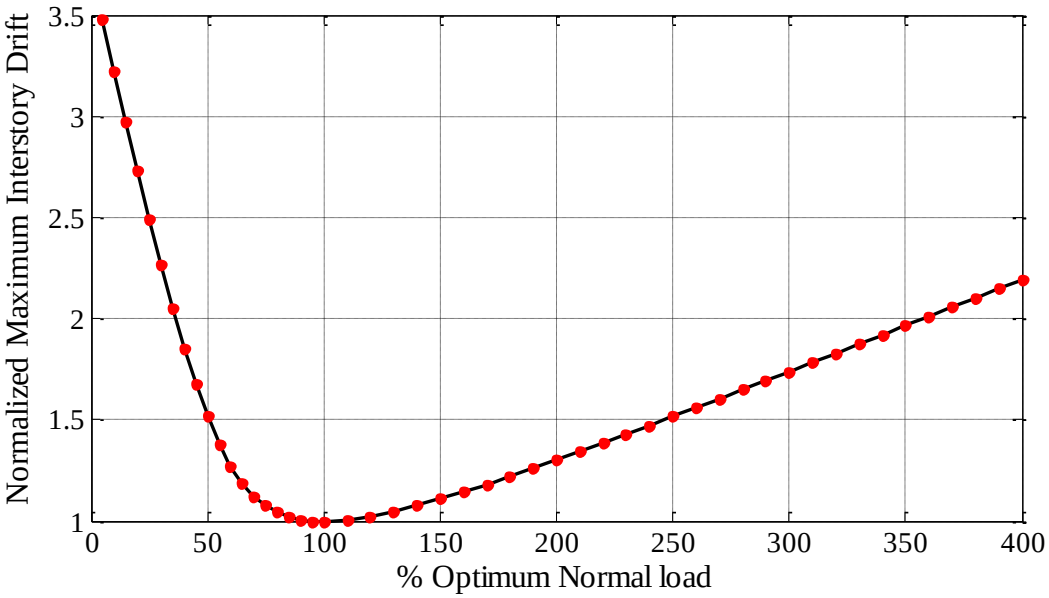

Figure 4.50 Verification plot - Case study 6

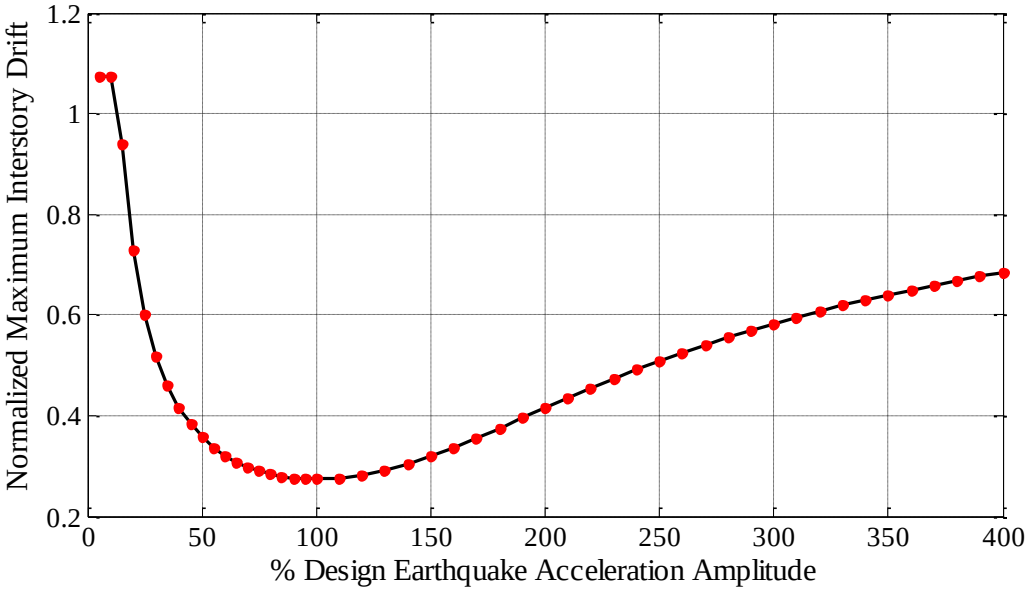

Figure 4.51 Response of the building for different design earthquake ground acceleration magnitudes - Case study 6

4.4.7. Case Study 7 - Optimization with a Single Damper

In this case study, integration of only a single damper is investigated and the optimum PS value and the location of the damper is determined.

At the end of the optimization, the optimum dry friction damper location is determined between the 1st and the 2nd story and the optimum value for PS is obtained as 1.8182. Results of the optimization are given in Table 4.8. The maximum interstory drift at 1.27 Hz is reduced to 13.05 mm as shown in Figure 4.52.

Figure 4.53 shows the verification of the results. Since the slope of Figure 4.53 at the right of the optimum value is less than the slope at the left of the optimum value, PS value slightly larger than the optimum value, i.e. 1.8182, should be used in the design. Figure 4.54 shows the response of the building with optimum dampers for different design earthquake ground acceleration magnitudes. For small design earthquake acceleration magnitudes, the damper can not slip so the normalized maximum interstory drift magnitude becomes constant as can be seen from the first four points of Figure 4.54 it can be concluded that at any earthquake ground acceleration value around the design earthquake ground acceleration, the optimized dampers have a very good performance and decreases the building response drastically.

Table 4.8 Results of case study 7

Damper Location	**Opt. PS Value**
Ground - 1st Story	X
1st Story - 2nd Story	1.8182
2nd Story - 3rd Story	X
3rd Story - 4th Story	X
4th Story - 5th Story	X
5th Story - 6th Story	X
Maximum Interstory Drift (mm)	**13.05**
Reduction for Maximum Interstory Drift (%)	**46.52**

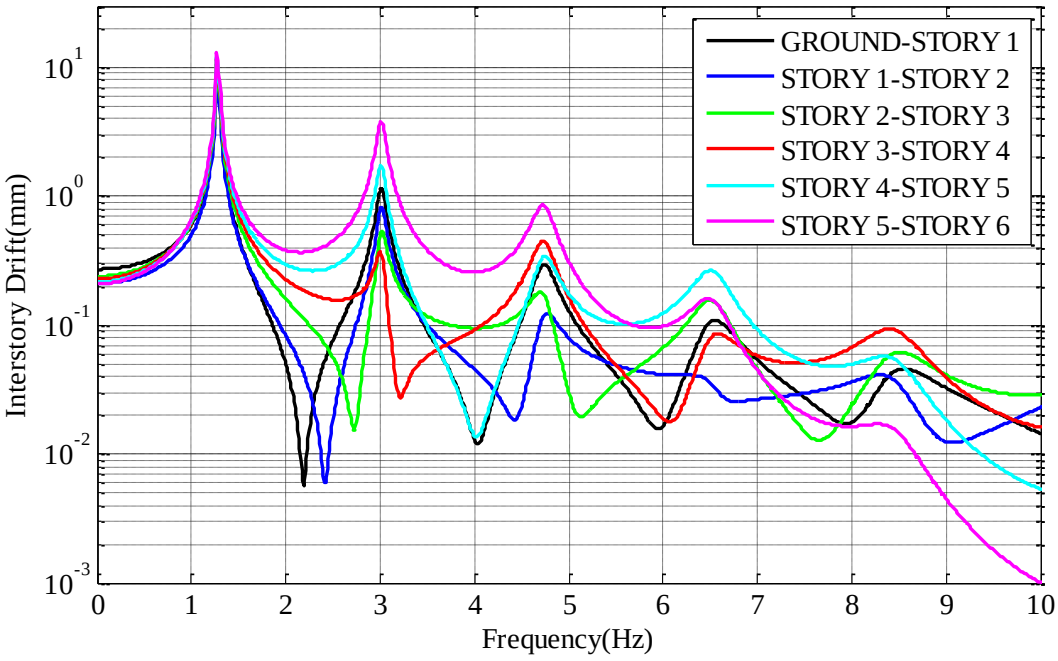

Figure 4.52 Interstory drift plot - Case study 7

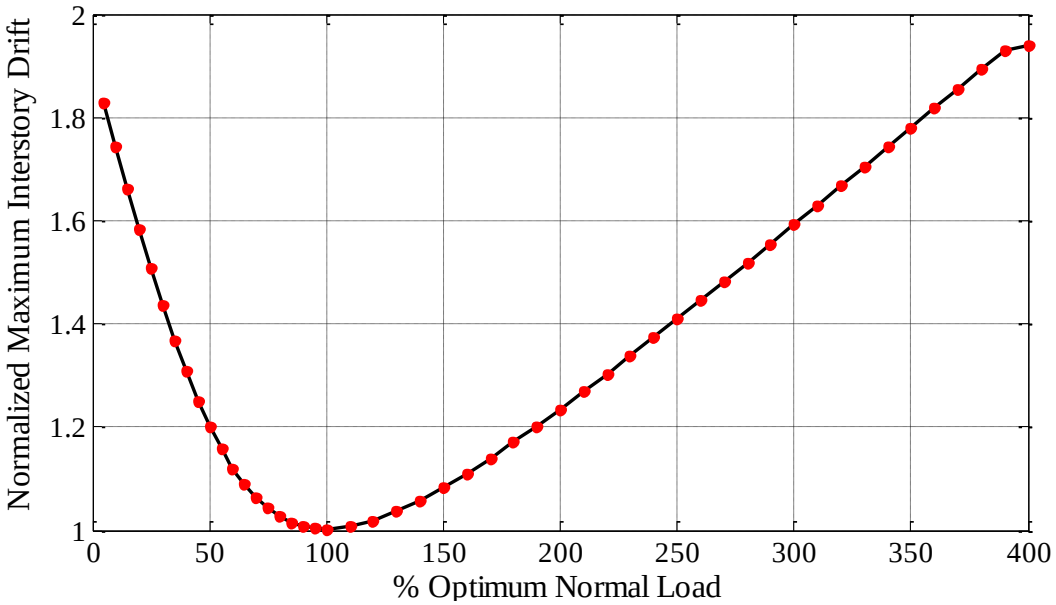

Figure 4.53 Verification plot - Case study 7

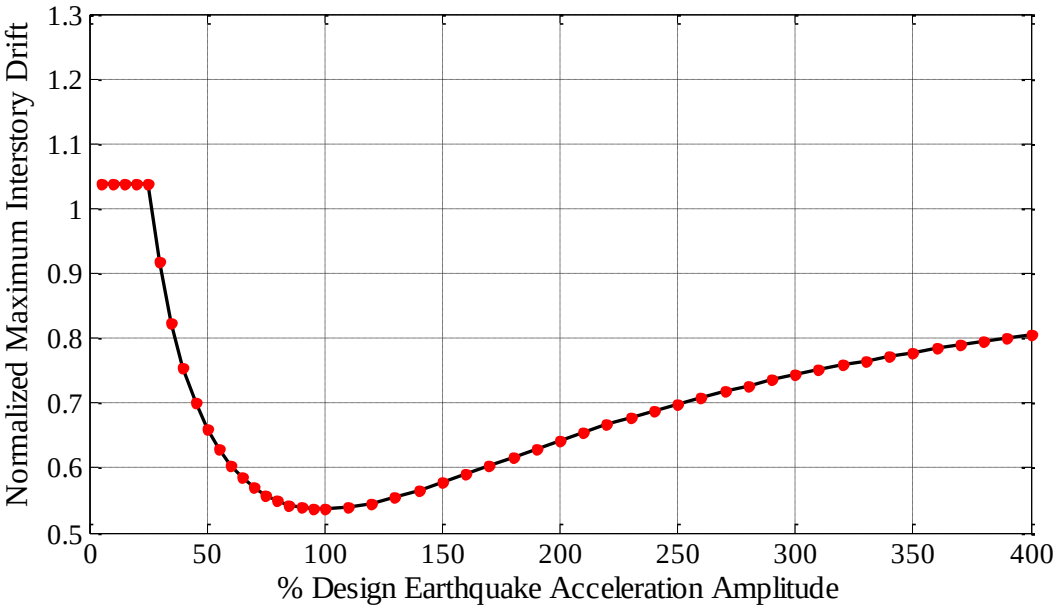

Figure 4.54 Response of the building for different design earthquake ground acceleration magnitudes - Case study 7

Optimization verification curves for identical dampers are given in Figure 4.55 and for different dampers are given in Figure 4.56. From these graphs, it can be seen that for all case studies, minimum interstory drift is obtained with the optimised damper determined during the optimization studies.

Comparison of the maximum interstory drift values for seven different cases investigated in this section is given in Figure 4.57 and Figure 4.58. From these results it is seen that maximum interstory drift can be decreased up to 84.8% if six different dampers are used. Another outcome of these case studies is, although the number of dampers are important for the reduction of the maximum interstory drift, instead of using different dampers identical dampers may be used since the difference between them is insignificant if dry friction dampers are accurately optimized.

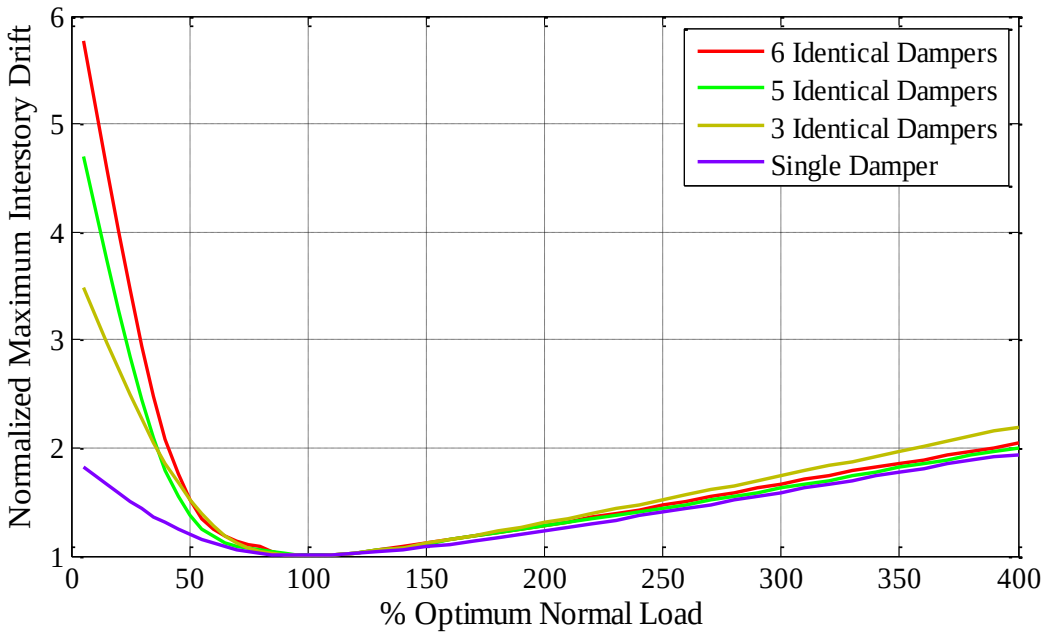

Figure 4.55 Verification plot - Identical friction dampers at adjacent stories

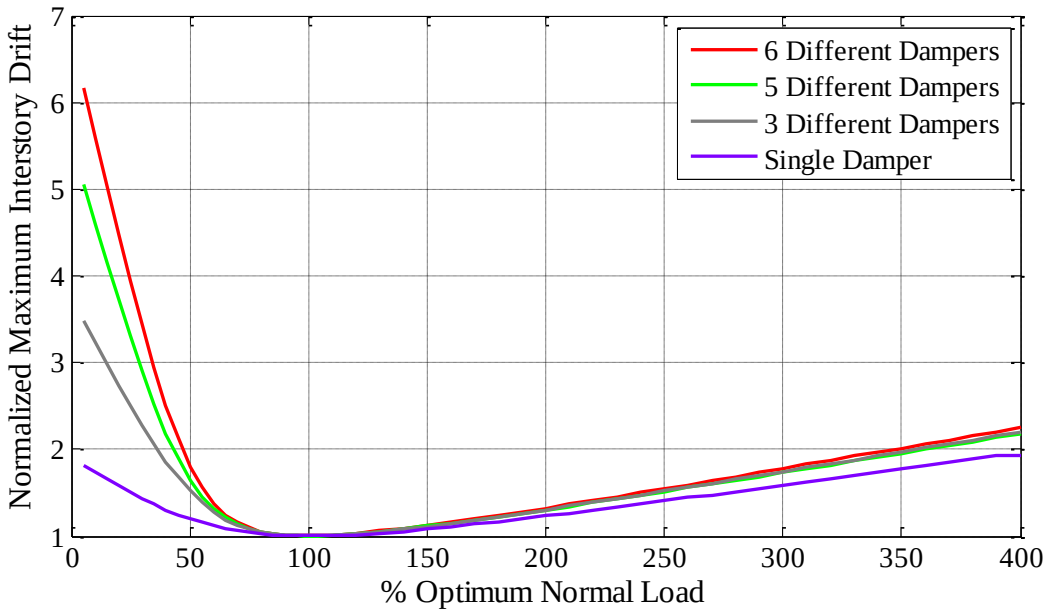

Figure 4.56 Verification plot - Different friction dampers at adjacent stories

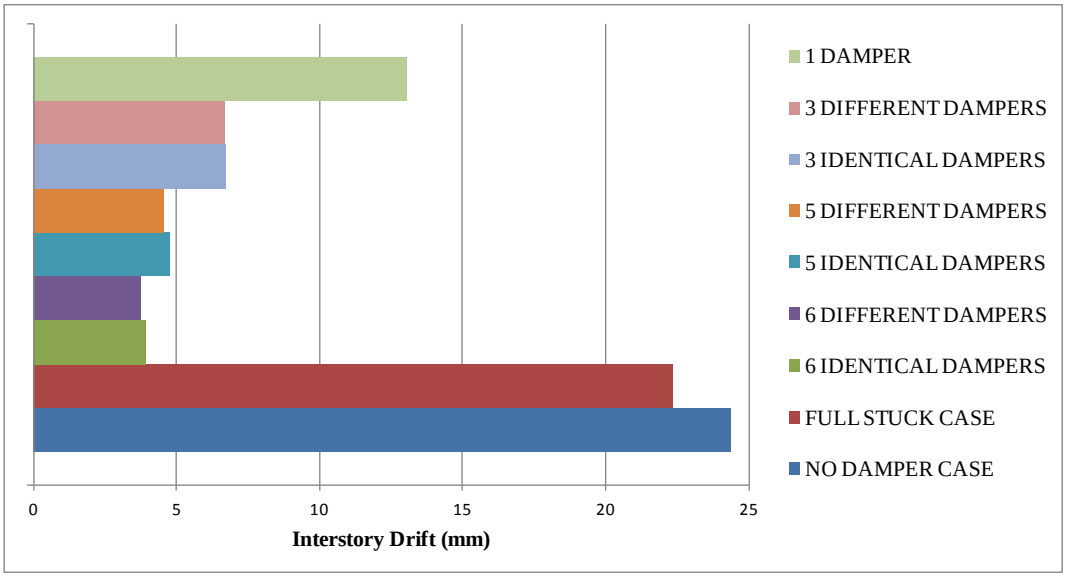

Figure 4.57 Comparison of maximum interstory drift values of the building having friction dampers only at adjacent stories

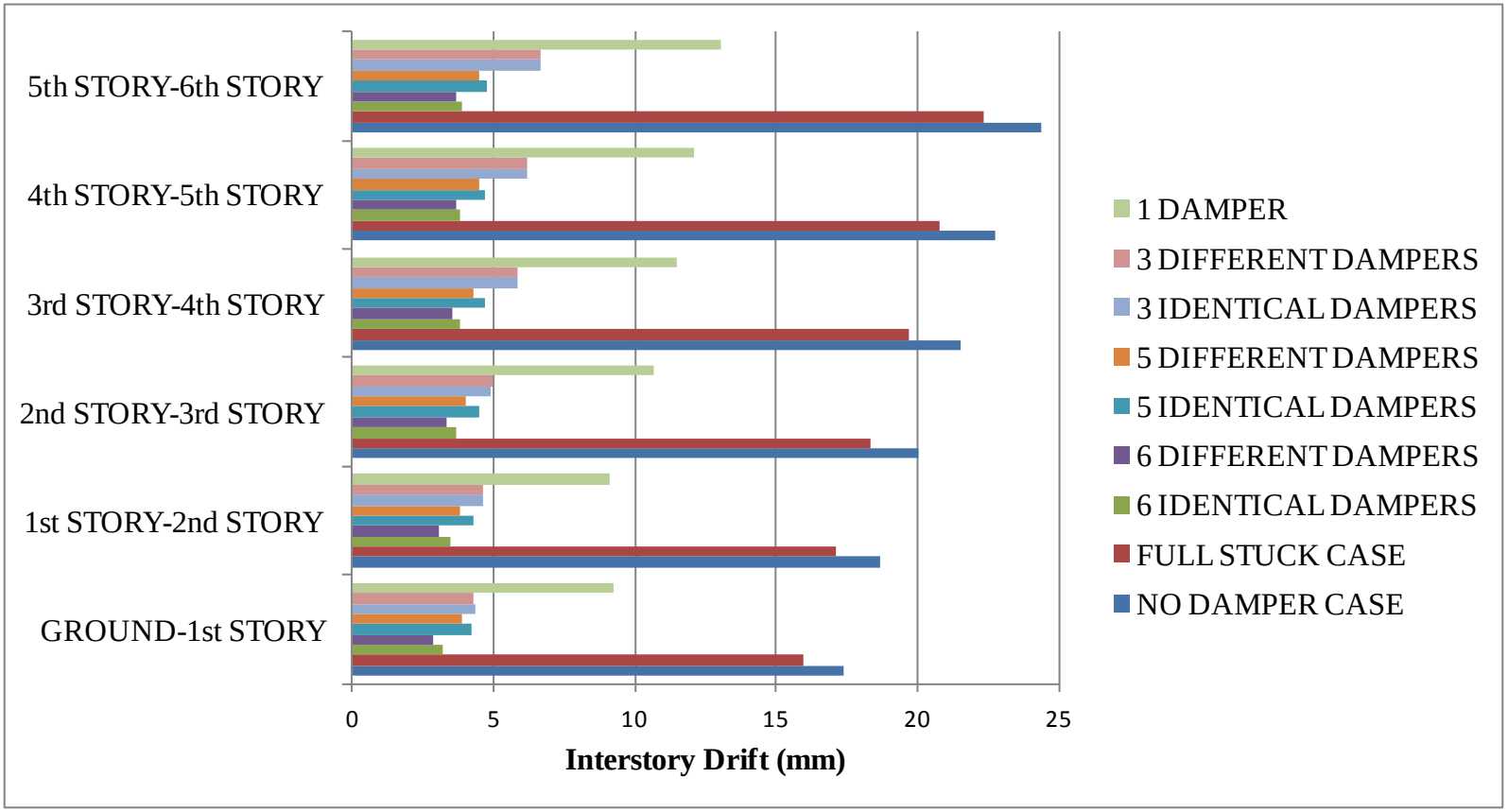

Figure 4.58 Comparison of interstory drift values of the building having friction dampers only at adjacent stories

4.5. Optimization Studies on a Multistory Building with Different Damper Configurations

In this part of the thesis, in order to determine the effect of damper configuration on building response, dry friction dampers are connected between q^{th} and $(q+2)^{th}$ stories as shown in Figure 4.59. Buildings are investigated under the same sinusoidal ground acceleration with a magnitude of 0.067m/s^2 and SR is kept constant as 0.2. Since the damper configurations change, the nonlinear forcing vector, $\{f_{NL}\}$, should be written for the new damper configurations.

For the building with full stuck dampers the maximum inter-story drift value is 16.74 mm at 1.67 Hz and it occurs between the 5th and the 6th stories as shown in Figure 4.60.

At the end of each case study, optimization results are verified and also response of the buildings with optimized dampers under different design earthquakes are investigated in the same manner as performed in Section 4.4.

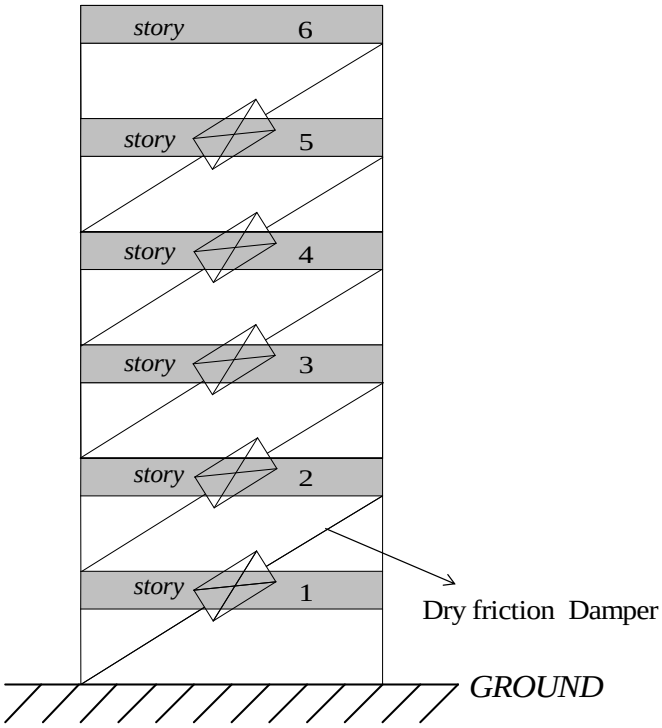

Figure 4.59 Shear building model for with alternative damper configuration

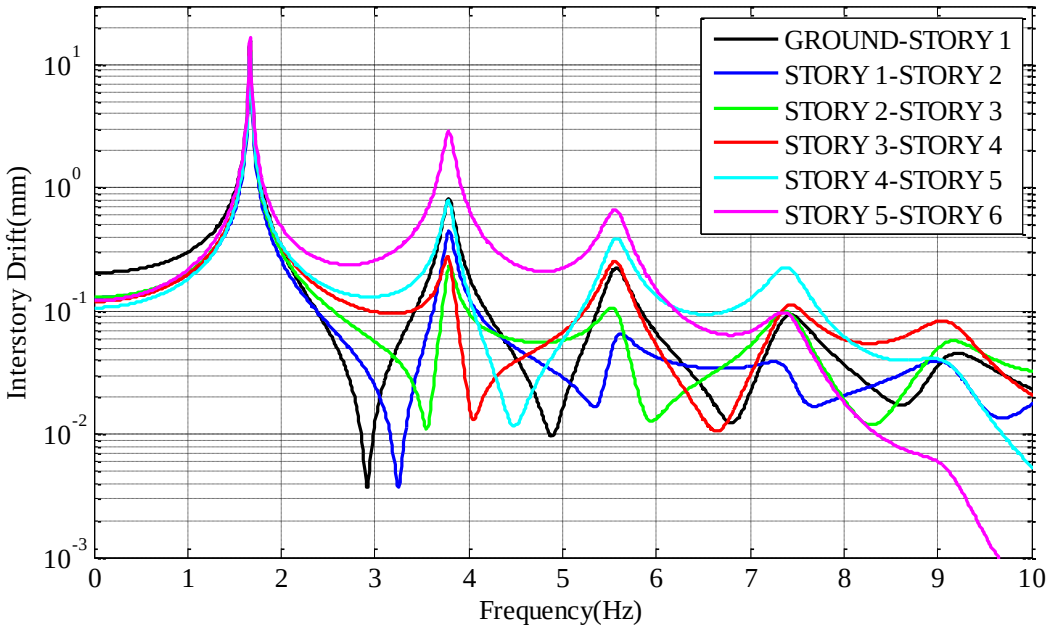

Figure 4.60 Interstory drift plot for alternative damper configuration (full stuck)

4.5.1. Case Study 8 - Optimization with 5 Identical Dampers for Alternative Damper Configuration

In this case study, installation of 5 identical dampers is investigated.

At the end of the optimization, the optimum value of *PS* is obtained as 0.2832 and the maximum interstory drift at 3.75 Hz is reduced to 1.23 mm as shown in Table 4.9 and Figure 4.61.

Figure 4.62 shows the verification of the results. It can be concluded that similar to the single story building, a correct choice of *PS* values should be different than the optimum values determined. Since the slope of Figure 4.62 at the right of the optimum value is less than the slope at the left of the optimum value, a *PS* value slightly larger than the optimum value, i.e. 0.2832, should be used in the design. Figure 4.63 shows the response of the building with optimum dampers for different design earthquake ground acceleration magnitudes and it can be concluded that at any earthquake ground acceleration value around the design earthquake ground acceleration, the optimized dampers have a very good performance and decreases the building response drastically.

Table 4.9 Results of case study 8

Damper Location	**Opt. PS Value**
Ground - 2nd Story	0.2832
1st Story - 3rd Story	0.2832
2nd Story - 4th Story	0.2832
3rd Story - 5th Story	0.2832
4th Story - 6th Story	0.2832
Maximum Interstory Drift (mm)	**1.23**
Reduction for Maximum Interstory Drift (%)	**94.96**

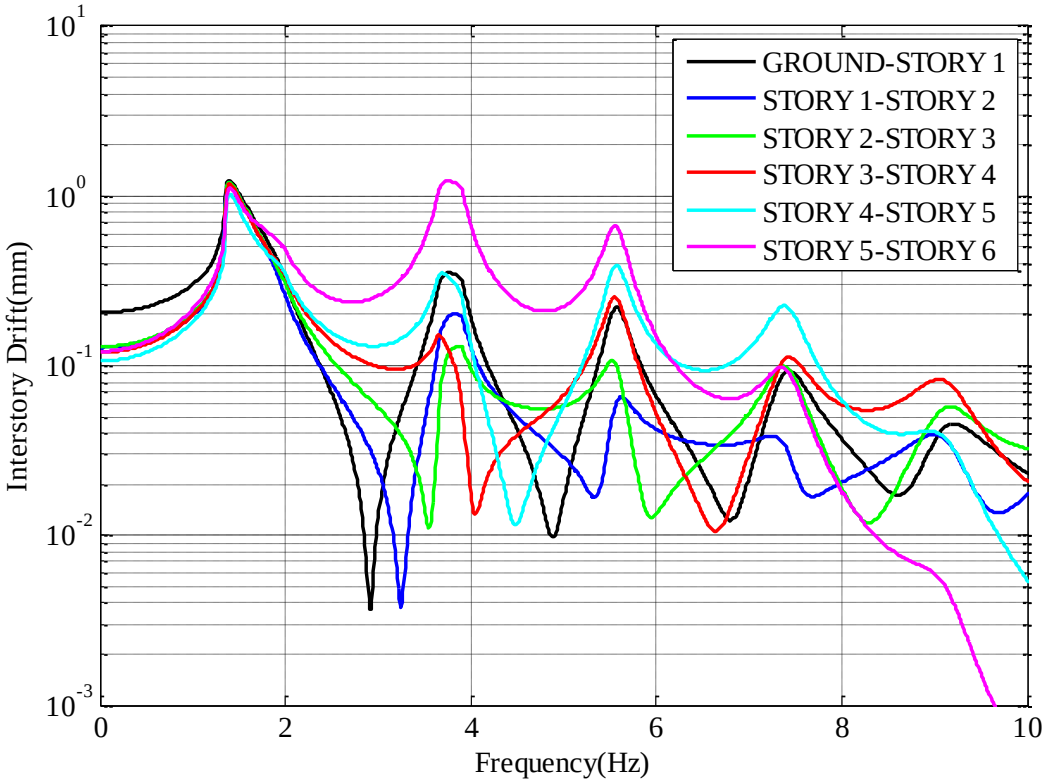

Figure 4.61 Interstory drift plot - Case study 8

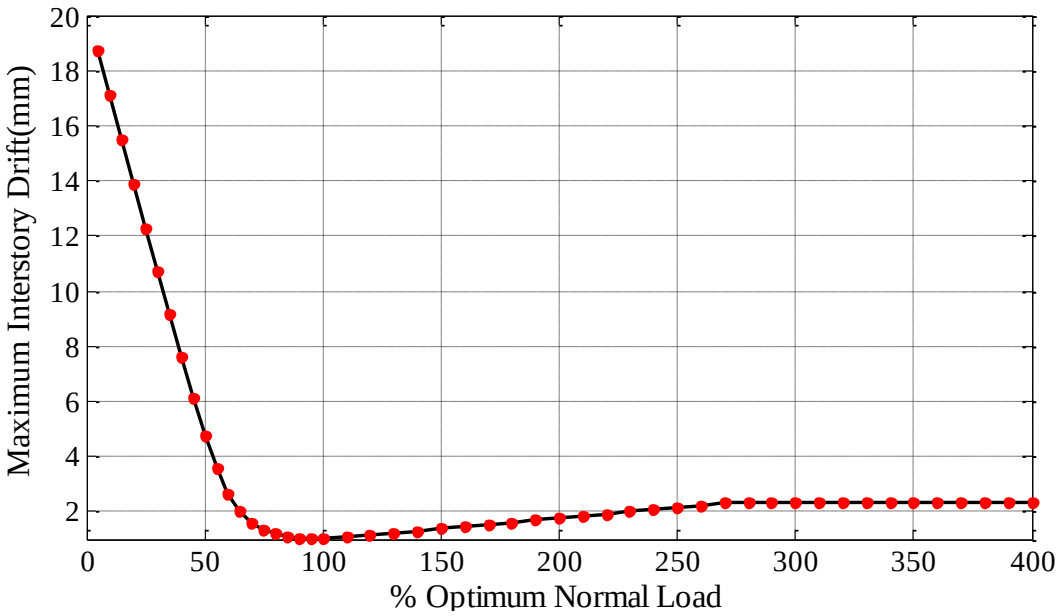

Figure 4.62 Verification plot - Case study 8

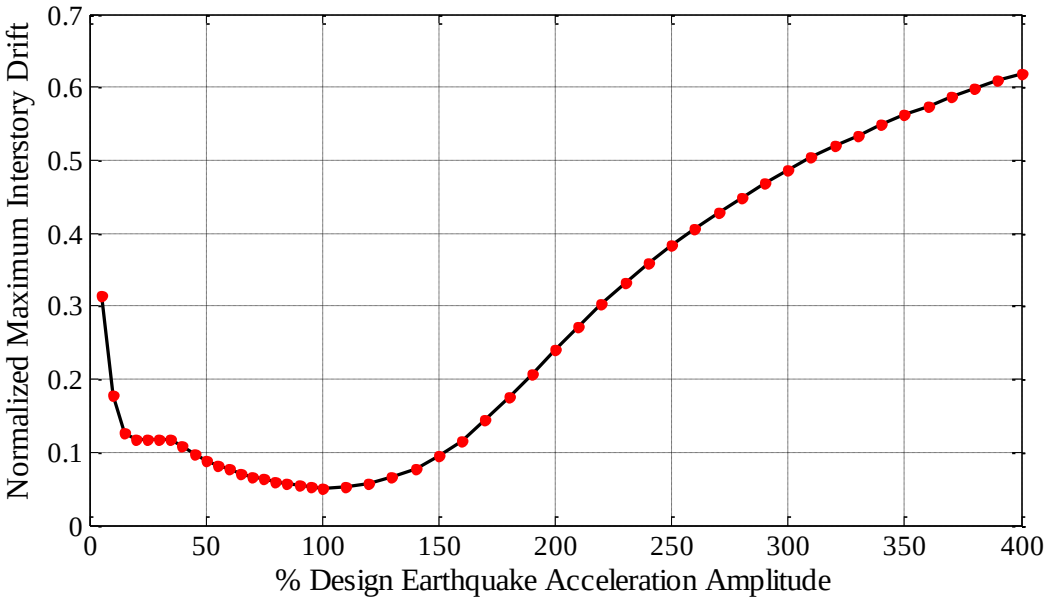

Figure 4.63 Response of the building for different design earthquake ground acceleration magnitudes - Case study 8

4.5.2. Case Study 9 - Optimization with 5 Different Dampers for Alternative Damper Configuration

In this case study, installation of 5 different dampers is investigated and the optimum PS values of all the dampers are determined.

Results of the optimization are given in Table 4.10 and the maximum interstory drift at 3.74 Hz is reduced to 1.10 mm as shown in Figure 4.64.

Figure 4.65 shows the verification of the results. Since the slope of Figure 4.65 at the right of the optimum value is less than the slope at the left of the optimum value, PS values slightly larger than the optimum values should be used in the design. Figure 4.66 shows the response of the building with optimum dampers for different design earthquake ground acceleration magnitudes and it can be concluded that at any earthquake ground acceleration value around the design

earthquake ground acceleration, the optimized dampers have a very good performance and decreases the building response drastically.

Table 4.10 Results of case study 9

Damper Location	**Opt. PS Value**
Ground - 2nd Story	0.3642
1st Story - 3rd Story	0.3222
2nd Story - 4th Story	0.261
3rd Story - 5th Story	0.2709
4th Story - 6th Story	0.2419
Maximum Interstory Drift (mm)	**1.1**
Reduction for Maximum Interstory Drift (%)	**95.49**

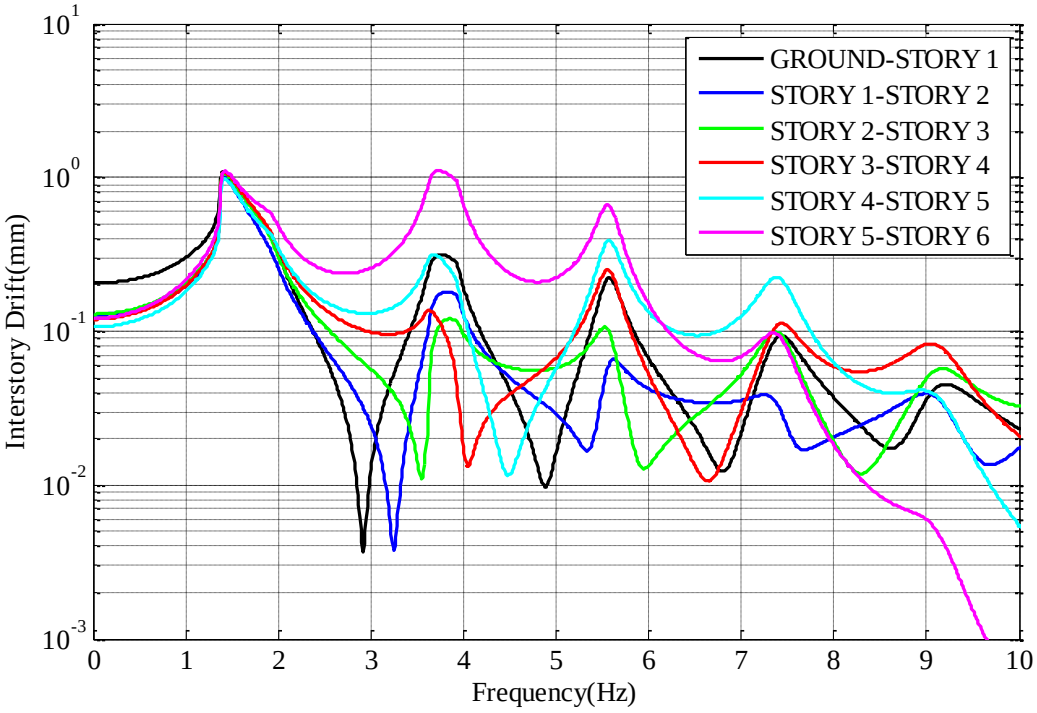

Figure 4.64 Interstory drift plot - Case study 9

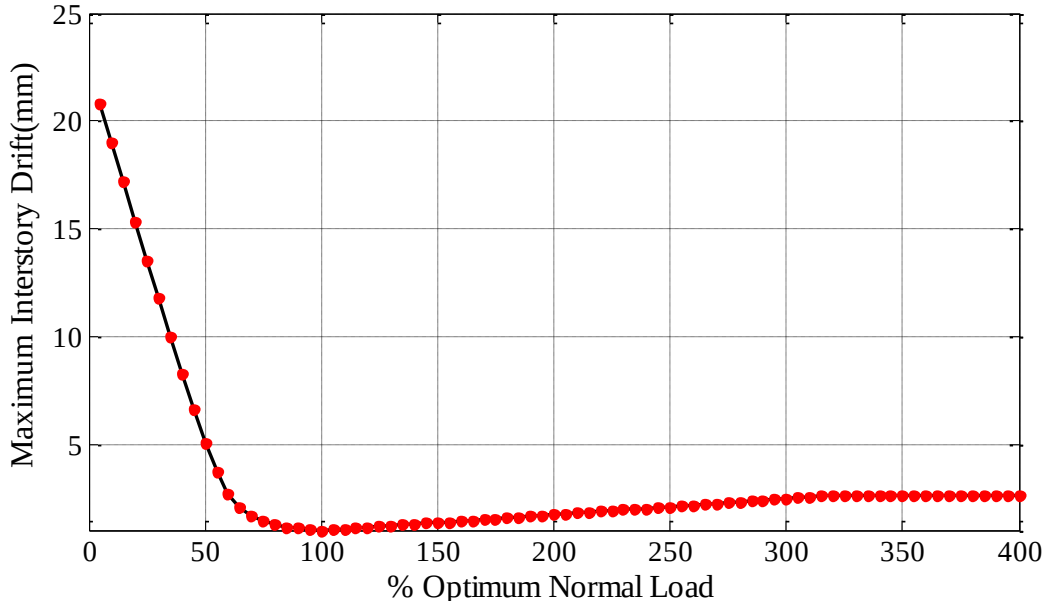

Figure 4.65 Verification plot - Case study 9

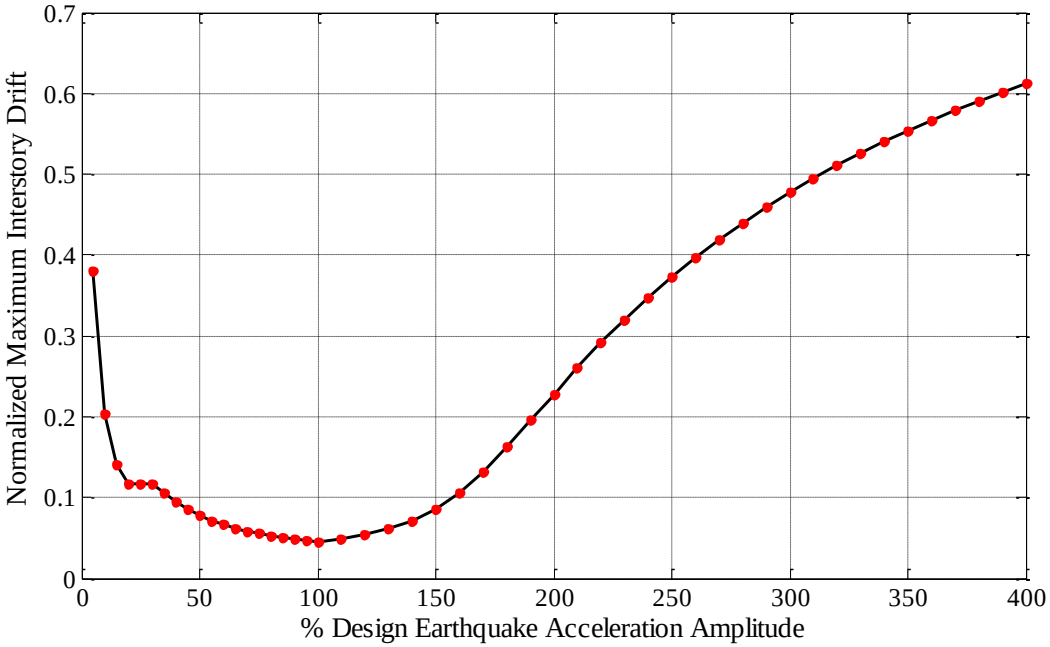

Figure 4.66 Response of the building for different design earthquake ground acceleration magnitudes - Case study 9

4.5.3. Case Study 10 - Optimization with 4 Identical Dampers for Alternative Damper Configuration

In this case study, installation of 4 identical dampers is investigated.

The optimum value for *PS* is obtained as 0.4126 and the location of no dry friction damper is determined to be between the 3rd and the 5th stories. The maximum interstory drift at 1.41 Hz is reduced to 1.51 mm as shown in Table 4.11 and Figure 4.67.

Figure 4.68 shows the verification of the results. Since the slope of Figure 4.68 at the right of the optimum value is less than the slope at the left of the optimum value, *PS* value slightly larger than the optimum value, i.e. 0.4126, should be used in the design. Figure 4.69 shows the response of the building with optimum dampers for different design earthquake ground acceleration magnitudes and it can be concluded that at any earthquake ground acceleration value around the design earthquake ground acceleration, the optimized dampers have a very good performance and decreases the building response drastically.

Table 4.11 Results of case study 10

Damper Location	**Opt. PS Value**
Ground - 2nd Story	0.4126
1st Story - 3rd Story	0.4126
2nd Story - 4th Story	0.4126
3rd Story - 5th Story	X
4th Story - 6th Story	0.4126
Maximum Interstory Drift (mm)	**1.51**
Reduction for Maximum Interstory Drift (%)	**93.81**

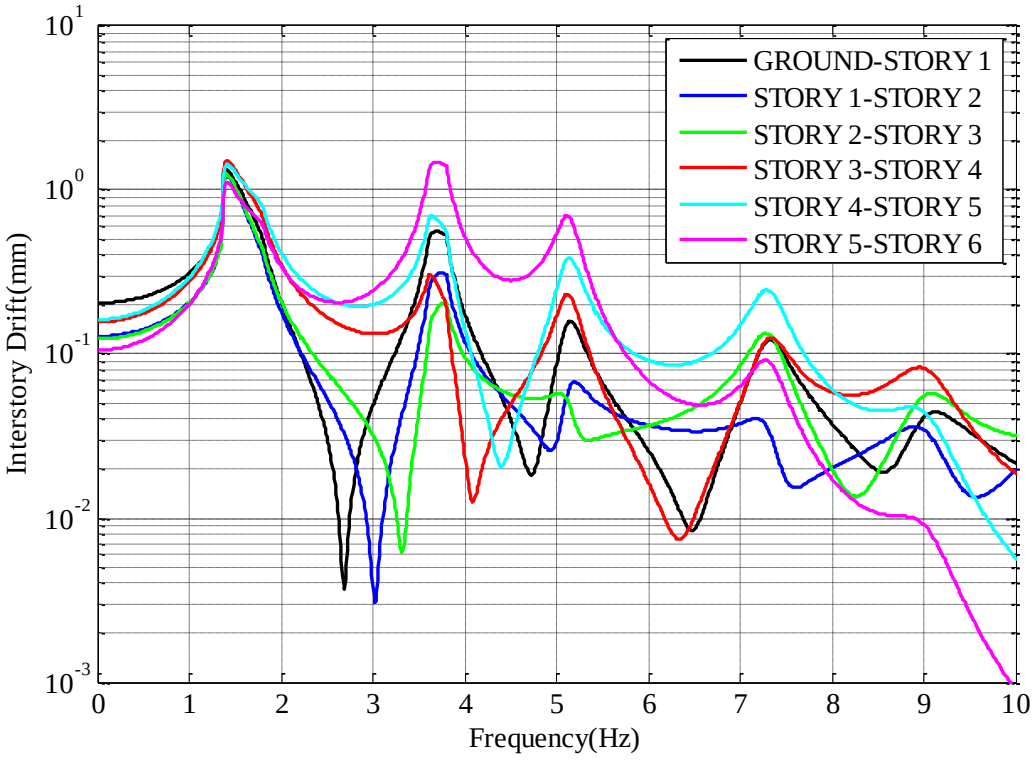

Figure 4.67 Interstory drift plot - Case study 10

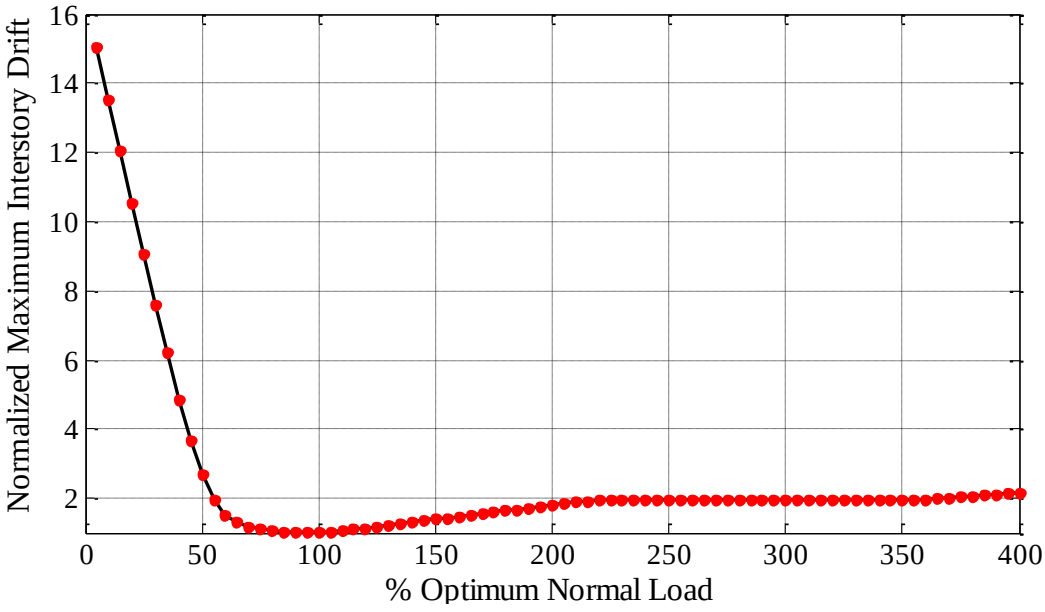

Figure 4.68 Verification plot - Case study 10

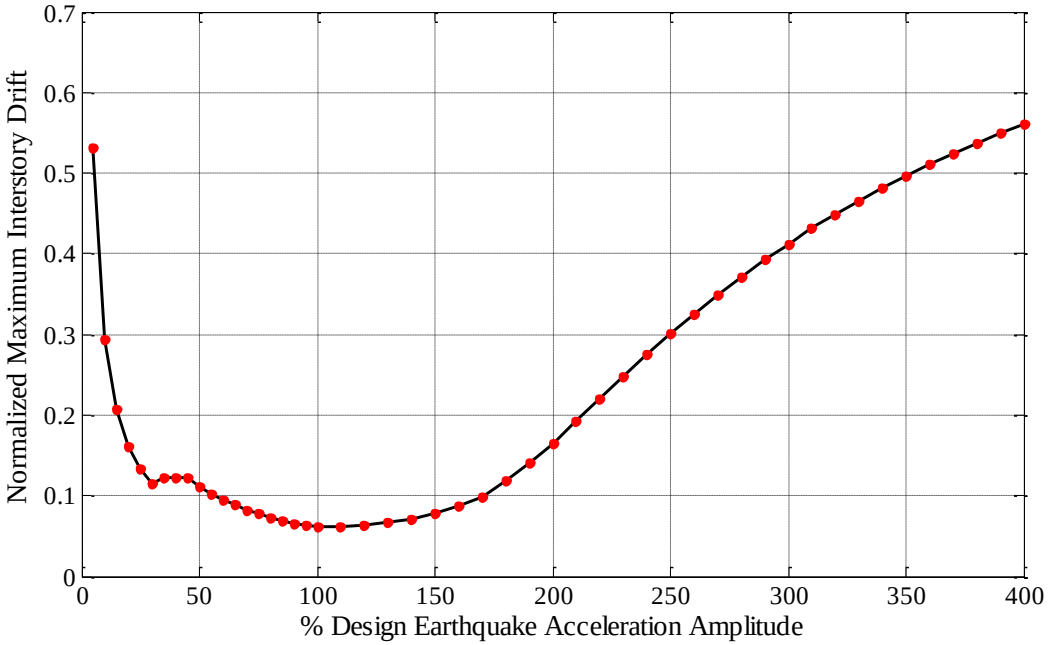

Figure 4.69 Response of the building for different design earthquake ground acceleration magnitudes - Case study 10

4.5.4. Case Study 11 - Optimization with 4 Different Dampers for Alternative Damper Configuration

In this case study, integration of 4 different dampers are investigated and the optimum PS values of all the dampers and their locations are determined.

Results of the optimization are given in Table 4.12 and the maximum interstory drift at 1.43 Hz is reduced to 1.44 mm as shown in Figure 4.70.

Figure 4.71 shows the verification of the results. Since the slope of Figure 4.71 at the right of the optimum value is less than the slope at the left of the optimum value, PS values slightly larger than the optimum values should be used in the design. Figure 4.72 shows the response of the building with optimum dampers for different design earthquake ground acceleration magnitudes and it can be concluded that at any earthquake ground acceleration value around the design

earthquake ground acceleration, the optimized dampers have a very good performance and decreases the building response drastically.

Table 4.12 Results of case study 11

Damper Location	**Opt. PS Value**
Ground - 2nd Story	0.5333
1st Story - 3rd Story	0.3855
2nd Story - 4th Story	0.4091
3rd Story - 5th Story	X
4th Story - 6th Story	0.3143
Maximum Interstory Drift (mm)	**1.44**
Reduction for Maximum Interstory Drift (%)	**94.10**

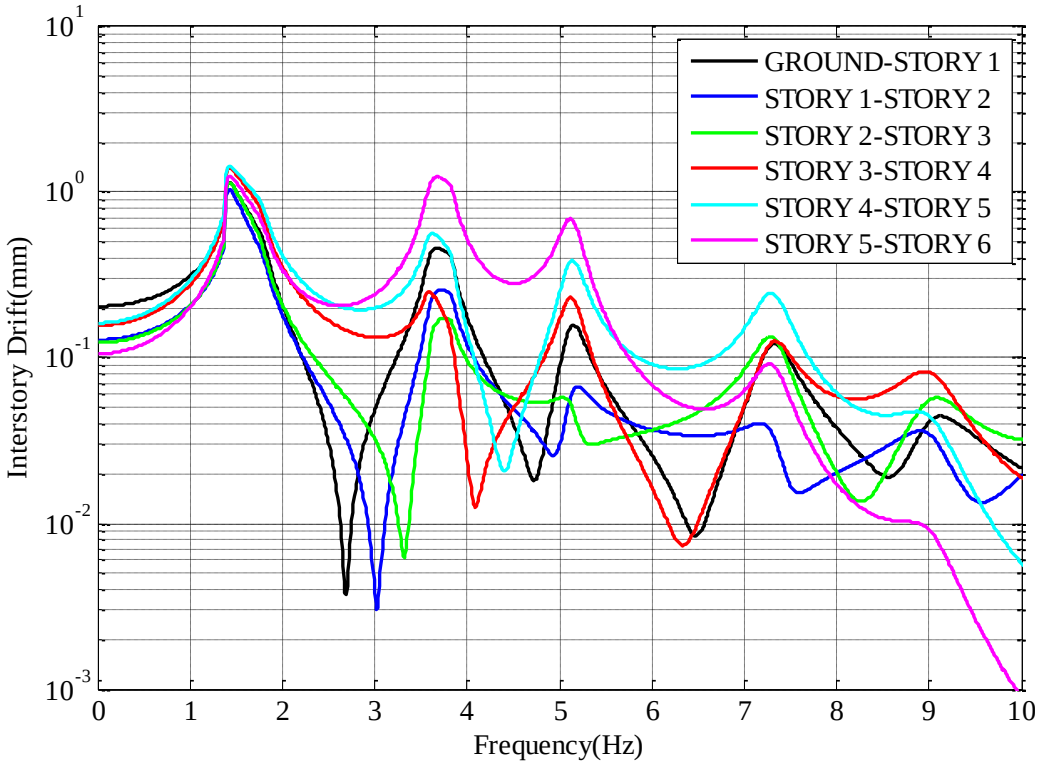

Figure 4.70 Interstory drift plot - Case study 11

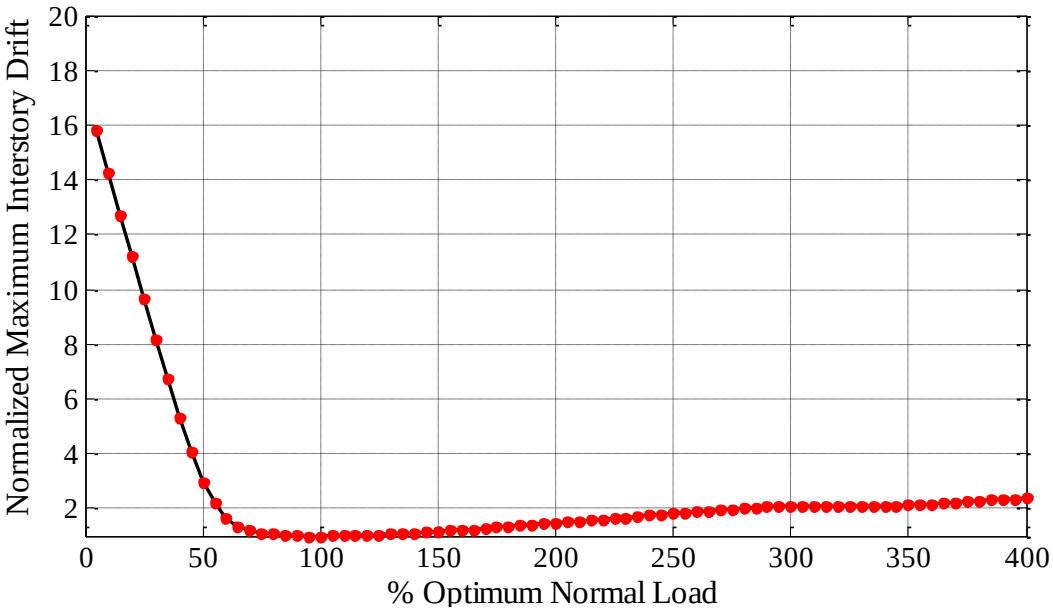

Figure 4.71 Verification plot - Case study 11

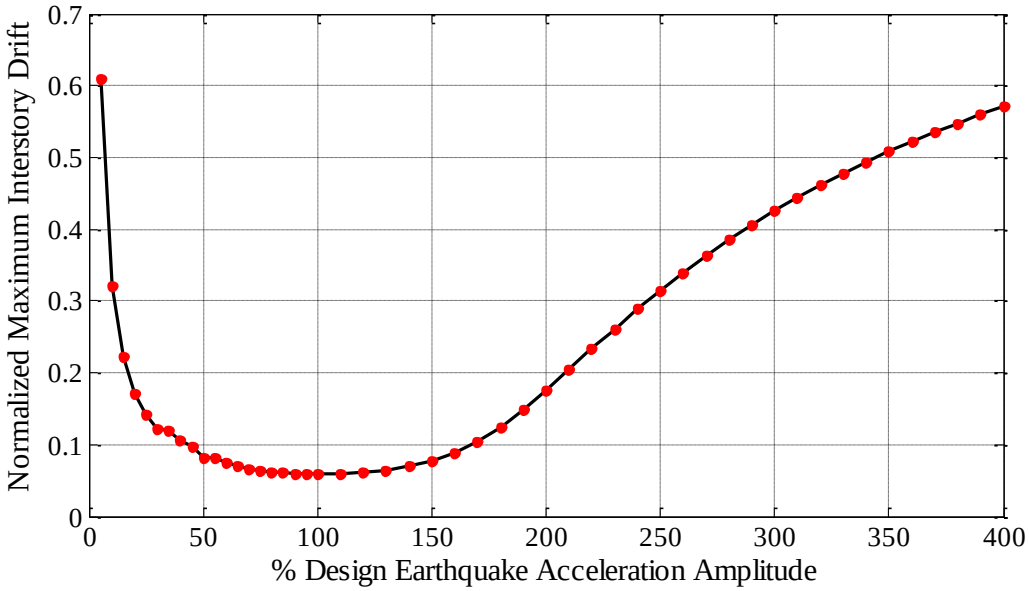

Figure 4.72 Response of the building for different design earthquake ground acceleration magnitudes - Case study 10

4.5.5. Case Study 12 - Optimization with 3 Identical Dampers for Alternative Damper Configuration

In this case study, installation of 3 identical dampers is investigated.

At the end of the optimization, the optimum value for *PS* is obtained as 0.5675. The maximum interstory drift at 1.41 Hz is reduced to 2,00 mm as shown in Table 4.13 and Figure 4.73.

Figure 4.74 shows the verification of the results. Since the slope of Figure 4.74 at the right of the optimum value is less than the slope at the left of the optimum value, *PS* value slightly larger than the optimum value, i.e. 0.5675, should be used in the design. Figure 4.75 shows the response of the building with optimum dampers for different design earthquake ground acceleration magnitudes and it can be concluded that at any earthquake ground acceleration value around the design earthquake ground acceleration, the optimized dampers have a very good performance and decreases the building response drastically.

Table 4.13 Results of case study 12

Damper Location	**Opt. PS Value**
Ground - 2nd Story	0.5675
1st Story - 3rd Story	X
2nd Story - 4th Story	0.5675
3rd Story - 5th Story	X
4th Story - 6th Story	0.5675
Maximum Interstory Drift (mm)	**2**
Reduction for Maximum Interstory Drift (%)	**91.80**

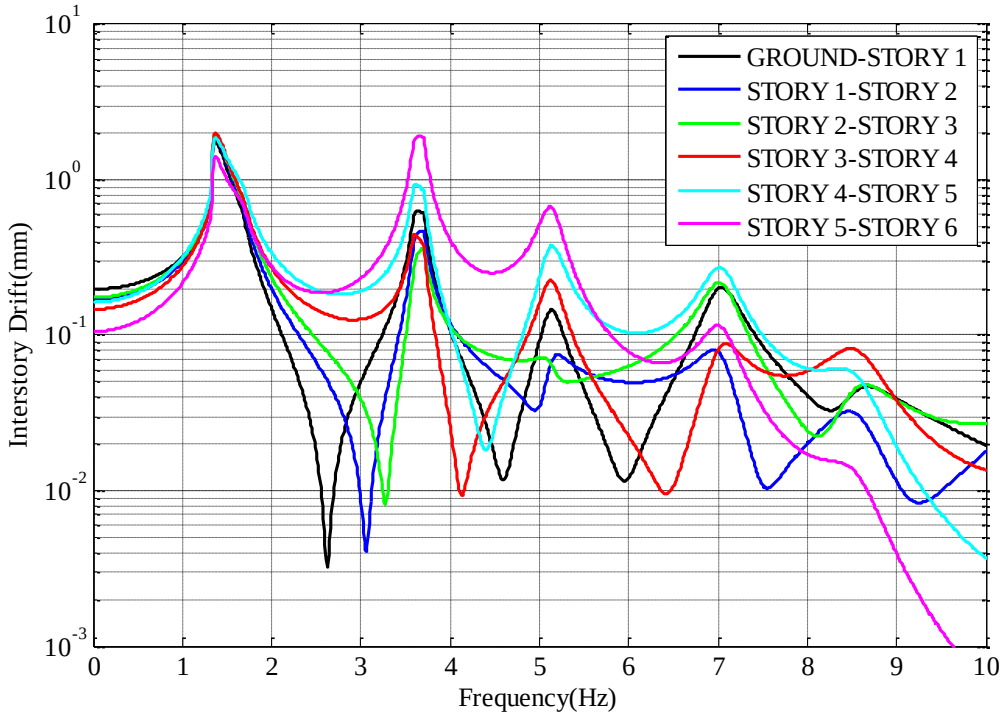

Figure 4.73 Interstory drift plot - Case study 12

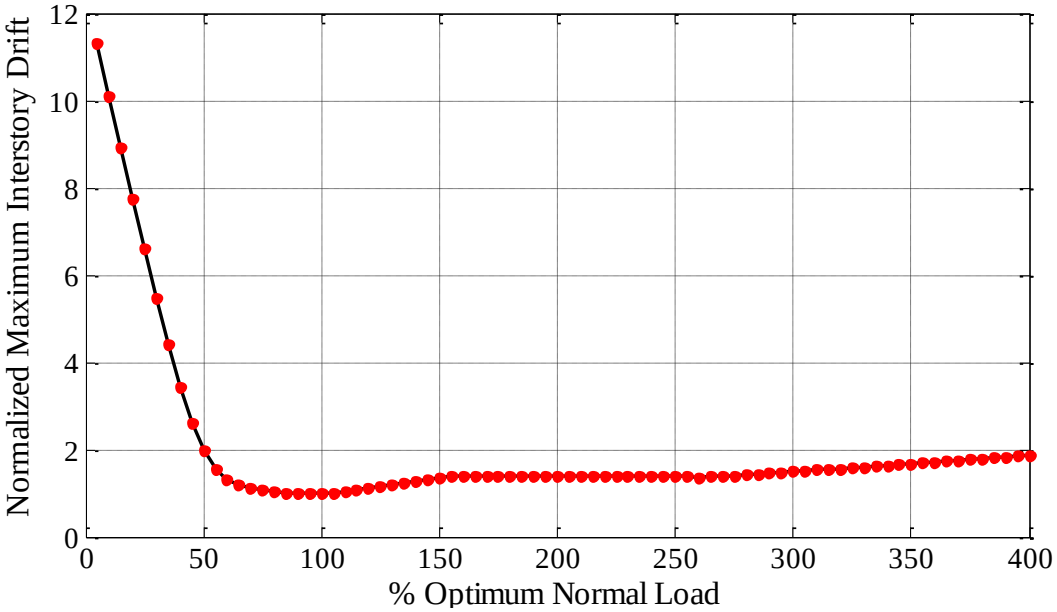

Figure 4.74 Verification plot - Case study 12

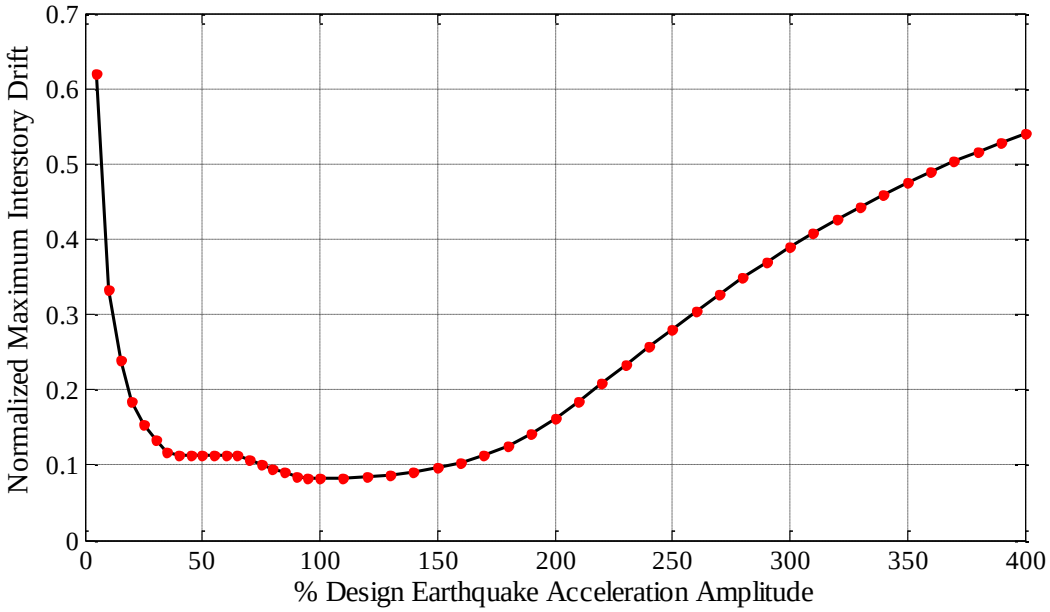

Figure 4.75 Response of the building for different design earthquake ground acceleration magnitudes - Case study 12

4.5.6. Case Study 13 - Optimization with 3 Different Dampers for Alternative Damper Configuration

In this case study, installation of 3 different dampers is investigated and the optimum PS values of all the dampers and their locations are determined.

Results of the optimization are given in Table 4.14 and the maximum interstory drift at 1.39 Hz is reduced to 1.76 mm as shown in Figure 4.76.

Figure 4.77 shows the verification of the results. Since the slope of Figure 4.77 at the right of the optimum value is less than the slope at the left of the optimum value, PS values slightly larger than the optimum values should be used in the design. Figure 4.78 shows the response of the building with optimum dampers for different design earthquake ground acceleration magnitudes and it can be concluded that at any earthquake ground acceleration value around the design

earthquake ground acceleration, the optimized dampers have a very good performance and decreases the building response drastically.

Table 4.14 Results of case study 13

Damper Location	**Opt. PS Value**
Ground - 2nd Story	0.6741
1st Story - 3rd Story	X
2nd Story - 4th Story	0.5663
3rd Story - 5th Story	X
4th Story - 6th Story	0.4332
Maximum Interstory Drift (mm)	**1.76**
Reduction for Maximum Interstory Drift (%)	**92.79**

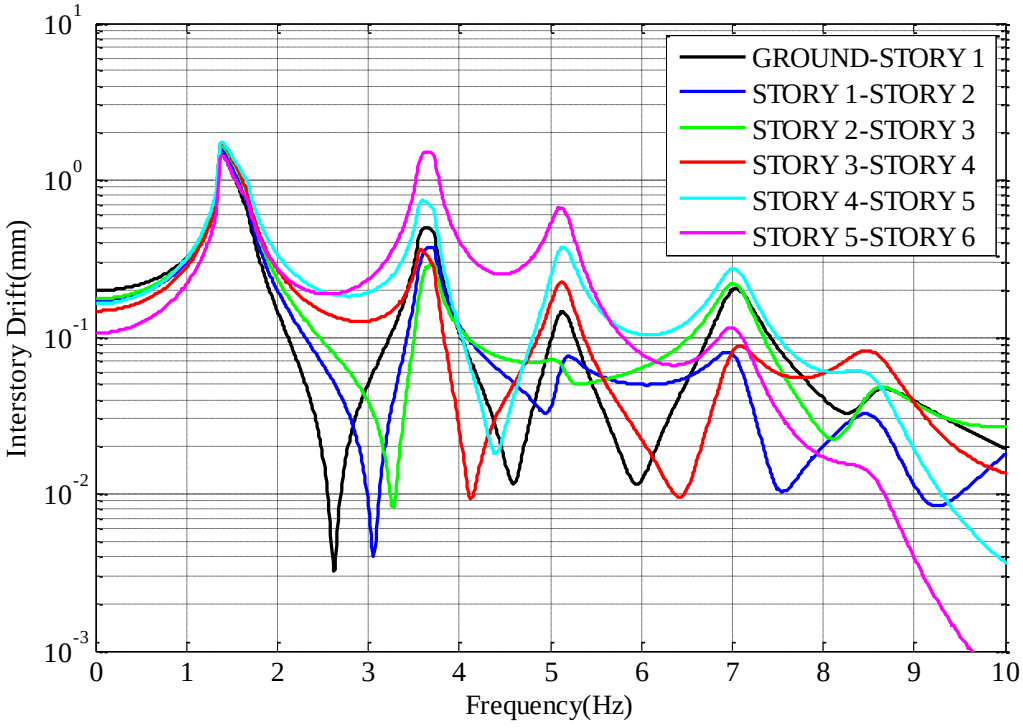

Figure 4.76 Interstory drift plot - Case study 13

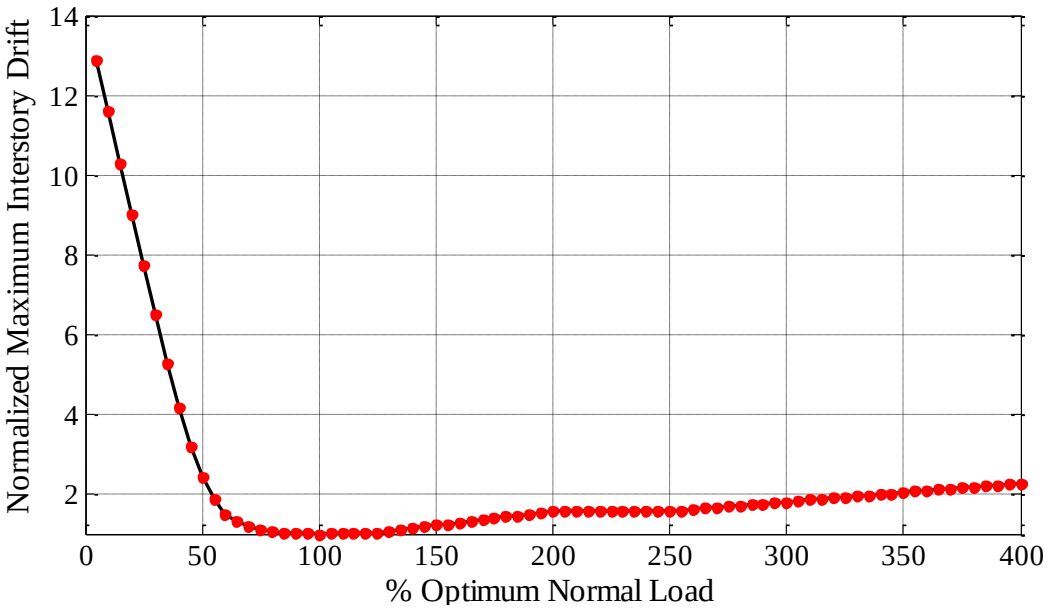

Figure 4.77 Verification plot - Case study 13

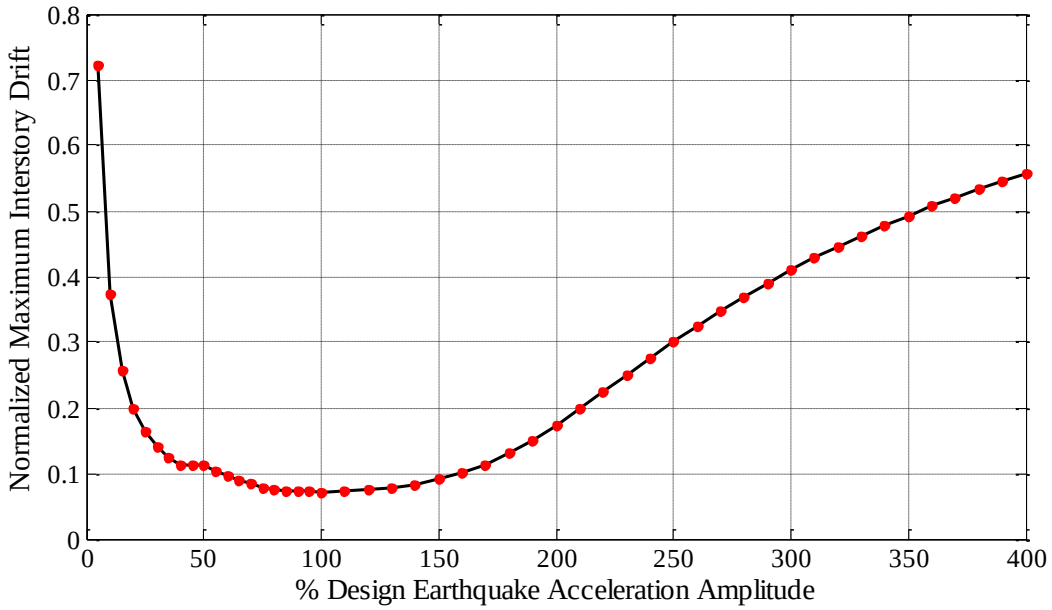

Figure 4.78 Response of the building for different design earthquake ground acceleration magnitudes - Case study 13

4.5.7. Case Study 14 - Optimization with a Single Damper for Alternative Damper Configuration

In this case study, integration of only a single damper is investigated and the optimum *PS* value and the location of the damper is determined.

At the end of the optimization, the optimum dry friction damper location is determined between the 1st and the 3rd stories and the optimum value for *PS* is obtained as 1.3532. Results of the optimization are given in Table 4.15. The maximum interstory drift at 1.3 Hz is reduced to 5.70 mm as shown in Figure 4.79.

Figure 4.80 shows the verification of the results. Since the slope of Figure 4.80 at the right of the optimum value is less than the slope at the left of the optimum value, *PS* value slightly larger than the optimum value, i.e. 1.3532, should be used in the design. Figure 4.81 shows the response of the building with optimum dampers for different design earthquake ground acceleration magnitudes and it can be concluded that at any earthquake ground acceleration value around the design earthquake ground acceleration, the optimized dampers have a very good performance and decreases the building response drastically.

Table 4.15 Results of case study 14

Damper Location	**Opt. PS Value**
Ground - 2nd Story	X
1st Story - 3rd Story	1.3532
2nd Story - 4th Story	X
3rd Story - 5th Story	X
4th Story - 6th Story	X
Maximum Interstory Drift (mm)	**5.7**
Reduction for Maximum Interstory Drift (%)	**76.64**

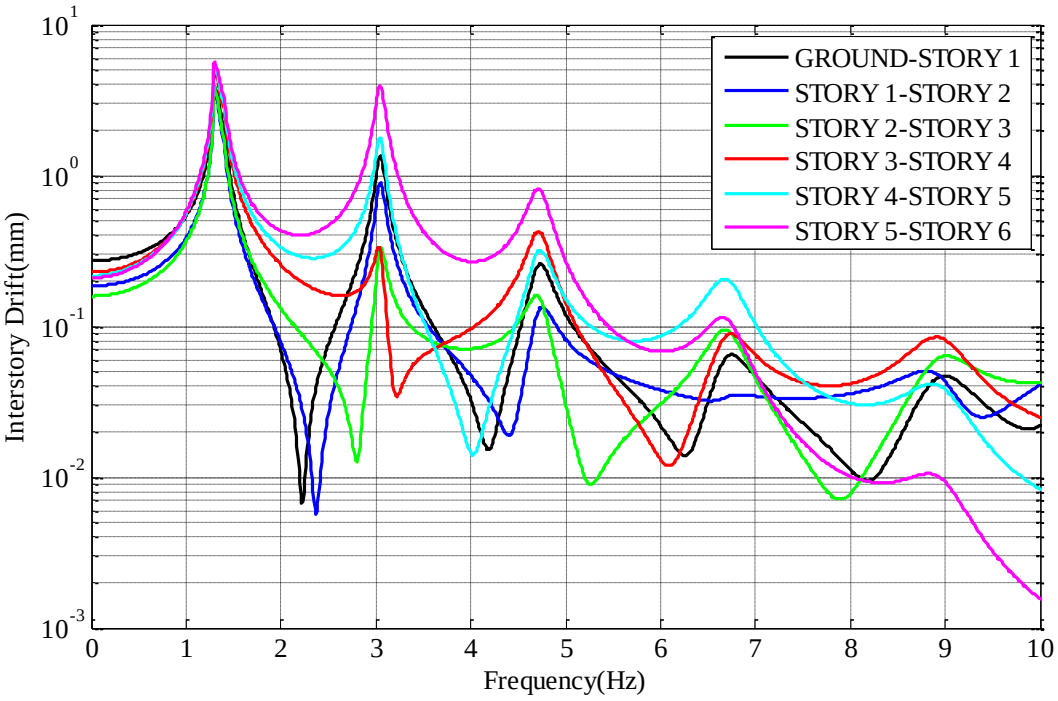

Figure 4.79 Interstory drift plot - Case study 14

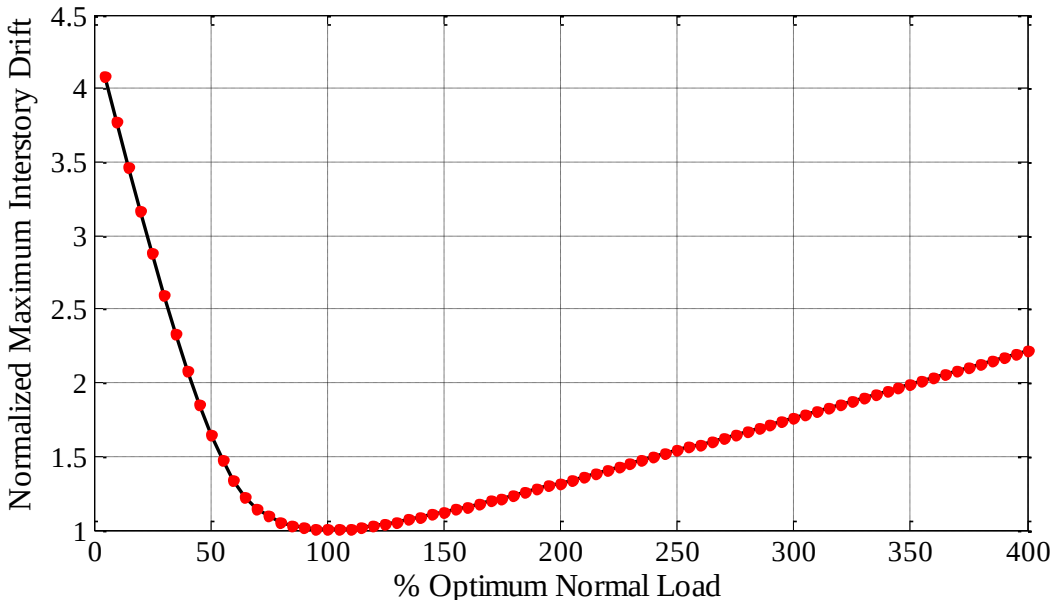

Figure 4.80 Verification plot - Case study 14

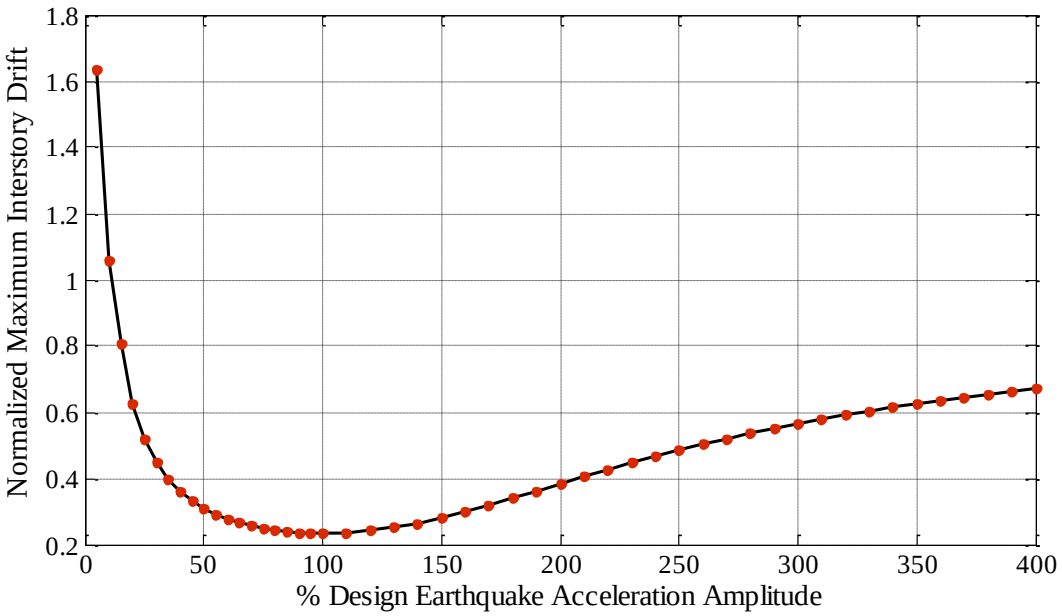

Figure 4.81 Response of the building for different design earthquake ground acceleration magnitudes - Case study 14

Optimization verification curves for identical dampers are given in Figure 4.82 and for different dampers are given in Figure 4.83. From these graphs, it can be seen that for all case studies, minimum interstory drift is obtained with the optimised damper determined during the optimization studies.

Comparison of the maximum interstory drift values for the seven different cases investigated in this section is given in Figure 4.84 and Figure 4.85. From these results it is seen that the maximum interstory drift can be decreased up to 95.49% if five different dampers are used at the proposed alternative configuration.

For the alternative damper connection, since the relative displacement between the ends of the damper increases compared with the adjacent story connection it is expected that at this configuration dampers will perform better which is as well verified with the results obtained in this section.

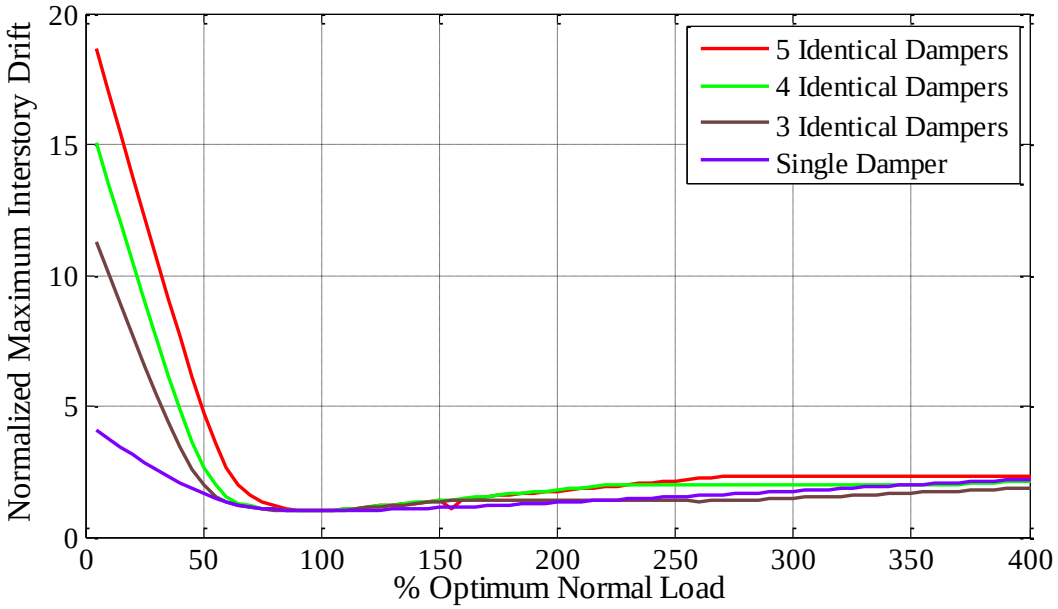

Figure 4.82 Verification plot - Identical friction dampers with alternative damper configuration

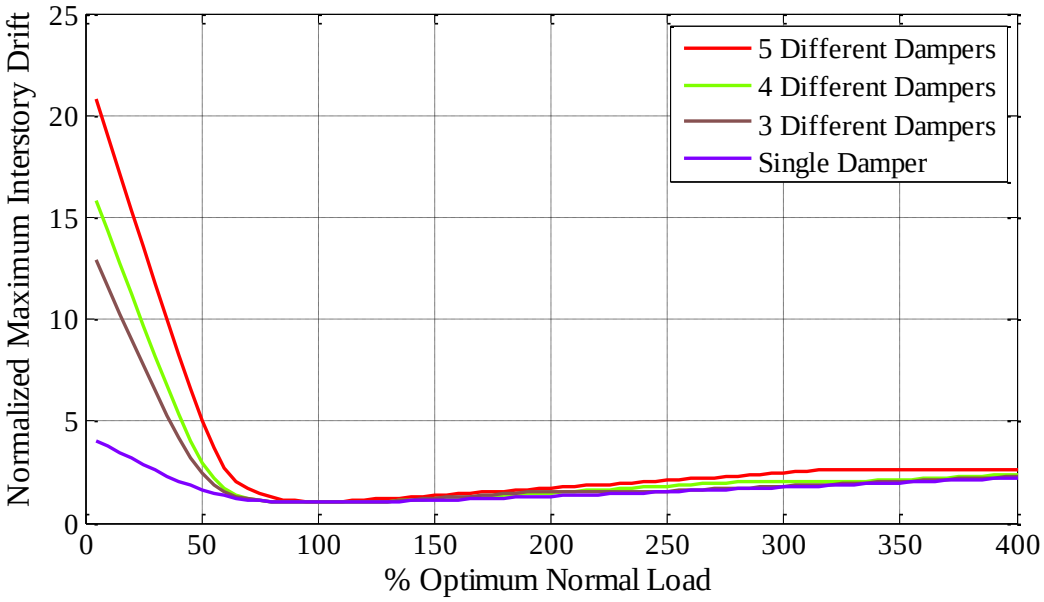

Figure 4.83 Verification plot - Different friction dampers with alternative damper configuration

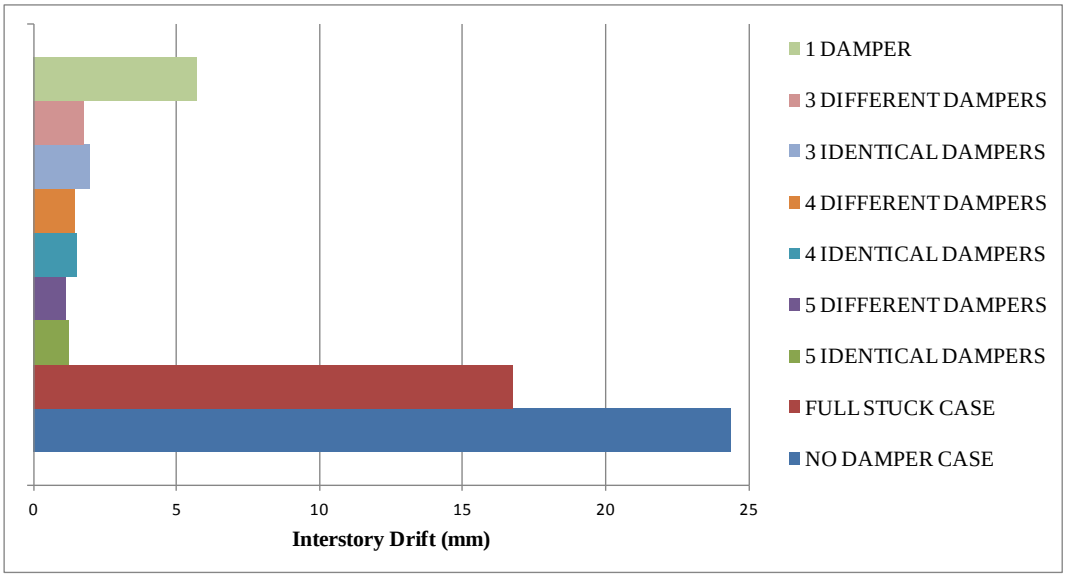

Figure 4.84 Comparison of maximum interstory drift values for alternative damper connection

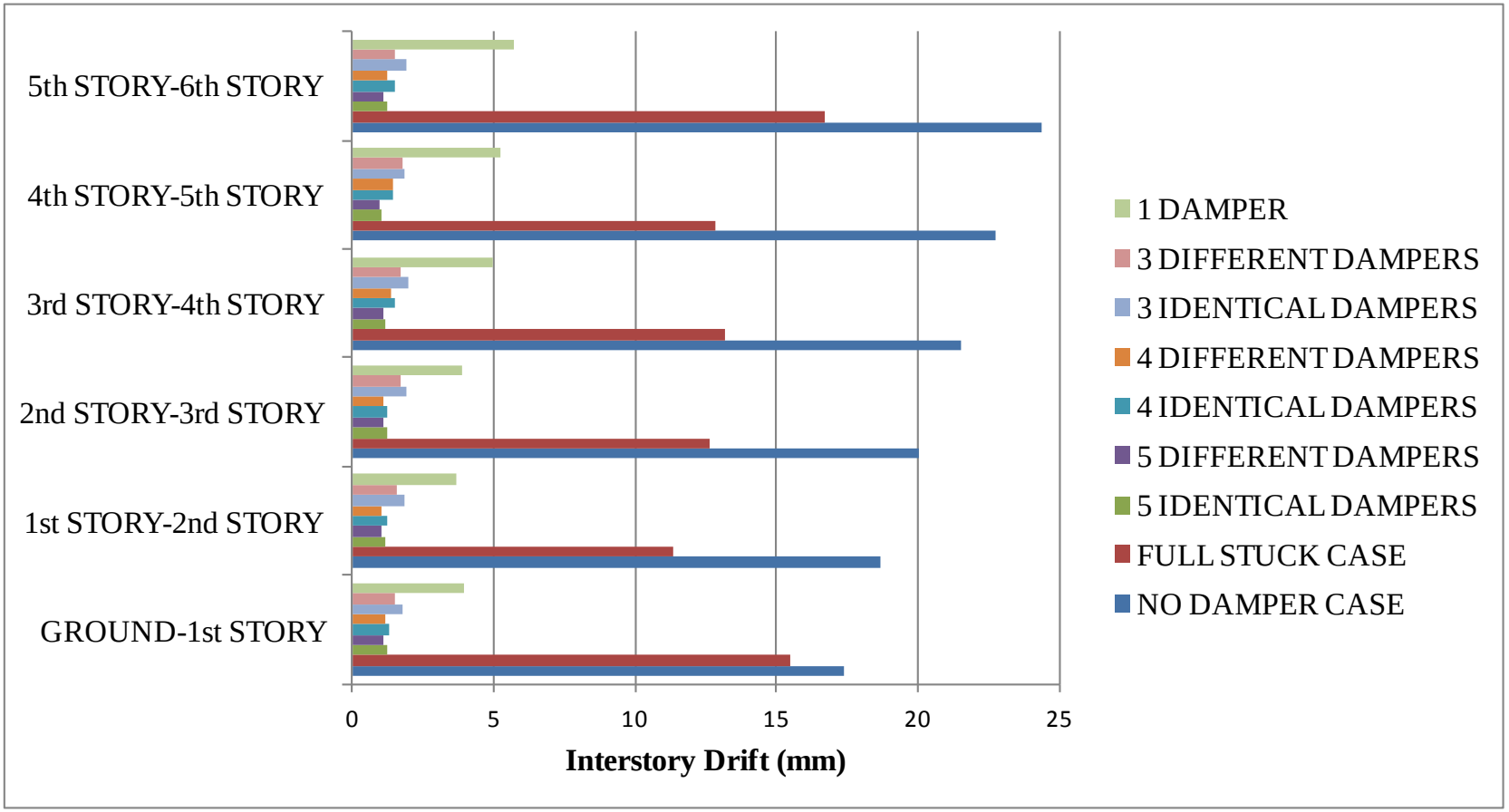

Figure 4.85 Comparison of interstory drift values for alternative damper connection

CHAPTER 5

CONCLUSION AND FUTURE WORK

5.1. Conclusion

In this thesis, a new method in frequency domain is proposed to design and optimize dry friction dampers integrated on a building to decrease the vibration response against an earthquake. With the proposed method, difficulties of time domain methods used in the literature are eliminated to an extent and computational expense is decreased.

Although, earthquake motion is totally random and cannot be expressed with harmonic components completely, for optimization purposes this method is advantageous compared to time domain optimizations, since frequency content and magnitude of an earthquake can be calculated by taking Fast Fourier Transform (FFT) of the recorded motion. Moreover, optimizations are not performed for a specific earthquake and; hence, obtained results can be applied for a wide range of earthquakes by properly selecting the ground acceleration amplitude.

For the analyses, displacements at each floor of the building are described as a single degree of freedom system by using shear building model and macro-slip friction model is used to model the friction at the dampers. Frictional contact at the dampers is represented as nonlinear complex stiffness using Describing Functions Method and nonlinear algebraic equations in frequency domain are solved with

Newton's method. During the optimizations, instead of calculating the response at each frequency at the interested frequency range, a method is developed for direct determination of resonance frequencies and building response is only calculated at these values. Using the advantage of the frequency domain solution and the direct determination of the resonance frequencies method, time expense for the calculations is decreased drastically compared with time domain solutions.

The validity of the solution method suggested in this thesis is demonstrated by comparing the results obtained from frequency domain and time marching solutions for a single story building and it is seen that they are in excellent agreement. Moreover, effects of slip load and stiffness of the supporting elements on building response are shown both for single and multi story building and importance of optimization of these parameters is denoted.

From the optimizations, it is seen that number and configuration of the dampers are also another important thing parameters that should be evaluated during the design of the building. It is shown that, responses are lower in alternative damper configuration when compared with the adjacent story connection. If an optimum slip force value is determined then identical dampers may be used at all locations instead of different dampers since results indicate that identical or different slip forces result in similar reductions in the maximum inter-story displacement in the case studies under consideration. By this way, initial cost of the dry friction dampers may be decreased. Another outcome of the optimization studies is that the optimum locations of the dampers do not change whether the dampers are identical or different. Therefore, in order to simplify the optimization problem for different dampers, locations of the dampers can be optimized initially by assuming dampers are identical and then slip forces of the dampers can be optimized

5.2. Future Work

Although the orientation of the dampers also affects the response of the building during an earthquake, in this thesis, it is not investigated. So with an improved building model, same solution method may be applied to optimize the orientation of the dampers together with the slip forces.

Some new methods may be developed to get more realistic results to simulate the earthquake in frequency domain instead of using the maximum amplitude of FFT of the earthquake data and frequency at that point. In the guidelines for earthquake resistant buildings, there are design earthquakes to use during the calculations however they are developed for time domain studies. Similar data can also be developed in frequency domain.

Another improvement which can be applied to get a lower response at the building is using different dampers between stories which are connected in series or parallel. Their effect should be studied and if it seems to perform better for a real earthquake some optimization methods can be developed for this type of configuration.

Finally, as mentioned in the thesis dry friction dampers do not have to be connected between stories of a building but can also be connected between adjacent buildings [20]. This study can also be adapted for this type of configuration and performance of the dampers can be investigated.

REFERENCES

[1] G. W. Housner et al., "Structural control: past, present, and future," *Journal of Engineering Mechanics*, vol. 123, no. 9, pp. 897–971, 1997.

[2] F. Păuleț-Crăiniceanu, "A lecture delivered to the 4th year students P100 Seismic Code," *Editura Cermi,* 1999.

[3] FEMA, "NEHRP guidelines for the seismic rehabilitation of buildings," 1997.

[4] BSSC, "NEHRP Recommended Provisions for Seismic Regulations for New Buildings and Other Structures," 1997.

[5] I. Takewaki, K. Fujita, K. Yamamoto, and H. Takabatake, "Smart passive damper control for greater building earthquake resilience in sustainable cities," *Sustainable Cities and Society*, vol. 1, no. 1, pp. 3-15, Feb. 2011.

[6] R. H. B. Fey, H. M. R. Suy, F. M. B. Galanti, and H. Nijmeijer, "Efficient analysis of the nonlinear dynamic response of a building with a friction-based seismic base isolation system," in *ECCOMAS Thematic Conference on Computational Methods in Structural Dynamics and Earthquake Engineering*, 2007.

[7] T.-shu Wu and R. W. Seidensticker, "Responses of an isolation system with distinct multiple frequencies," 1991.

[8] T. Soong, "Active, semi-active and hybrid control of structures," *Bulletin of the New Zealand National Society for*, pp. 1-16, 2000.

[9] N. A. Alexander, "Simplified multi-storey shear building model," in *Academic notes, University of Bristol*, pp. 41-62.

[10] B. Bhushan, *Principles and applications of tribology*, vol. 9, no. 2. Wiley-Interscience, 1999, pp. 89-89.

[11] K.-W. Min, J.-Y. Seong, and J. Kim, "Simple design procedure of a friction damper for reducing seismic responses of a single-story structure," *Engineering Structures*, vol. 32, no. 11, pp. 3539-3547, Nov. 2010.

[12] H. Olsson, K. J. Åström, C. Canudas de Wit, M. Gafvert, and P. Lischinsky, "Friction models and friction compensation," *European journal of control*, vol. 4, pp. 176–195, 1998.

[13] E. Cigeroglu and H. Ozguven, "Nonlinear vibration analysis of bladed disks with dry friction dampers," *Journal of Sound and Vibration*, vol. 295, no. 3-5, pp. 1028-1043, Aug. 2006.

[14] I. Mualla, "Performance of steel frames with a new friction damper device under earthquake excitation," *Engineering Structures*, vol. 24, no. 3, pp. 365-371, Mar. 2002.

[15] C. Pasquin, N. Leboeuf, R. T. Pall, and A. Pall, "Friction dampers for seismic rehabilitation of Eaton building, Montreal," in *Proceeding of the 4th Structural Specialty Conference of the Canadian Society for Civil Engineering*, 2002, pp. 1-10.

[16] C. Y. L. Chang, A. Pall, and J. J. C. Louie, "The use of friction dampers for seismic retrofit of the Monterey county government center," in *8th US National Conference on Earthquake Engineering*, 2006.

[17] L. Lu, L. Chung, L. Wu, and G. Lin, "Dynamic analysis of structures with friction devices using discrete-time state-space formulation," *Computers & Structures*, vol. 84, no. 15-16, pp. 1049-1071, Jun. 2006.

[18] J. Marko, D. Thambiratnam, and N. Perera, "Study of Viscoelastic and Friction Damper Configurations in Medium-Rise Structures," *Materials and Structures*, vol. 1, 2006.

[19] W.-I. Liao, I. Mualla, and C.-H. Loh, "Shaking-table test of a friction-damped frame structure," *The Structural Design of Tall and Special Buildings*, vol. 13, no. 1, pp. 45-54, Mar. 2004.

[20] A. Bhaskararao and R. Jangid, "Harmonic response of adjacent structures connected with a friction damper," *Journal of Sound and Vibration*, vol. 292, no. 3-5, pp. 710-725, May 2006.

[21] A. V. Bhaskararao and R. S. Jangid, "Seismic Response of Adjacent Buildings Connected with Friction Dampers," *Bulletin of Earthquake Engineering*, vol. 4, no. 1, pp. 43-64, Feb. 2006.

[22] M. Tabeshpour and H. Ebrahimian, "Seismic Retrofit of Existing Structures Using Friction Dampers," *Asian Journal of Civil Engineering (Building and Housing)*, vol. 11, no. 4, pp. 509–520, 2010.

[23] S. Lee, “Allocation and slip load of friction dampers for a seismically excited building structure based on storey shear force distribution,” *Engineering Structures*, vol. 30, no. 4, pp. 930-940, Apr. 2008.

[24] J. Kim, “Behavior and design of structures with buckling-restrained braces,” *Engineering Structures*, vol. 26, no. 6, pp. 693-706, May 2004.

[25] J. F. Hall, “Finite element analysis in earthquake engineering,” in *International Handbook of Earthquake and Engineering Seismology*, vol. 1, Academic Pr, 2003, pp. 1133-1158.

[26] O. Tanrikulu, M. Imregun, B. Kuran, and H. N. Ozguven, “Forced harmonic response analysis of nonlinear structures using describing functions,” *AIAA Journal*, vol. 31, no. 7, pp. 1313-1320, Jul. 1993.

[27] E. Cigeroglu, N. An, and C.-H. Menq, “Forced Response Prediction of Constrained and Unconstrained Structures Coupled Through Frictional Contacts,” *Journal of Engineering for Gas Turbines and Power*, vol. 131, no. 2, p. 022505, 2009.

[28] G. Orbay, “Nonlinear vibration of mistuned bladed disk assemblies,” MS Thesis Middle East Technical University, 2008.

[29] M. Crisfield, “A fast incremental/iterative solution procedure that handles ‘snap-through’,” *Computers & Structures*, vol. 13, no. 1-3, pp. 55-62, Jun. 1981.

[30] U. Pillai, “Application of Homotopy Continuation Methods to Computation of Line Spectral Pairs,” *Computer Engineering*, 1989.

[31] E. P. Petrov, “Direct Parametric Analysis of Resonance Regimes for Nonlinear Vibrations of Bladed Disks,” *Journal of Turbomachinery*, vol. 129, no. 3, p. 495, 2007.

[32] S. H. Lee, J. H. Park, B. W. Moon, K. W. Min, and J. Kim, “Design of a bracing-friction damper system for seismic retrofitting,” *Smart Structures and Systems*, vol. 4, no. 5, pp. 685–696, 2008.

APPENDIX A

CONFERENCE PROCEEDING

A.1 IMAC XXX: Conference & Exposition on Structural Dynamics, January 30 - February 02, 2012, Jacksonville, Florida, USA

Frequency Domain Optimization of Dry Friction Dampers on Buildings Under Harmonic Excitation

Z. Eren Erisen , Ender Cigeroglu
Mechanical Engineering Department, Middle East Technical University, 06800 Ankara, TR

ABSTRACT

Friction mechanism has an extensive usage in many different fields for energy dissipation. It is also used at buildings to reduce the displacement that is caused by ground acceleration during an earthquake. Despite friction damper is a simple device to use on structures, due to its nonlinear characteristic, analysis and design of a structure equipped with a friction damper is difficult. In this paper, Harmonic Balance Method (HBM) is employed to represent the frictional contact as a nonlinear complex stiffness in order to find the steady state displacement of each story of a multi-story building under harmonic ground acceleration. Application of HBM results in a set of nonlinear algebraic equations in frequency domain which can be solved by an iterative method. As a result of this, the solution method presented reduces the computational effort compared to time integration methods; therefore, optimization of friction dampers can be performed in a reasonable time. Accuracy and validation of the presented method is demonstrated on a single-story shear building model equipped with a single friction damper by comparing the frequency domain solution with time marching results. A multi-story building is considered as a case study where the slip force of each dry friction damper is optimized in order to minimize the relative displacement between the stories.

1. INTRODUCTION

As a result of structural vibrations that occur during an earthquake, structural damage or even failure may occur at buildings. In order to minimize the effects of earthquakes on buildings, passive or active control systems can be utilized. The ways to accomplish a seismic response control are [1];

- Decreasing the energy transmission of the earthquake ground motion to the structure.
- Isolating the natural frequency of the building from the dominant frequency of the earthquake.
- Achieving the non-stationary and non-resonant state by providing nonlinear characteristics.
- Applying control forces to the building.
- Utilizing energy absorption mechanisms.

Friction can be defined as the resistance to motion during sliding or rolling when one body is in tangentially contact with another body [2]. Since there is no requirement of an external power supply or a sensor, usage of dry friction dampers on buildings is a passive vibration control method and an energy absorption mechanism. Analysis of buildings equipped with dry friction dampers is complicated and requires high computational effort due to the nonlinear characteristic of dry friction. Frequency domain and time domain solution methods are utilized for structures with dry friction dampers; however, for the solution of buildings equipped with dry friction dampers, time domain methods based on time integration have been frequently used in the literature which require more computation effort and significant computation times compared to frequency domain methods. Moreover, by utilizing time domain analysis, it is hard to guess the most unfavorable ground motion for a building that may occur at the specified site and this brings another difficulty for the analysis [3].

There are many factors which effect the building performance and they depend on both earthquake characteristics such as amplitude and frequency of the ground motion and also building properties such as mass, stiffness, damping and ductility of the building. Since passive control systems are not adaptive to changes in the excitation, an optimum damping ratio and damping distribution along the building is very important.

As can be seen from Fig. 1, ground motion at a site is superposition of different frequencies with different amplitudes. If one of the dominant frequencies of an earthquake is far from the natural frequency of the building, then the vibration amplitude of the building will be low; however, it is not always possible to isolate the natural frequency of the building from these dominant frequencies due to constructive challenges and due to the fact that most of the earthquakes are dominant in the frequency range of 0 Hz - 15 Hz.

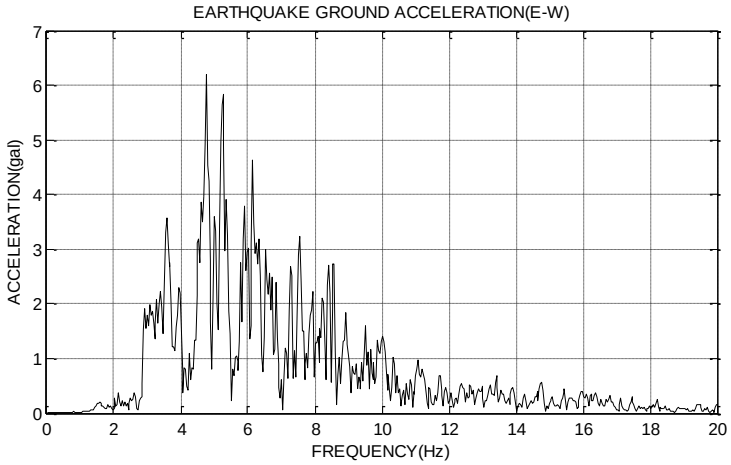

Fig. 1 Frequency response function of 1992 ERZINCAN earthquake

2. MODELLING OF THE SYSTEM

In this paper, orientation of the dampers will not be investigated and at each floor, response will be studied only in one direction for optimization purposes; hence, using shear building model will be sufficient. Placement of the dampers also play an important role in modeling of the building. In this study, shear building model given in Fig. 2 is used where the dampers are placed between the successive floors; however, different damper configurations are as well possible.

2.1. Shear Building Model

Schematic representation of a n-story building model used for the simulations is given in Fig. 2. Equation of motion of the system can be given as follows;

$$\begin{aligned} &[M]\{\ddot{x}\}+[C]\{\dot{x}\}+[K]\{x\}+\{f_{NL}\}=\{f_{exc}\} \\ &\{f_{exc}\}=-[M]\ddot{x}_g \end{aligned} \tag{1}$$

In this equation, $[M]$, $[C]$ and $[K]$ represent mass, damping and stiffness matrices of the building and $\{x\}$, $\{\dot{x}\}$, $\{\ddot{x}\}$ are displacement, velocity and acceleration vectors of the stories, respectively, $\{f_{NL}\}$ is the nonlinear forcing vector consisting of the nonlinear forces due to friction dampers, $\{f_{exc}\}$ is the excitation vector, and $\ddot{x}_g$ is ground acceleration due to earthquake. The details of these matrices and vectors are given as;

$$[M]=diag(m_1, m_2, m_3 \cdots m_{n-1}, m_n) \tag{2}$$

$$[C]=\begin{bmatrix} c_1+c_2 & -c_2 & 0 & \cdots & \cdots & \cdots & 0 \\ -c_2 & c_2+c_3 & -c_3 & \cdots & \cdots & \cdots & 0 \\ 0 & -c_3 & c_3+c_4 & \cdots & \cdots & \cdots & 0 \\ 0 & 0 & -c_4 & \cdots & \cdots & \cdots & 0 \\ 0 & 0 & 0 & \cdots & \cdots & \cdots & 0 \\ 0 & 0 & 0 & \cdots & -c_{n-1} & c_{n-1}+c_n & -c_n \\ 0 & 0 & 0 & \cdots & \cdots & -c_n & c_n \end{bmatrix} \tag{3}$$

$$[K]=\begin{bmatrix} k_1+k_2 & -k_2 & 0 & \cdots & \cdots & \cdots & 0 \\ -k_2 & k_2+k_3 & -k_3 & \cdots & \cdots & \cdots & 0 \\ 0 & -k_3 & k_3+k_4 & \cdots & \cdots & \cdots & 0 \\ 0 & 0 & -k_4 & \cdots & \cdots & \cdots & 0 \\ 0 & 0 & 0 & \cdots & \cdots & \cdots & 0 \\ 0 & 0 & 0 & \cdots & -k_{n-1} & k_{n-1}+k_n & -k_n \\ 0 & 0 & 0 & \cdots & \cdots & -k_n & k_n \end{bmatrix} \tag{4}$$

$$\{x\}=\left[x_1, x_2, x_3 \cdots x_{n-1}, x_n\right]^T \tag{5}$$

Details of $\{f_{NL}\}$ vector is given in Section 3.1.

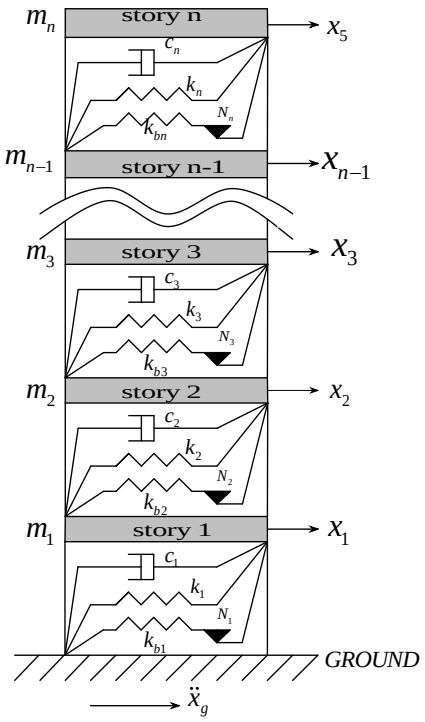

Fig. 2 MDOF shear building model

2.2. Modeling of Dry Friction

In this paper, macro-slip friction model which is composed of a spring and a frictional contact with a slip load μN as shown in Fig. 3, is used. In this model, k_f, μ, N and x represent the stiffness of the friction damper, coefficient of friction, normal load acting across the contact surface and relative motion across the damper, respectively. When the force on the spring is less than the slip load (force), μN, the damper is in stick state and the friction force is defined as;

$$F_f = k_f x \tag{6}$$

Damper remains in stick state until the friction force reaches to the slip force where further increase of the relative motion results in slip state. During the slip state, friction force equals to the slip force which can be expressed as;

$$F_f = \mu N \tag{7}$$

The damper continues to slip until the relative velocity becomes zero (i.e. $\dot{x} = 0$) and at this point damper sticks again.

In the literature, friction is idealized by rigid perfectly plastic models and modeled as a fictitious spring having infinite stiffness during stick phase and zero stiffness during slip phase. In another words;

$$k_f = \begin{Bmatrix} \infty \text{ if the damper sticks} \\ 0 \text{ if the damper slips} \end{Bmatrix} \tag{8}$$

While modeling the dry friction damper, flexibility of the elements that are used to support and connect the damper to the main structure should also be introduced as shown in Fig. 4, where k_b represents the stiffness of the bracing. Stiffness of the damper assemblage, k_{bd}, can be given as follows;

$$\frac{1}{k_{bd}} = \frac{1}{k_b} + \frac{1}{k_f} \tag{9}$$

From Eq. (8), during stick state Eq. (9) reduces to

$$k_{bd} = k_b \tag{10}$$

Therefore, dry friction damper is modeled with a spring of stiffness k_b, for which the hysteresis diagram for a simple harmonic motion is given in Fig. 5 and the corresponding equation for the friction force is given in Eq. (13).

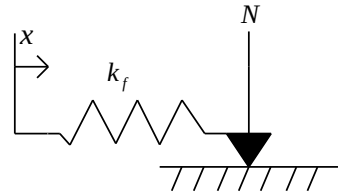

Fig. 3 Macro-slip friction model

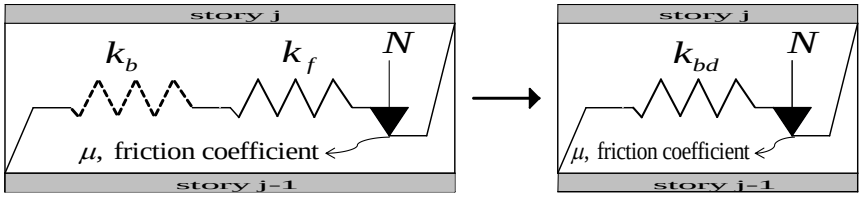

Fig. 4 Modeling of dry friction damper connection to the building

3. SOLUTION METHOD

For frequency domain solution, $\{f_{exc}\}$ is assumed to be sinusoidal in the form of ;

$$\{f_{exc}\} = \mathrm{Im}\left(\{F\} e^{i\varphi}\right), \tag{11}$$

where $\varphi = \omega t$, $\{F\}$ and $\{\omega\}$ are the complex vector of amplitudes of external forces and excitation frequency, respectively. Assuming that the structure vibrates harmonically the response can be expressed as follows;

$$\{x\} = \mathrm{Im}\left(\{X\} e^{i\varphi}\right) \tag{12}$$

where $\{X\}$ is the complex vector of displacement amplitudes.

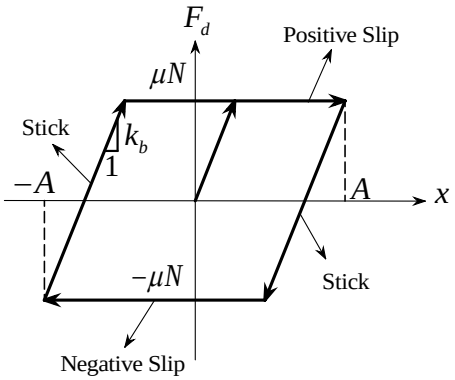

Fig. 5 Hysteresis diagram of dry friction damper

$$F_d = \begin{cases} \mu N & \text{Positive Slip} \\ \mu N + k_b\left(x - A\right) & \text{Stick} \\ -\mu N & \text{Negative Slip} \\ -\mu N + k_b\left(x + A\right) & \text{Stick} \end{cases} \tag{13}$$

3.1. Harmonic Balance Method

Sanliturk et al. [4], used harmonic balance method (HBM) for vibration analysis of turbine blades with friction dampers. In this part, short information about HBM will be given.

HBM is based on finding linearized coefficients which, in general, depend on both the frequency and the amplitude of the oscillations. For the given harmonic displacement in Eq. (12), linearized stiffness coefficient for the friction damper is expressed as;

$$k^*_{eq}(A) = k^r_{eq}(A) + ik^i_{eq}(A) \tag{14}$$

where (A) is the displacement amplitude of the relative motion across the damper as shown in Fig. 5, k^r_{eq} , k^i_{eq} are the real and imaginary parts of amplitude-dependent equivalent stiffness, respectively.

In this paper, only the fundamental harmonic term is considered as suggested by Chen et al. [5] and Cigeroglu et al. [6]. Then, equivalent stiffness coefficients can be calculated as follows;

$$\begin{aligned} k^r_{eq}(A) &= \frac{1}{\pi A}\int_0^{2\pi} F_d(A\sin\varphi)\cos\varphi \; d\varphi \\ k^i_{eq}(A) &= \frac{1}{\pi A}\int_0^{2\pi} F_d(A\sin\varphi)\sin\varphi \; d\varphi, \end{aligned} \tag{15}$$

Up to now, general information about defining a nonlinear force as a complex stiffness is given. For the macro-slip friction model having the hysteresis curve shown in Fig. 5, the nonlinear stiffnesses expressed in Eq. (15) are given as follows;

$$\begin{aligned} k^r_{eq}(A) &= \left\{ \begin{array}{l} \dfrac{1}{\pi}\left(\dfrac{2\mu N}{A} - k_b\right)\sqrt{1-\left(\dfrac{k_b A - 2\mu N}{k_b A}\right)^2} + k_b\dfrac{\gamma}{\pi} - \dfrac{k_b}{2} \quad \text{if} \quad k_b A > \mu N \\ k_b \quad \text{if} \quad k_b A \le \mu N \end{array} \right\} \\ k^i_{eq}(A) &= \left\{ \begin{array}{l} -\dfrac{4\mu N(\mu N - Ak_b)}{\pi k_b A^2} \quad \text{if} \quad k_b A > \mu N \\ 0 \quad \text{if} \quad k_b A \le \mu N \end{array} \right\} \\ \gamma &= \pi - \sin^{-1}\left(\frac{\mu N}{Ak_b} - 1\right) \end{aligned} \tag{16}$$

From Eq. (16), the nonlinear friction forces on each damper can be obtained as follows

$$F_{d_j} = k_{eq}^{*}\left(Y_j\right)\cdot Y_j \tag{17}$$

where,

$$\begin{aligned} Y_j &= X_j \quad \text{for} \quad j=1 \\ Y_j &= X_j - X_{j-1} \quad \text{for} \quad j \geq 2. \end{aligned} \tag{18}$$

Using Eq. (17), nonlinear forcing vector, $\{f_{NL}\}$, can be defined as follows

$$\{f_{NL}\} = \mathrm{Im}\left(\left\{F_{NL}\left(\{X\}\right)\right\}e^{i\varphi}\right). \tag{19}$$

where $\left\{F_{NL}\left(\{X\}\right)\right\}$ is expressed as

$$\left\{F_{NL}\left(\{X\}\right)\right\} = \left[F_{d_1} - F_{d_2}, F_{d_2} - F_{d_3}, F_{d_3} - F_{d_4}, \cdots, F_{d_{n-1}} - F_{d_n}, F_{d_n}\right]^T. \tag{20}$$

Then, Eq. (1) can be re-written for harmonic motion as follows;

$$\left[[K] - \omega^2[M] + i\omega[C]\right]*\{X\} + \left\{F_{NL}\left(\{X\}\right)\right\} = \{F\}. \tag{21}$$

3.2. Solution of Resulting Nonlinear Equations

Since the nonlinear force given in Eq. (21) is displacement dependent, an iterative method is required for the solution. Eq. (21) can be expressed as a residual vector as follows;

$$\left\{R\left(\{X\},\omega\right)\right\} = \left[[K] - \omega^2[M] + i\omega[C]\right]*\{X\} + \left\{F_{NL}\left(\{X\}\right)\right\} - \{F\} = \{0\}, \tag{22}$$

Solution of Eq. (22) can be obtained for values of $\{X\}$ that result in $\left\{R\left(\{X\},\omega\right)\right\} = 0$. Using Newton's method the following iterative formula can be written for the solution of Eq. (22);

$$\{X\}_{k+1} = \{X\}_k - \left[\frac{\partial\{R(\{X\},\omega)\}}{\partial\{X\}}\right]^{-1}\Bigg|_{\{X\}_k,\omega} \{R(\{X\}_k,\omega)\} \tag{23}$$

where k is the iteration number and $\left[\partial\{R(\{X\},\omega)\}/\partial\{X\}\right]$ is the Jacobian matrix and should be calculated either analytically or numerically. This iteration for $\{X\}$ continues until a pre-defined error tolerance, either on the relative difference between $\{X\}_{k+1}$ and $\{X\}_k$ or on $\{R(\{X\},\omega)\}$ or on both, is satisfied.

4. RESULTS

4.1. Validation of the method

The validation of the solution method suggested is demonstrated by comparing the results obtained from frequency domain and time domain solutions. For this reason, a single story building equipped with a dry friction damper connected between ground and the floor is investigated under a harmonic ground acceleration. In order to have a scale for the parameter values used in the study, the stiffness and the slip load of the damper is normalized as follows;

$$SR = \frac{k_{b1}}{k_1}, \quad PS = \frac{F_s}{m_1 g}100, \tag{24}$$

where SR and PS demonstrates stiffness ratio and percentage slip load, respectively and g is gravitational acceleration. The response of the 1-dof system is studied by keeping the amplitude of ground acceleration, $\ddot{x}_g$, and SR constant at 0.2m/s^2 and 0.2 respectively and PS is changed between 0.7 and 6. The investigated 1-dof system is modeled such that; its mass, stiffness and viscous damping coefficient are equal to 5000 kg, 805000 N/m and 1280 N/m, respectively. In this analysis, $PS = 0$ is the case corresponding to no damper.

Fig. 6 shows the comparison of displacement values of the building calculated by using the frequency domain solution and time domain simulation. When the results are compared, it is seen that the values are in excellent agreement although single harmonics is used at harmonic balance method.

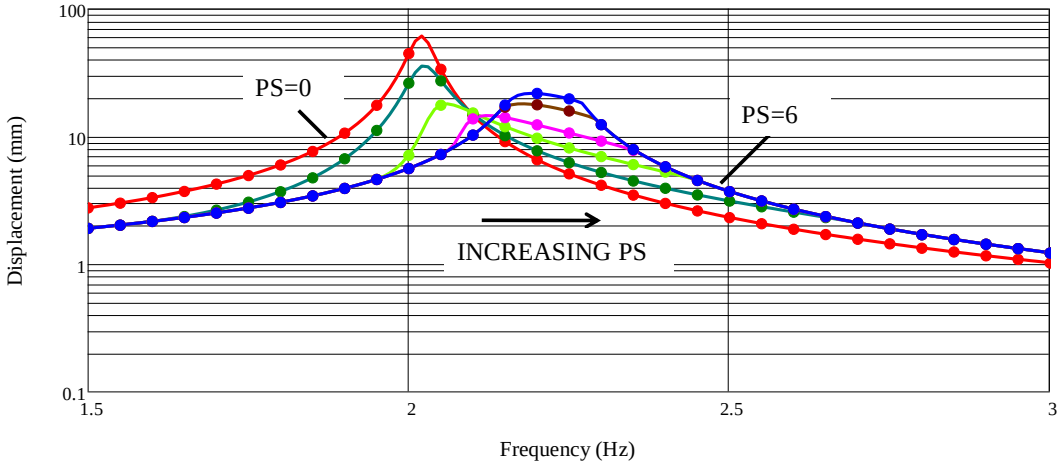

Fig. 6 Displacement vs. frequency curve for time and frequency domain solutions comparison and PS values as 0, 0.7, 1.5, 2.5, 4.5 and 6. Full lines are frequency domain solutions and discrete points are time domain simulations.

4.2. Effect of damper parameters on displacement

In this section, the effect of brace stiffness and slip load on building displacement response will be demonstrated with a simple analysis. For this reason, the same system studied in Section 4.1 is investigated under a constant harmonic ground acceleration which has a magnitude of 0.2m/s^2 .

The response of the 1-dof system is studied by varying PS and SR from 0 to 10 . It should be noted that, in real life, it is difficult to achieve values of SR much greater than 1 as Tabeshpour et al. [7] mentioned; however, there exists several studies in the literature where values of SR are much larger than 1 are considered for bracing systems [8] [9] [10].

Fig. 7, Fig. 8 and Fig. 9 show the effect of PS on the displacement amplitude and resonance frequency of the building when SR is kept constant at 0.2. As already mentioned before, $PS = 0$ is the case corresponding to no damper. As can be seen from Fig. 8, there is an optimum point of PS which results in minimum displacement amplitude. It should also be noted that, for high values of PS , damper cannot slip and the system behaves like a linear one with an equivalent stiffness of $k_1 + k_{b_1}$ and the resonance frequency of the building becomes identical to the stuck case resonance frequency.

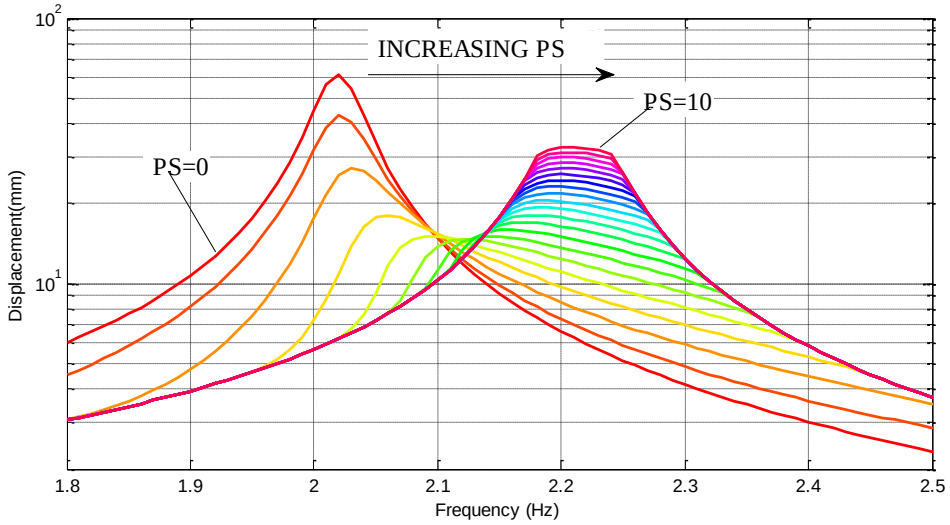

Fig. 7 Frequency-displacement curve for SR=0.2 and PS values as 0, 0.5, 1, 1.5,...,10.

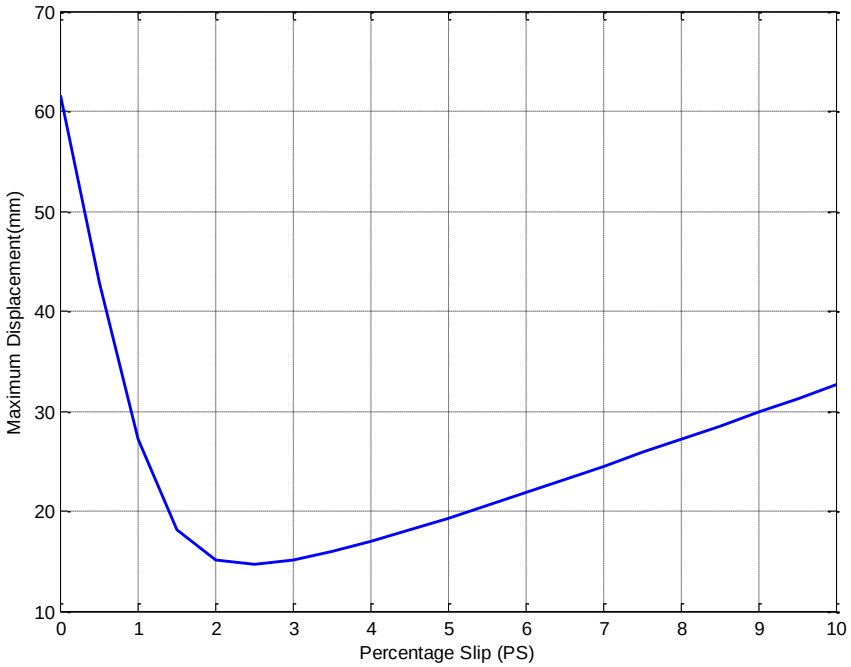

Fig. 8 Maximum displacement versus PS curve for SR=0.2

Fig. 10, Fig. 11 and Fig. 12 show the effect of *SR* on the displacement amplitude and the resonance frequency of the building when *PS* is kept constant at 2. In this analysis, $SR = 0$ is the case corresponding to no damper. From these graphs, it is observed that, the maximum displacement amplitude decreases and the resonance frequency increases with increasing SR.

Effect of *SR* and *PS* on the maximum displacement is as well demonstrated on a 3D graph given in Fig. 13. From this figure, it can be seen that optimum *PS* is a function of *SR*.

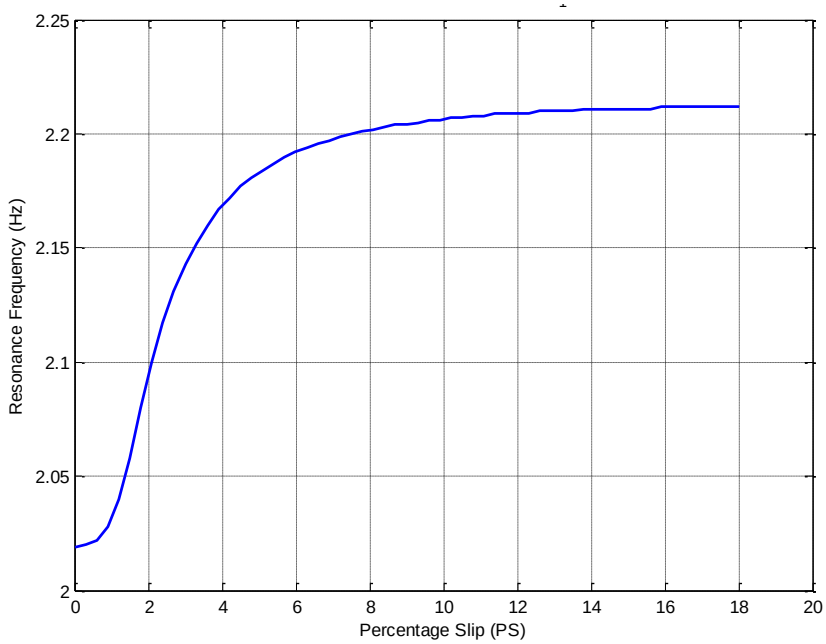

Fig. 9 Resonance frequency versus PS curve for SR=0.2

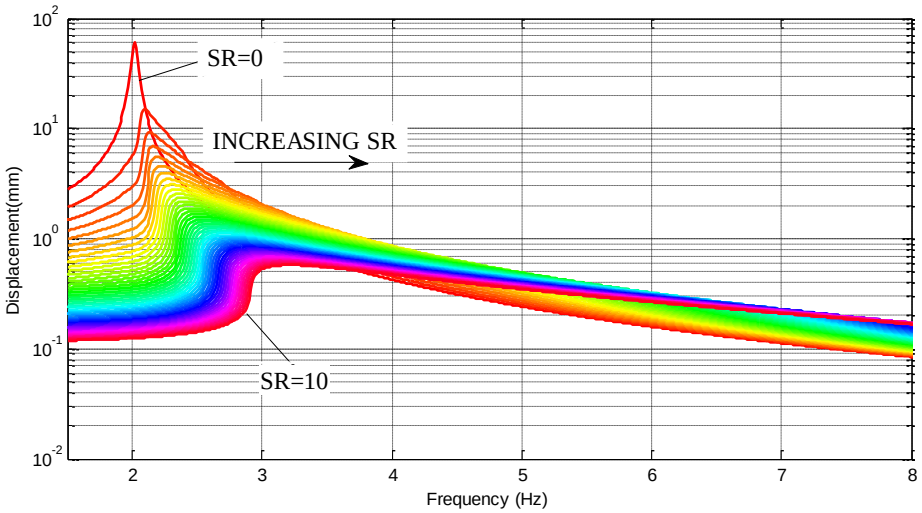

Fig. 10 Frequency-displacement curve for PS=0.2 and SR values as 0, 0.5, 1, 1.5,...,10.

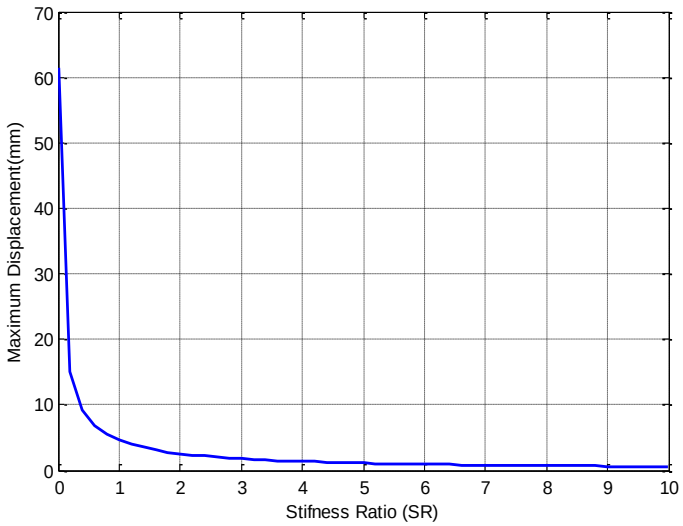

Fig. 11 Maximum displacement versus SR curve for PS=2

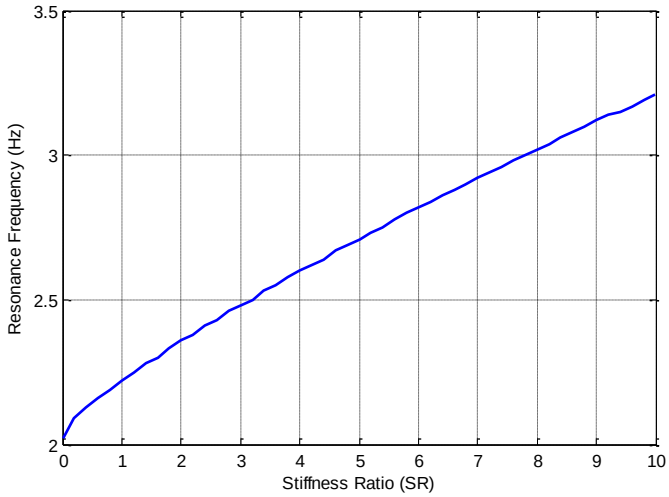

Fig. 12 Resonance frequency versus SR curve for PS=2

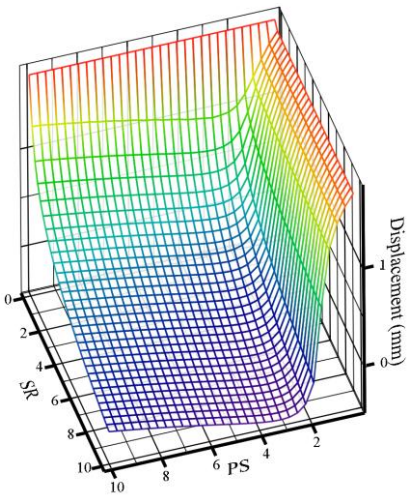

Fig. 13 Effect of PS and SR on maximum displacement

4.3. Optimization Studies

In this section a 6-story building with the following properties is studied;

$$m_j = 50000 \text{ kg for } j = 1,2,3\cdots 6$$

$$k_1 = 74000 \text{ kN/m}, k_2 = 66000 \text{ kN/m}, k_3 = 56000 \text{ kN/m}, k_4 = 44000 \text{ kN/m}, k_5 = 31000 \text{ kN/m}, k_6 = 16000 \text{ kN/m}$$

$$c_1 = 120 \text{ kNs/m}, c_2 = 90 \text{ kNs/m}, c_3 = 75 \text{ kNs/m}, c_4 = 65 \text{ kNs/m}, c_5 = 45 \text{ kNs/m}, c_6 = 32 \text{ kNs/m}.$$

The 6-story building is analyzed by adding dry friction dampers between each story and between the first story and the ground. *SR* is kept constant at 0.2 for all dampers and ground acceleration is kept constant at 0.067 m/s^2 which is the maximum frequency response value of the 1999 Bolu earthquake in east-west direction. In order to obtain the global optimum value of *PS*, a hybrid optimization method is utilized in MATLAB which applies Genetic Algorithm at first and then uses fmincon, a gradient based optimization, in order to enhance the results further. The cost function used in the optimization problem is defined as the minimization of the relative displacement between two successive floors i.e. inter-story drift and the design variables are the slip forces of each damper. As can be seen from Fig. 14, maximum inter-story drift value for the building without any damper is 24.4 mm at 1.25 Hz and it is between 5th and 6th story.

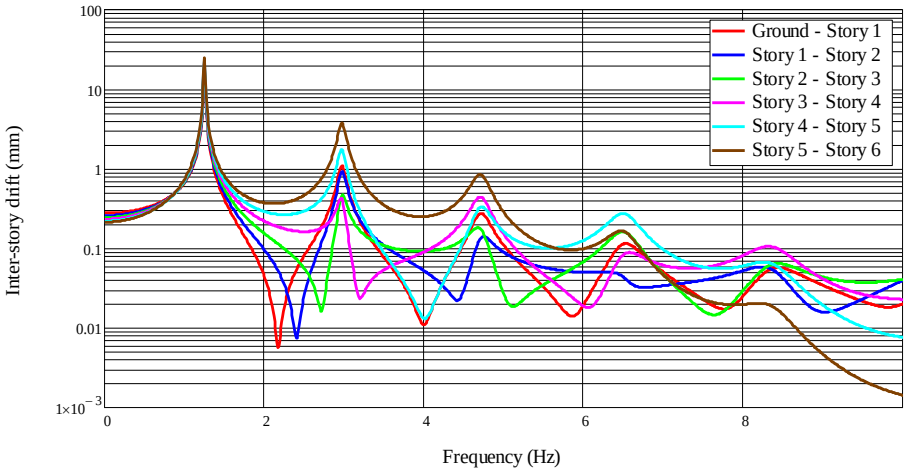

Fig. 14 Inter-story drift plot (no damper)

In the first part of the study, it is assumed that the slip load on each damper is identical and it is optimized. The optimum value for *PS* is obtained as 0.5631 and the maximum inter-story drift at 1.26 Hz is reduced to 3.92mm as seen in Fig. 15.

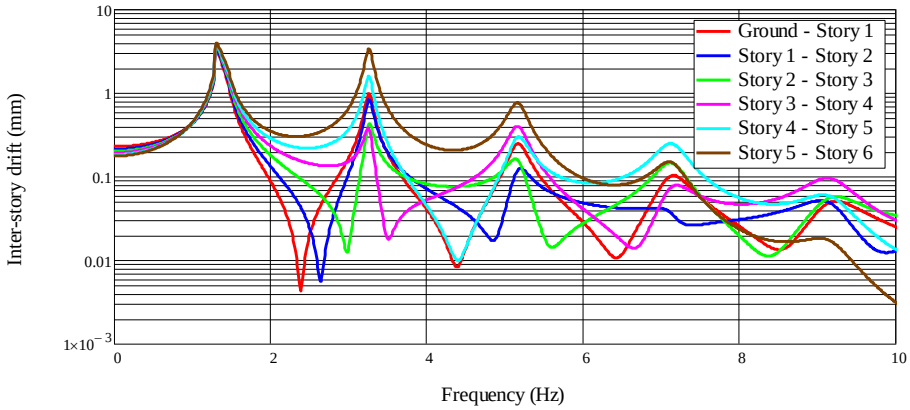

Fig. 15 Inter-story drift plot (PS=0.5631 for all dampers)

In the second part of the study, slip loads on the dampers are considered to be independent from each other and all of these values are optimized. The optimum *PS* values are obtained as follows;

$$PS_1 = 0.6767,\ PS_2 = 0.6443,\ PS_3 = 0.5832,\ PS_4 = 0.4922,\ PS_5 = 0.3912,\ PS_6 = 0.3279$$

and the maximum inter-story drift at 1.3 Hz is reduced to 3.71mm as shown in Fig. 16.

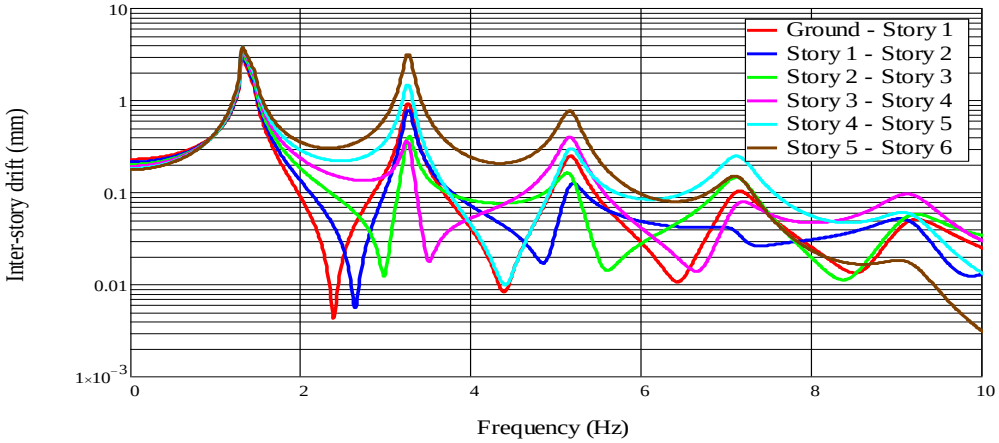

Fig. 16 Inter-story drift plot (optimum PS values)

5. CONCLUSION

In this paper, a multi story building equipped with dry friction dampers is studied under harmonic acceleration. Shear building and macro-slip friction model is used to mathematically model the building and dampers, respectively. In order to overcome the difficulties of time domain methods used in the literature and also decrease the computational expense, a frequency domain solution method is used utilizing Harmonic Balance Method. Although, earthquake motion is totally random and cannot be expressed with harmonic components completely, for optimization purposes this method is very advantageous compared to time domain optimizations, since frequency content and magnitude of an earthquake can be easily calculated by taking Fast Fourier Transform (FFT) of the recorded motion. Moreover, optimizations are not performed for a specific earthquake and; hence, obtained results can be applied for a wide range of earthquakes by properly selecting the ground acceleration amplitude. The validity of the solution method suggested here is demonstrated by comparing the results obtained from frequency domain and time marching solutions and it is seen that they are in excellent agreement. Moreover, it is observed that damper properties such as slip load and stiffness of the supporting elements have a great effect on inter-story drift and should be optimized for minimum inter-story drift. However, due to challenges in construction, it is not practical to change the stiffness of the damper, i.e. brace stiffness. Therefore, the main important variable in optimization is the slip force of the dampers. Hence, the slip force on each friction damper for a multi story building is optimized by using a hybrid optimization method. It is observed that if the identical slip force on each damper is applied, the maximum inter-story drift is

decreased by 83.9% and if the slip loads on the dampers are considered to be independent from each other, then the maximum inter-story drift is decreased by 84.8% for the case study considered in this paper. These results indicate that identical or different slip forces result in similar reductions in the maximum inter-story displacement in the case study under consideration.

REFERENCES

[1] F. Păuleţ-Crăiniceanu, "A lecture delivered to the 4th year students P100 Seismic Code," Editura Cermi, 1999.

[2] B. Bhushan, Principles and applications of tribology, vol. 9, no. 2. Wiley-Interscience, 1999, pp. 89-89.

[3] I. Takewaki, K. Fujita, K. Yamamoto, and H. Takabatake, "Smart passive damper control for greater building earthquake resilience in sustainable cities," Sustainable Cities and Society, vol. 1, no. 1, pp. 3-15, Feb. 2011.

[4] K. Y. Sanliturk, M. Imregun, and D. J. Ewins, "Harmonic Balance Vibration Analysis of Turbine Blades With Friction Dampers," Journal of Vibration and Acoustics, vol. 119, no. 1, p. 96, 1997.

[5] C. H. Chen, J. J., and Menq, "Periodic Response of Blades Having Three-Dimensional Nonlinear Shroud Constraints," ASME J. Eng. Gas Turbines Power, vol. 123, pp. 901-909, 2001.

[6] E. Cigeroglu, N. An, and C.-H. Menq, "Forced Response Prediction of Constrained and Unconstrained Structures Coupled Through Frictional Contacts," Journal of Engineering for Gas Turbines and Power, vol. 131, no. 2, p. 022505, 2009.

[7] M. Tabeshpour and H. Ebrahimian, "Seismic Retrofit of Existing Structures Using Friction Dampers," Asian Journal of Civil Engineering (Building and Houısing), vol. 11, no. 4, pp. 509–520, 2010.

[8] S. Lee, "Allocation and slip load of friction dampers for a seismically excited building structure based on storey shear force distribution," Engineering Structures, vol. 30, no. 4, pp. 930-940, Apr. 2008.

[9] J. Kim, "Behavior and design of structures with buckling-restrained braces," Engineering Structures, vol. 26, no. 6, pp. 693-706, May. 2004.

[10] L. Lu, L. Chung, L. Wu, and G. Lin, "Dynamic analysis of structures with friction devices using discrete-time state-space formulation," Computers & Structures, vol. 84, no. 15-16, pp. 1049-1071, Jun. 2006.

APPENDIX B

EARTHQUKE GROUND ACCELERATION PLOTS

B.1 1992 Erzincan Earthquake in East-West Direction Measured at Erzincan Merkez Meteoroloji Mudurlugu

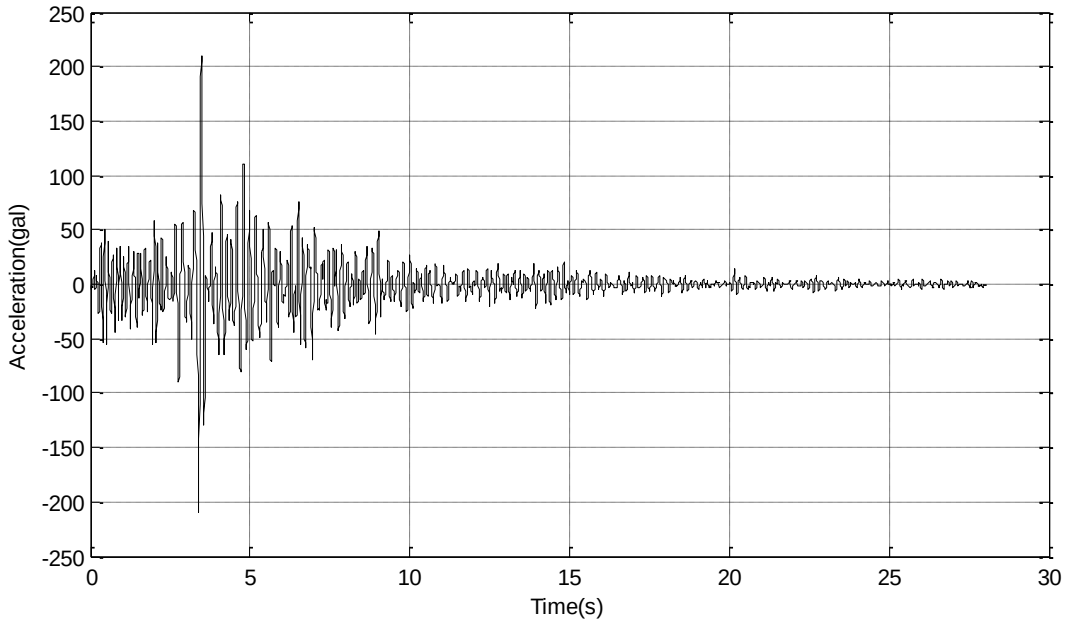

Figure B.1 Time history record of 1992 Erzincan Earthquake (E-W direction)

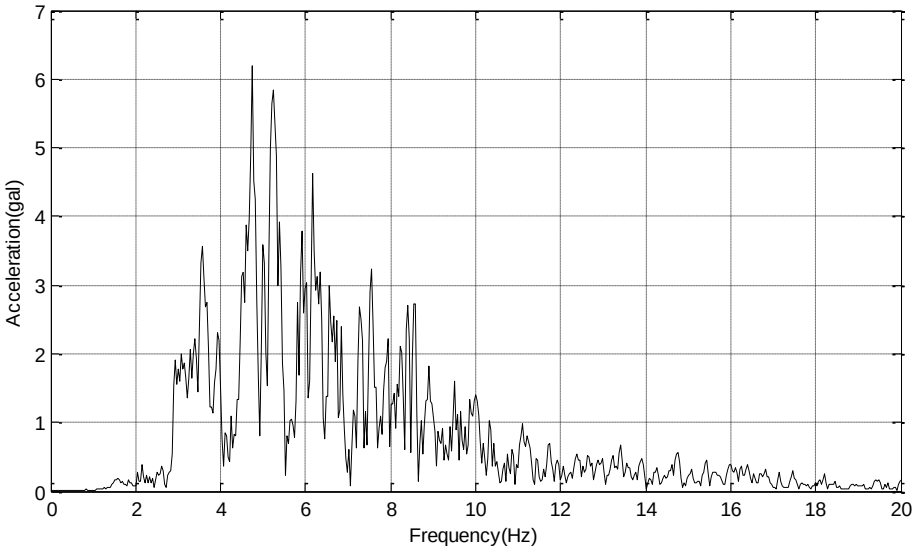

Figure B.2 FFT of 1992 Erzincan Earthquake (E-W direction)

B.2 1976 Denizli Earthquake in East-West Direction Measured at Denizli Merkez Meteoroloji Mudurlugu

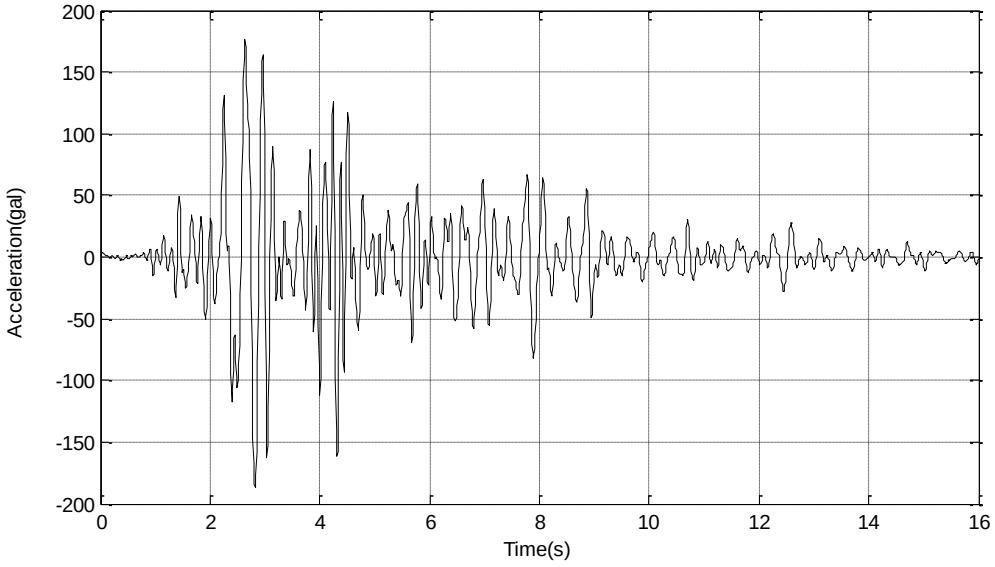

Figure B.3 Time history record of 1976 Denizli Earthquake (E-W direction)

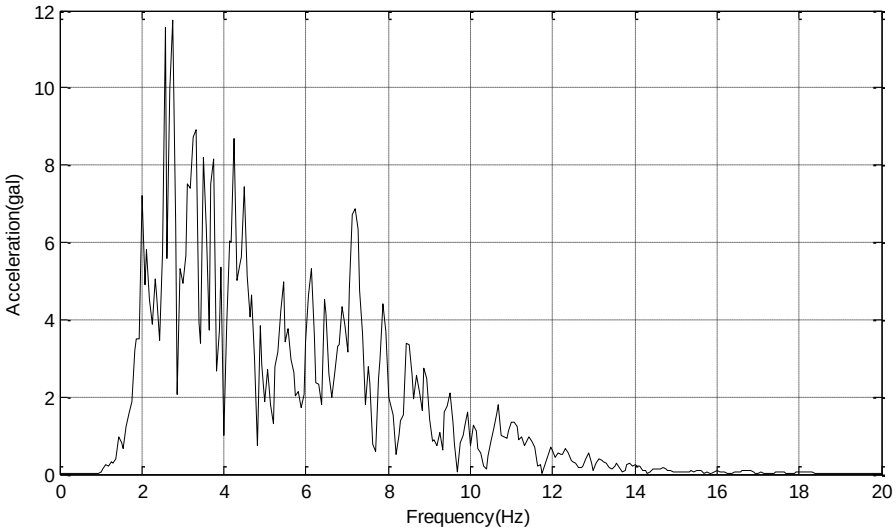

Figure B.4 FFT of 1976 Denizli Earthquake (E-W direction)

B.3 2002 Afyon Earthquake in East-West Direction Measured at Afyon Merkez Bayındırlık ve İskan Müdürlüğü

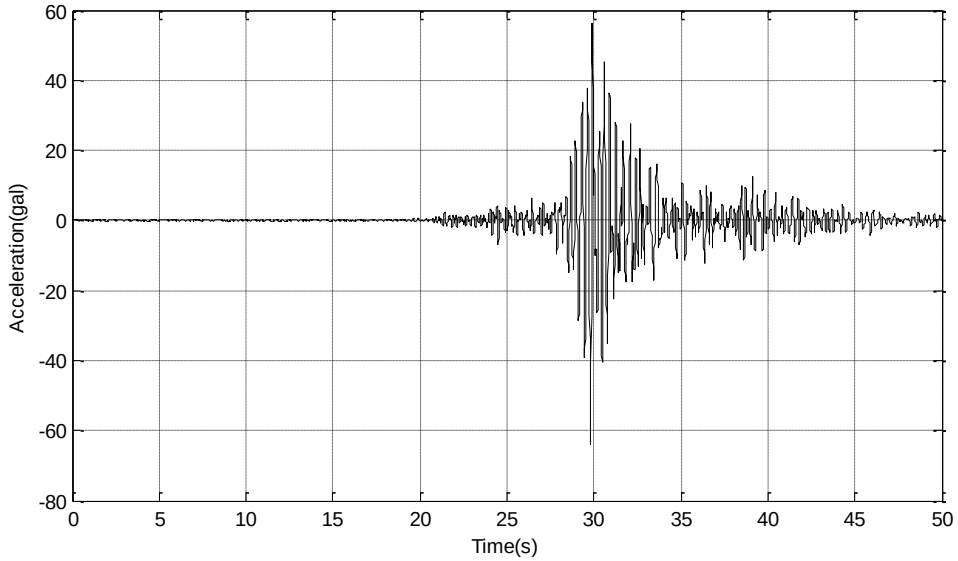

Figure B.5 Time history record of 2002 Afyon Earthquake (E-W direction)

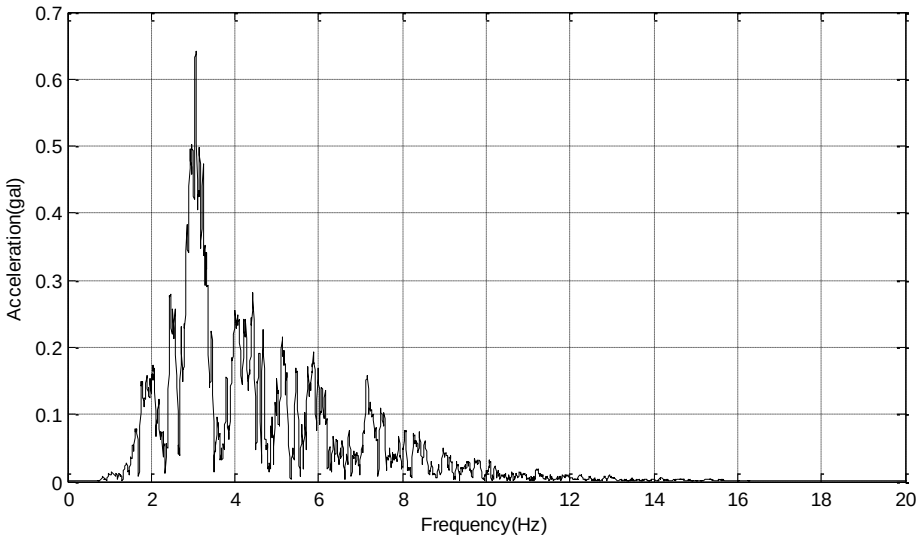

Figure B.6 FFT of 2002 Afyon Earthquake (E-W direction)